

SEARCH FOR NEW HEAVY PARTICLES

by

Walter H. Toki

A.B., University of California, Berkeley

1973

SUBMITTED IN PARTIAL FULFILLMENT

OF THE REQUIREMENTS FOR THE

DEGREE OF DOCTOR OF

PHILOSOPHY

at the

MASSACHUSETTS INSTITUTE OF TECHNOLOGY

April 30, 1976

Signature redacted

Signature of Author.....
Department of Physics, (April 30, 1976)

Signature redacted

Certified by.....
Thesis Supervisor

Signature redacted

Accepted by.....
Chairman, Departmental Committee





Room 14-0551
77 Massachusetts Avenue
Cambridge, MA 02139
Ph: 617.253.2800
Email: docs@mit.edu
<http://libraries.mit.edu/docs>

DISCLAIMER OF QUALITY

Due to the condition of the original material, there are unavoidable flaws in this reproduction. We have made every effort possible to provide you with the best copy available. If you are dissatisfied with this product and find it unusable, please contact Document Services as soon as possible.

Thank you.

The images contained in this document are of the best quality available.

SEARCH FOR NEW HEAVY PARTICLES

Walter H. Toki

Submitted to the Department of Physics on April 30, 1976
in partial fulfillment of the requirements
for the degree of
Doctor of Philosophy

Abstract

Experiments were done at the proton synchrotron at Brookhaven National Laboratory with a 28.5 Gev incident proton beam and a pair spectrometer to detect hadrons and electrons; The first search yielded the discovery of the "J". Here we describe subsequent searches for other long lived particles decaying into $K^- \pi^+$, $K^+ \pi^-$, $P\bar{P}$, $K^- K^+$, $K^+ \bar{P}$, $K^- P$, $\pi^- \pi^+$, $\pi^- p$, and $\pi^+ \bar{P}$. The result based on 2×10^7 events shows to a sensitivity of $\sigma_B \approx 10^{-34} \text{ cm}^2$ no such states were found. The cross sections of all pairs decrease like $d^2\sigma/dx dm \propto e^{-5m}$ and can be grouped into three bands; $\pi^- P$; $\pi^- \pi^+$, $P\bar{P}$, $K^- P$; and $K^- \pi^+$, $\pi^+ \bar{P}$. Within a given band the yield is the same to $\pm 20\%$ and different groups are separated by a factor ~ 10 from each other. A measurement of electron-hadron pairs yielded no indication of a new phenomena and sets limits on $e^+ K^-$ and $e^+ \bar{P}$ cross sections to less than 10^{-33} and 10^{-34} cm^2 respectively.

Thesis Supervisor: Ulrich J. Becker
Title: Associate Professor of Physics

TABLE OF CONTENTS

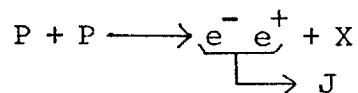
I.	Motivation	5
II.	Experimental Setup at B.N.L.	
	A. Design Considerations for $pp \rightarrow e^-e^+ + X$	8
	B. Double Arm Magnetic Spectrometer for e^-e^+ pairs	
	1. General Description	11
	2. Magnets	15
	3. Scintillation Counters	18
	4. Cerenkov Counters	21
	5. Lead-glass and Shower Counters	31
	6. Proportional Wire Chamber System	33
	7. Shielding	38
	C. Target Preparation and Beam Monitoring	
	1. Target	39
	2. Beam Characteristics	41
	3. Beam Position Monitors	43
	4. Beam Intensity Monitor	44
	D. Instrumentation	
	1. Trigger Electronics	45
	2. Data Acquisition System	47
	3. On-line Analysis	52
III.	Experiment on h^-h^+ Pairs	
	A. Experimental Modifications	55
	B. Spectrometer Checks	59
	C. Data Runs	66
	D. Analysis	71
	E. Results	77
	F. Cross Section	88
IV.	Experiment on e^-h^+ and e^+h^- Pairs	
	A. Data Runs	97
	B. Analysis	101
	C. Results	103

Table of Contents (cont'd.)

V.	Summary and Conclusions111
	Acknowledgements113
	Biographical Note114

MOTIVATION

The discovery of the J particle in August 1974 at Brookhaven National Laboratory by the M.I.T. group¹ was completely unexpected. It was the result of the first high sensitivity and high resolution experiment studying the reaction,



Theoretical speculations before the discovery asked for neutral particles but with a mass larger than 10 GeV to mediate weak interactions as photons do in electromagnetic interactions.² The only prediction in the e^-e^+ mode was a continuum, made by the Drell-Yan model of parton-antiparton annihilation.³

Since the J discovery there has been a flood of theoretical models attempting to explain the J as well as $\psi(3700)$ later discovered at Spear.⁴ Almost all models predict additional long lived particles, which due to their quantum numbers, decay into modes other than e^-e^+ .

The charm model interprets the J particle as a bound quark-antiquark state with the new heavy fourth quark containing the quantum number charm. The charmed quark originally was introduced to eliminate unobserved strangeness changing weak current of the Salam-Weinberg theory.⁵ Using a nonrelativistic four quark model with the J mass as input, theorists predict many sharp states. If J is orthocharm⁶ there must be a parastate, near 3 GeV with probably a

large coupling (decay) to $P\bar{P}$.

The charm model mainly predicts sharp states containing charm in the mass region between 2.0 and 2.5 Gev. Using the Salam-Weinberg theory these charmed states are predicted to have specific weak decay modes and branching ratios. The hypothetical D^0 meson decays slowly because this is charm-forbidden into nonleptonic modes like $D^0 \rightarrow K^- \pi^+$ and also semileptonic into $D^0 \rightarrow K^- e^+ \nu$. With θ being the Cabbibo angle one expects branching ratios,

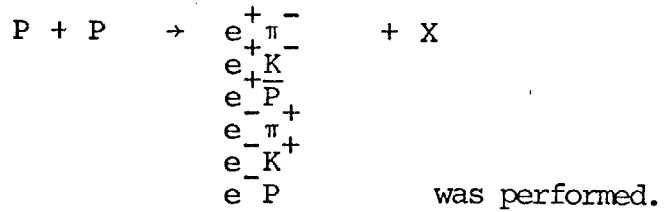
$$\frac{\Gamma(D^0 \rightarrow K^- e^+ \bar{\nu})}{\Gamma(D^0 \rightarrow \pi^- e^+ \bar{\nu})} \approx \cot^2 \theta$$

Aside from theoretical speculations, the experimental question is, are there other long lived states that are unable to decay into $e^- e^+$ pairs but can decay into hadron pairs $h^- h^+$ and is there an electron-hadron pair $e^- h^+$ signal, possibly from a three body decay.

To answer these questions the $e^- e^+$ pair spectrometer at B.N.L. was modified to perform a systematic search of hadron pairs in the reactions

$$P + P \rightarrow \begin{array}{l} \pi^- P^+ \\ \pi^- \pi^+ \\ \pi^- K^+ \\ K^- P^+ \\ K^- \pi^+ \\ K^- K^+ \\ \bar{P} P^+ \\ \bar{P} \pi^+ \\ \bar{P} K^+ \end{array} + X$$

Also a systematic search for $e^- h^+$ and $e^+ h^-$ pairs in the reactions



In the next chapter we describe the e^-e^+ pair spectrometer used for the e^-e^+ pair search. This allows for an orderly description of the apparatus as it was designed, constructed and later modified. In the following chapter, the modifications and the hadron pair experiment are fully described, followed by the e^+h^+ experiment.

1. J.J. Aubert et. al., Phys. Rev. Lett. 33, 1404 (1974).
2. S. Weinberg, Phys. Rev. Lett. 19, 1264 (1967).
3. S.D. Drell and T.M. Yan, Phys. Rev. Lett. 25, 316 (1970).
4. G.S. Abrams et. al., Phys. Rev. Lett. 33, 1453 (1974).
5. S.L. Glashow, J. Iliopoulos and L. Maiani, Phys. Rev O2, 1285 (1970).
6. T. Appenquist et al., Phys. Rev. Lett. 34, 365 (1975)

DESIGN CONSIDERATIONS FOR e^+e^- PAIR MEASUREMENT

The design considerations for the MIT spectrometer¹ were for measuring $pp \rightarrow e^-e^+ + X$ with high sensitivity and high resolution to detect long-lived particles. The primary problem is measuring a very small e^+e^- pair signal against an intense hadronic background.

To detect e^+e^- pair events at an acceptable rate, a high beam intensity is required. Estimating the rate from a previous experiment² that measured a $\mu^+\mu^-$ continuum in $P+U \rightarrow \mu^+\mu^- + X$, the design beam intensity of 2×10^{12} protons/AGS beam pulse was chosen. This led to predictions of 20×10^6 hz single arm rates of hadrons, based upon Hagedorn and Ranft calculations.³ Furthermore, estimates of the hadron pair rates were quite high. A naive estimate of the e^+e^- pairs rate over the hadron pair rate is the ratio of the electromagnetic to strong coupling. With the strong coupling $g^2 \approx 10$, if we compare an s-channel exchange with an electromagnetic coupling to an exchange with strong coupling, the ratio becomes,

$$\frac{\alpha}{g^4} \approx 10^{-6}$$

The main design requirements emerging are a spectrometer that can accept 2×10^7 hz single arm rates and can detect electrons with a rejection efficiency against hadrons of 10^8 . All this is coupled with the requirement of high resolution.

To detect electrons but reject hadrons with high efficiency two Cerenkov counters are used. Furthermore, to reduce knock-on electrons (elastically-scattered atomic electrons) and photon conversion, all material in spectrometer arm is minimized.

The key to detect an e^+e^- pair signal with estimated 10 khz single arm electron rates and 2×10^7 single arm hadron rates, will be fast timing with detectors with short resolution times and small dead time. Using 4 planes of hodoscopes in addition to the Cerenkov, a many-fold coincidence can be formed to reduce background in the trigger, as well as provide a fast trigger with resolving times in the 10's of nanoseconds.

To sensitively momentum analyze particles, magnetic deflection should be measured to the limit imposed by multiple scattering. This deflection measurement can be accomplished by the use of proportional wire chambers to determine track position to 2 mm accuracy.

Finally, assuming that the production of particles that decay into e^-e^+ pairs have a similar production mechanism to vector mesons, produced in pp collisions, namely,⁴

$$\frac{d\sigma}{dp_{\perp}^2} \propto e^{-bp_{\perp}^2}$$

then the best kinematic region is at rest in the CM frame. Choosing to detect the decay particles symmetrically in the lab system or at 90° in the CM frame. One finds the pair opening

angle for 28.5 Gev incident protons to be;

$$\theta_{lab} = \tan(P_{\perp}/P_L^{lab}) = \tan(P_{\perp}/\gamma(P_L^{cm} + \beta E^{cm})) = \tan(P_{\perp}/\gamma\beta\sqrt{P^2 + m_e^2}) \approx \tan(1/\gamma\beta) \approx 14.6^\circ$$

This is for particles with $m \ll P$ such as e, K and π and then it is independent of the pair mass.

1. J.J. Aubert et al., Nucl. Phys. B89, 1 (1975).
2. J.H. Christensen et. al., Phys. Rev. Lett. 25, 1523 (1970).
3. H. Grote, R. Hagedorn and J. Ranft, Particle Spectra (1970).
4. V. Blobel et. al., Phys. Lett. 48B, 73 (1974).

GENERAL DESCRIPTION

The layout of the electron pair spectrometer is shown in fig. 1 and 2. The symmetric arms are positioned at 14.6° relative to the beam to detect electrons at 90° in the CM frame for an incident 28.5 Gev proton beam.

The three dipole magnets M0, M1 and M2 bend the charged secondaries in the vertical plane. The momentum is determined from the total vertical deflection through the magnets by measuring the track positions beyond the last magnet in four proportional wire chambers AO, A, B and C.

Behind A and B chamber are a set of 8x8 hodoscopes to provide a fast timing signal for the trigger electronics.

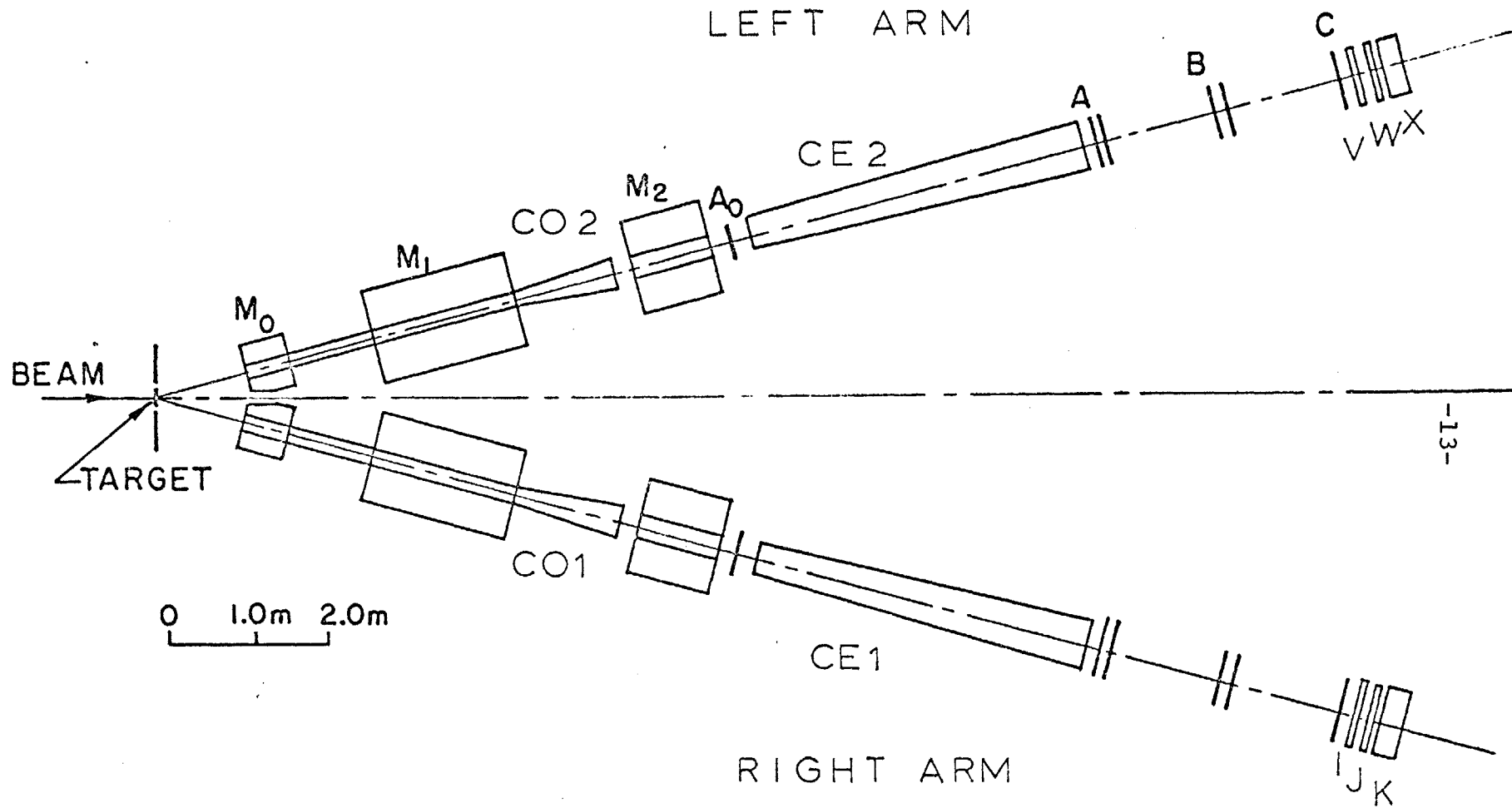
The electrons /positrons were identified by two threshold Cerenkov counters and a set of lead-glass and lead-lucite shower counters. CO Cerenkov counter was built into M1 magnet and CE Cerenkov counter was beyond the last magnet M2. This configuration decoupled charged particles passing through each counter magnetically to provide rejection against delta rays. The lead-glass and shower counters at the end of the arm provided an additional check for an electron shower and improved track identification in the case of two or more track ambiguities.

CB, a large angular acceptance wedge shaped Cerenkov counter, was placed below M0 magnet to count electrons

(positrons) bent downward radially from the center of MO. A coincidence from CB and a positron (electron) in the spectrometer arm indicated a pair event entered the arm, primarily from $\pi^0 \rightarrow \gamma e^- e^+$, which was rejected.

Plan view of e^-e^+ pair spectrometer.

Fig. 1



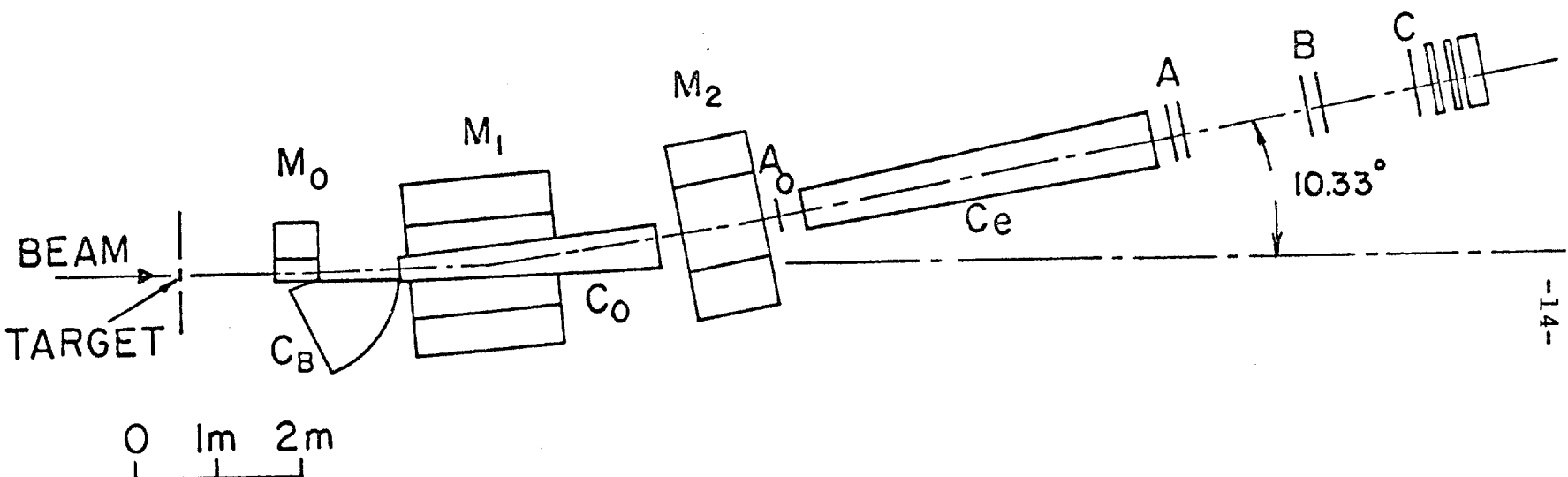


Fig. 2

Side view of one arm of e^-e^+ pair spectrometer

MAGNETS

The three magnets M0, M1 and M2 of fig. 2 were mapped in January of 1974. An aluminum trough with a small wheeled cart holding a 3-dimensional hall probe was surveyed into each magnet. All field components were measured stepping along the horizontal lines in 1" intervals. For each point the hall probe output was fed into a Hewlett-Packard 3485A digital voltmeter whose output punched the 3 field values on cards. The current was monitored by the voltage drop across a high precision shunt. Roughly 10^5 points were measured in 3 complete magnet settings.

The hall probe was calibrated against a Nuclear Magnetic Resonance probe in a dipole magnet with a known highly homogeneous field. The calibration corrected field strength, rotation and position. All cards with DVM values were put onto magnetic tape and corrected accordingly. Then for each horizontal trace, done with the probe, the total integrated field was calculated. All other intermediate values were determined by interpolating between measured ones.

To calculate the momentum along the central ray axis we first note that the amount of bending of a particle of momentum P(GeV) through a magnet of given Bdl (kilogauss-inches) is:

$$\theta_{out} = \sin^{-1} ([\int Bdl / (P \times 1313.2) + \sin\theta_{in}])$$

where θ_{in} and θ_{out} are the angles with the normal. We may

estimate the momentum along the central ray axis by determining the momentum a particle that enters M0 at 0° must have to leave M2 at 10.33° to the horizontal, entering normal to the wire chambers. This roughly corresponds to the average path in phase space or the principle momentum axis (P_0) a particle follows through the spectrometer arm. From Monte Carlo calculations the angular acceptance of each spectrometer arm is $\theta \pm \Delta\theta = 14.6^\circ$ and $\phi = \pm 2^\circ$ with momentum acceptance of $0.6 P_0 < P < 1.8 P_0$. In table 1, are the results at three different magnet settings along with the invariant mass of an e^+e^- pair that occurs when each secondary is on the principle momentum axis of each spectrometer arm.

Table 1. Center $\int B dl$ values (kilogauss-inch)

<u>SETTING</u>	<u>M\emptyset(8C20)</u>	<u>M1(18D72)</u>	<u>M2(18D40)</u>	<u>P(Gev)</u>	<u>M_{pair}^{ee}(Gev)</u>
HIGH P	219.02	1498.25	474.17	9.26	4.6
MED P	219.02	1086.94	417.94	7.2	3.6
LOW P	219.02	568.495	320.04	4.6	2.3

SCINTILLATION COUNTERS

Scintillation counters of the right and left arm are E(8), F(8), G(8), and H(8) and R(8), S(8), T(8) and U(8), respectively. All are 1.6 mm thick scintillators. The counters with their tube base positions are drawn for the right arm in fig. 3. All counters used 56 DVP (2" dia.) phototubes with 2 ns clips. The vertical scintillators were all of equal widths, whereas the 4 top horizontal counters were half the widths of the bottom four. This was an attempt to more evenly distribute the rates since low momentum particles with higher rates were bent up higher into the hodoscopes. All phototubes pointed away from the beam in order to reduce background.

The counters were all voltage plateaued (measure detection efficiency versus high voltage) in the AGS east test beam. The setup is shown in fig. 4. It used three small test counters to define the beam. All cables (H.V. and signal) used between the counter and the electronics were the same as those to be used for the experiment. The efficiency was the 4-fold coincidence with the counter under test divided by the 3-fold coincidence excluding that counter. To incorporate light attenuation, the end opposite to the phototube was placed in the test beam. All final voltages were set 50 volts above the knee (where the efficiency curve stops rising and flattens out). All counters had measured efficiencies of better than 99%.

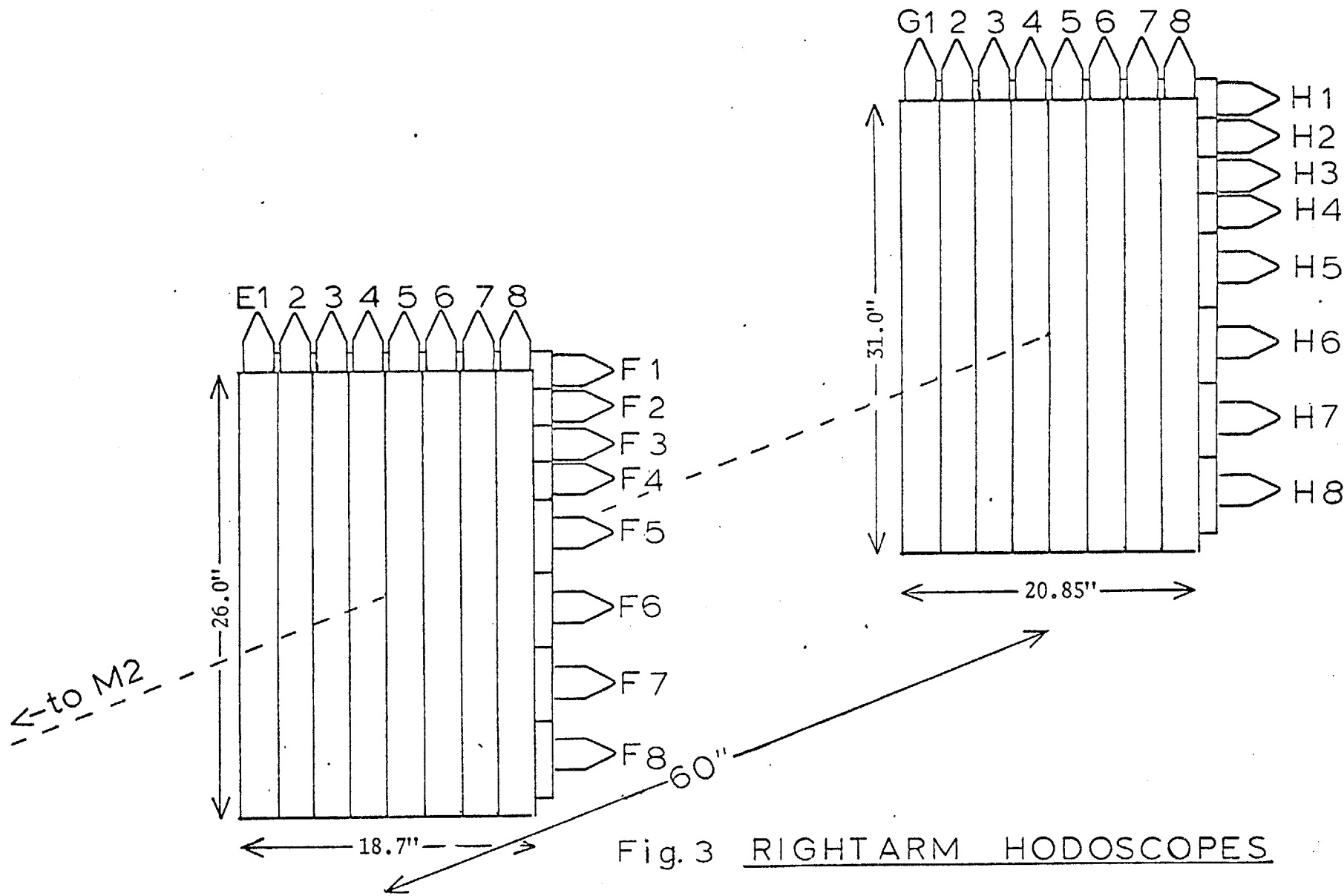


Fig. 3 RIGHT ARM HODOSCOPES

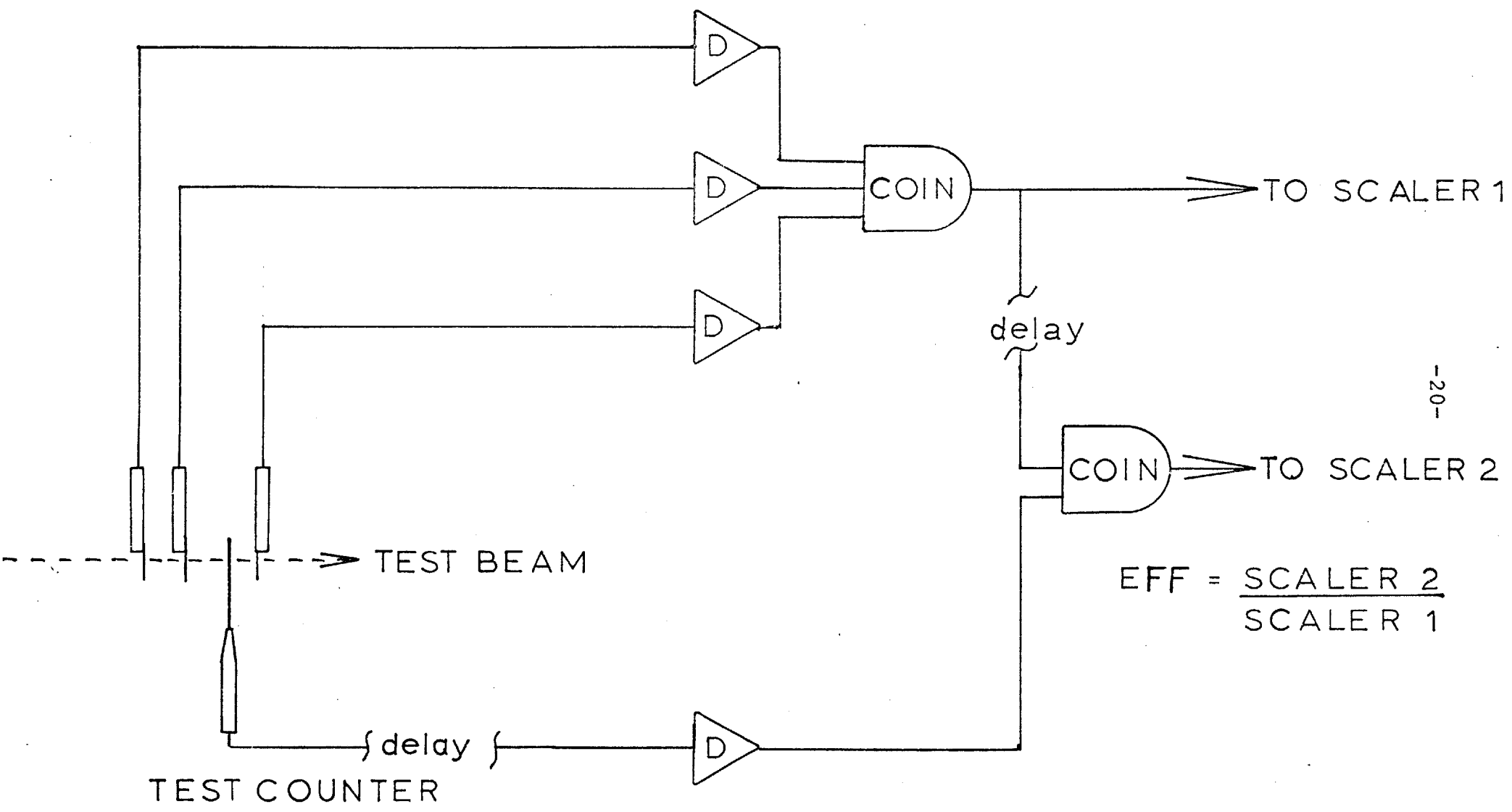


Fig. 4 Test Setup for Hodoscope Efficiencies.

CERENKOV COUNTERS

The Cerenkov effect occurs in mediums when the velocity of a charge particle exceeds the velocity of light radiation. The effect is characterized by the Cerenkov eqn:

$$\cos \theta = 1/\beta n$$

where θ is the angle of emission, $\beta = v/c$ and $n =$ index of refraction. The onset or threshold of Cerenkov light occurs at $\cos\theta = 1$. The number of photons emitted per unit length, calculated classically by Tamm & Frank,¹ is given by

$$\frac{\partial N}{\partial L} = 2\pi\alpha Z^2 \int_{\lambda_2}^{\lambda_1} (1 - 1/\beta^2 n^2) \frac{d\lambda}{\lambda^2}$$

For experimental uses the expression is simplified to

$$N = A L \sin^2 \theta = A L (1 - 1/\beta^2 n^2)$$

where N is the number of photoelectrons ejected off the photocathode of the photomultiplier. The $A(\text{cm}^{-1})$ factor characterizes the wavelength dependent efficiency of the photocathode and the optical system. Assuming one photoelectron to yield a count, then from Poisson statistics the efficiency of the photomultiplier is given as

$$\epsilon = 1 - e^{-N}$$

Hence for +99% detection efficiencies, at least 5 photoelectrons are required.

The spectrometer contains three large aperture gas threshold Cerenkov counters, CB, CØ and CE, to identify electrons. Table 2 summarizes the design characteristics of the counters. The index of refractions^{of the gases} are given at 25°C and 1 atm and the A values are from published values.²

CB counter (fig. 5) has four mirrors and phototubes positioned radially from M0 magnet so each system is partially momentum selective. Only electrons of less than 1 Gev can be detected. The top surface of CB used a very thin stainless steel window (0.25 mm) to minimize conversion of gamma rays from the target and electron bremsstrahlung in the foil. CB was aligned with a laser and not tested before placement into the spectrometer. Later, tests will be described using electron converter plates. CB was filled with Isobutane gas, a denser gas than hydrogen, otherwise used for electron detection, because its short length allowed the particle track to emit little Cerenkov light. Thus a denser gas was used to increase the photon yield of the electrons, however at the cost of lowering the threshold of the pions and increasing CB's background rate.

CO counter (fig. 6) extended all the way through M1 magnet. It used the highly sensitive RCA 31000M phototube and a lucite spherical mirror and a parabolic mirror near the phototube. The front and rear window of CO was thin mylar

(125 μ m and 250 μ m respectively) and the mirror was 3 mm lucite so as to minimize multiple coulomb scattering and knock on electrons. The test beam setup used a Cerenkov counter efficient on pions and four small scintillation counters to define the beam. Initially CO was voltage-plateaued to find the knee. All cables (HV and signal) used, between CO and the electronics, were the same as later used in the spectrometer. The efficiency was the 5 fold coincidence of all counters divided by the 4 fold coincidence excluding C \emptyset . Filling C \emptyset with CO₂ gas at 1 atm and setting the voltage at 50% detection efficiency, the output was fed into a PHA and the photoelectron peaks were clearly discernable (fig. 7)*. This is a special feature of the newly developed 31000M tube. Next the detection efficiency as a function of gas pressure was investigated. For dilute gases, the relation between n, index of refraction and density can be calculated classically and results in the Lorentz-Lorenz Law.²

$$\frac{n^2 - 1}{n^2 + 2} = A d$$

d = gas density, A = atomic refractivity (constant), consequently

$$\frac{P_2}{T_2} \left(\frac{n_1^2 - 1}{n_1^2 + 1} \right) = \frac{P_1}{T_1} \left(\frac{n_2^2 - 1}{n_2^2 + 1} \right)$$

*This checks $\langle n \rangle$.

P_i = pressure, T_i = temperature, and simplifying, for
 $0 < \eta \ll 1$, $\eta = n-1$

$$P (273^\circ/T) \eta_o = \eta$$

$P(\text{atm})$, $T(K^\circ)$ and $\eta_o = \eta_o - 1$, at 1 atm. at 0°C . Since,

$$N = A L (1 - 1/\beta^2 n^2)$$

then for $\beta \approx 1$ and $n \approx 1$

$$N = A L (n^2 - 1) = 2 A L (n - 1) = 2 A L \eta$$

$$N = 2 A L P (273^\circ \eta_o / T)$$

Hence the efficiency dependency of P was checked to be,

$$\epsilon = 1 - e^{-P\kappa} , \quad \kappa = 2 A L 273^\circ \eta_o / T$$

To check the A parameter value against published values³, the efficiency of the counter as a function of beam momentum was measured and compared. The resulting values were in rough agreement with the published value of 150 cm^{-1} . Finally, the optics of various regions of phase space were mapped by tilting the counter in different positions relative to the beam (fig. 8)

CE counter has similar optical system to CO except it has a larger angular acceptance. Again CE had thin mylar windows and a lucite mirror. It was designed to operate near or at 1 atm. The test beam runs were identical to those of CO.

However, it was found that the uniformity of the photocathode surface was very important. This was discovered by changing the efficiency by rotating the phototube. This was later corrected by replacing the mirror and trying several different 3100M phototubes.

¹I. M. Frank and I. Tamm, Dokl. Akad. Nauk SSSR, 14, 109(1937)

²J. Litt and R. Meunier, Ann. Rev. Nucl. Sci., 23, 1(1973)

³D. D. Yovanovitch et al., Nucl. Inst. and Meth., 94, 477(1971)

Fig. 5 Plan and side view of the CB counter shown in its location in the experiment.

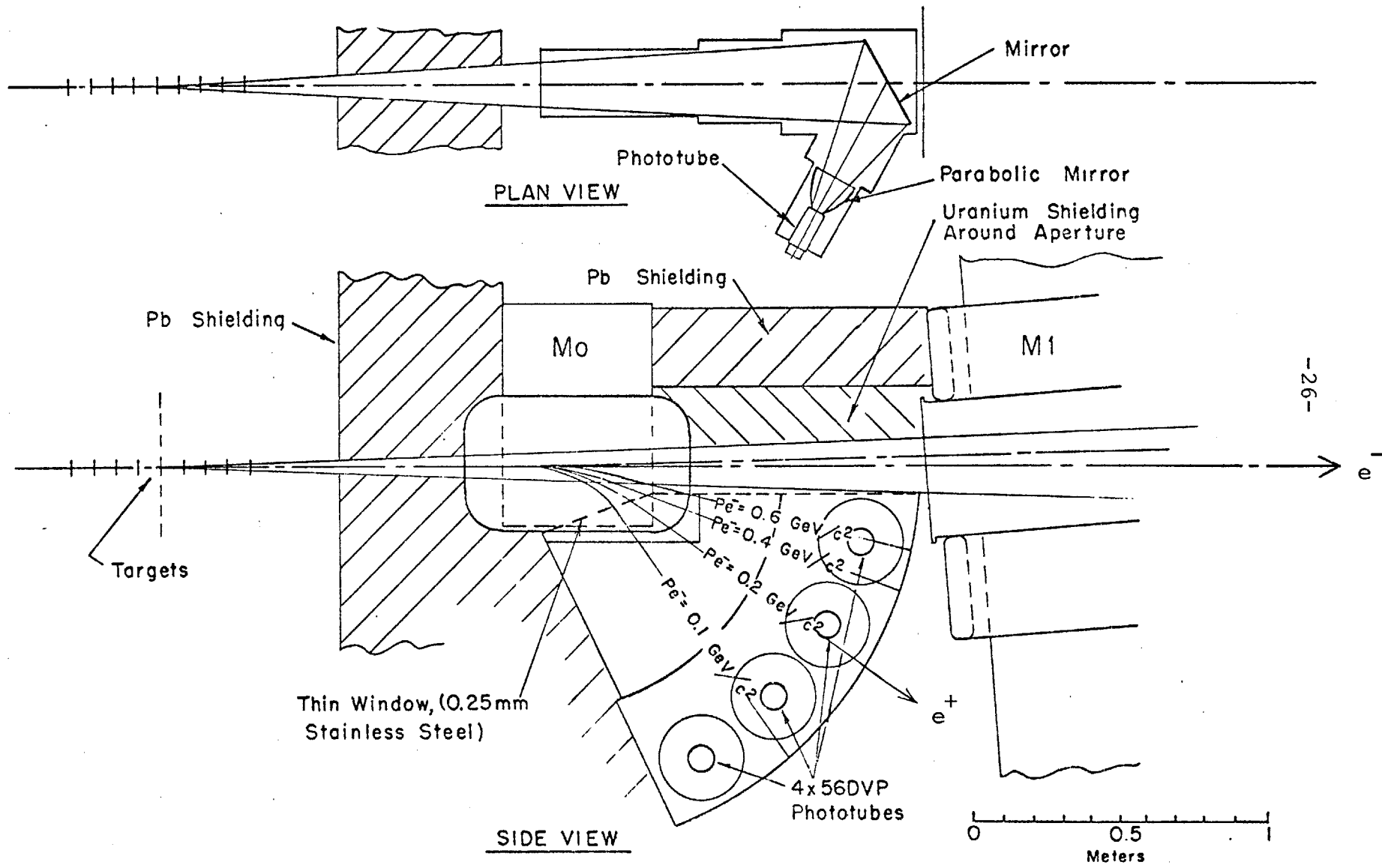
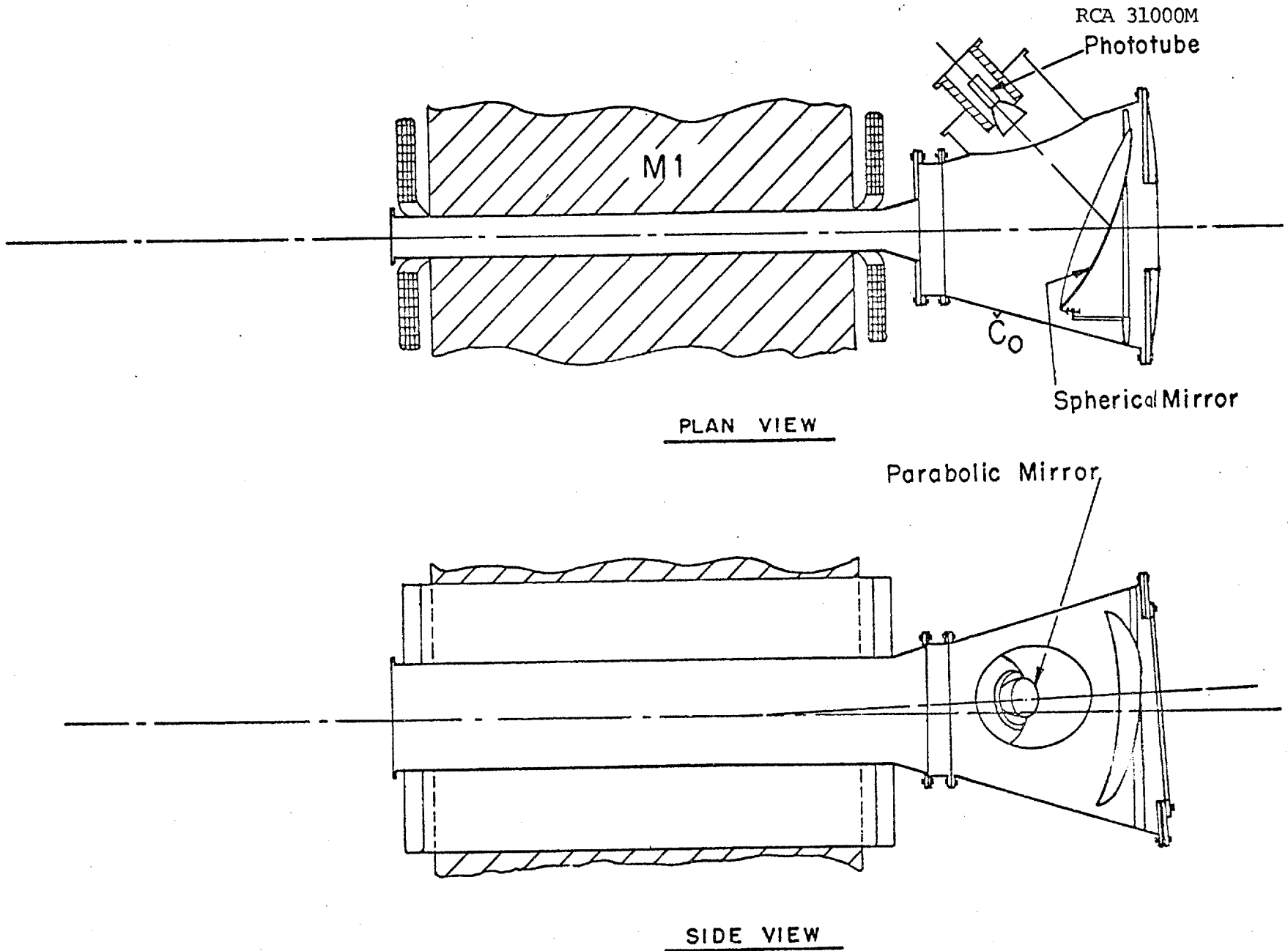


Fig. 6 Plan and side view of the $C\bar{O}$ counter shown in its location in the experiment.



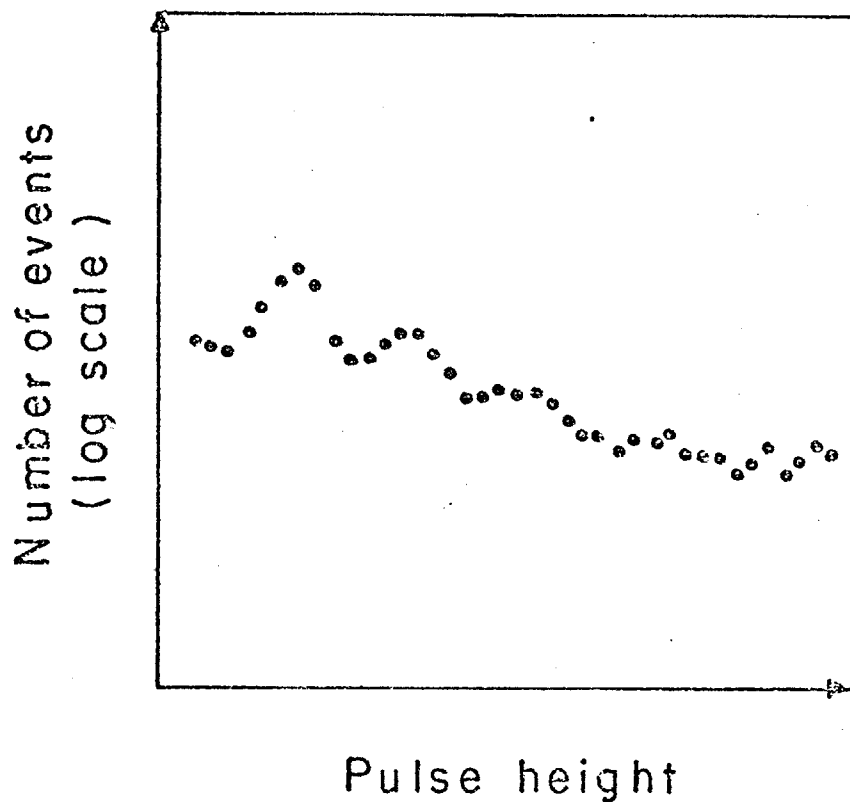


Fig. 7 Pulse height spectrum from the phototube (RCA C31000M) of the $C\emptyset$ in Helium Cerenkov counter. Clearly visible are the one, two and three photoelectron peaks.

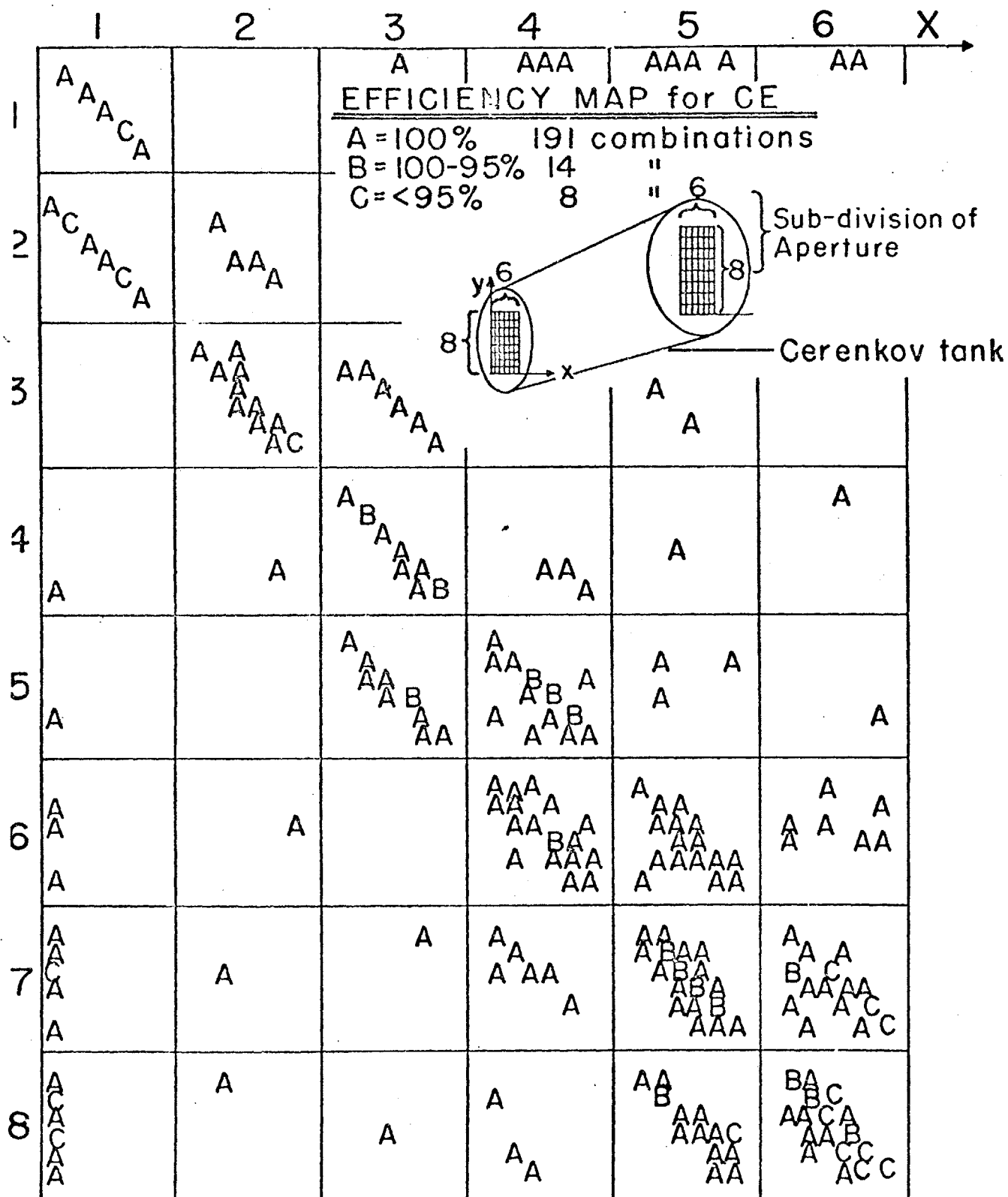


Fig. 8 Mapping of the efficiency of CE counter over its whole phase space. The letters on the plot refer to efficiencies measured for trajectories between the corresponding points marked on the grid at each end on the counter.

TABLE 2 CERENKOV COUNTER CHARACTERISTICS

COUNTER	GAS	PRESS.	LENGTH	A	$n(n-1)$	γ	N_e	p_{thres}^e	p_{thres}^π
CB	C_4H_{10}	1 atm	90 cm	100 cm^{-1}	1.364×10^{-3}	19.1	25	9.7 Mev	2.7 Bev
CØ	H_2	1	283	150	1.505×10^{-4}	57.6	13	29	8.0
CE	H_2	0.8	388	150	1.204×10^{-4}	64.4	14	33	9.0

$$\gamma = \frac{1}{\sqrt{1-\beta^2}}$$

LEAD-GLASS AND SHOWER COUNTERS

The lead-glass and shower counters are shown in fig. 9 . The $^{12+}_{13}$ lead-glass counters that form the first and second banks, are each 3 radiation lengths thick. Their horizontal and vertical positions provide partial spatial selection. The last bank contains 7 horizontal shower counters that are a lead-lucite sandwich 10 radiation lengths thick. Each lead-glass counter uses one Amperex XP-1031 (3") phototube and each shower counter has two 58DVP(5") phototubes on each end.

Connected at the end opposite to the phototube in the lead-glass counters and in the center of the shower counters were fiber optic light pipes all fed from one tight emitting diode. This provided absolute and relative calibration of the counters.

The counters were voltage plateaued in the test beam with pairs so only their Cerenkov light was detected. The calibration with electrons will be described later in the section, Spectrometer Checks.

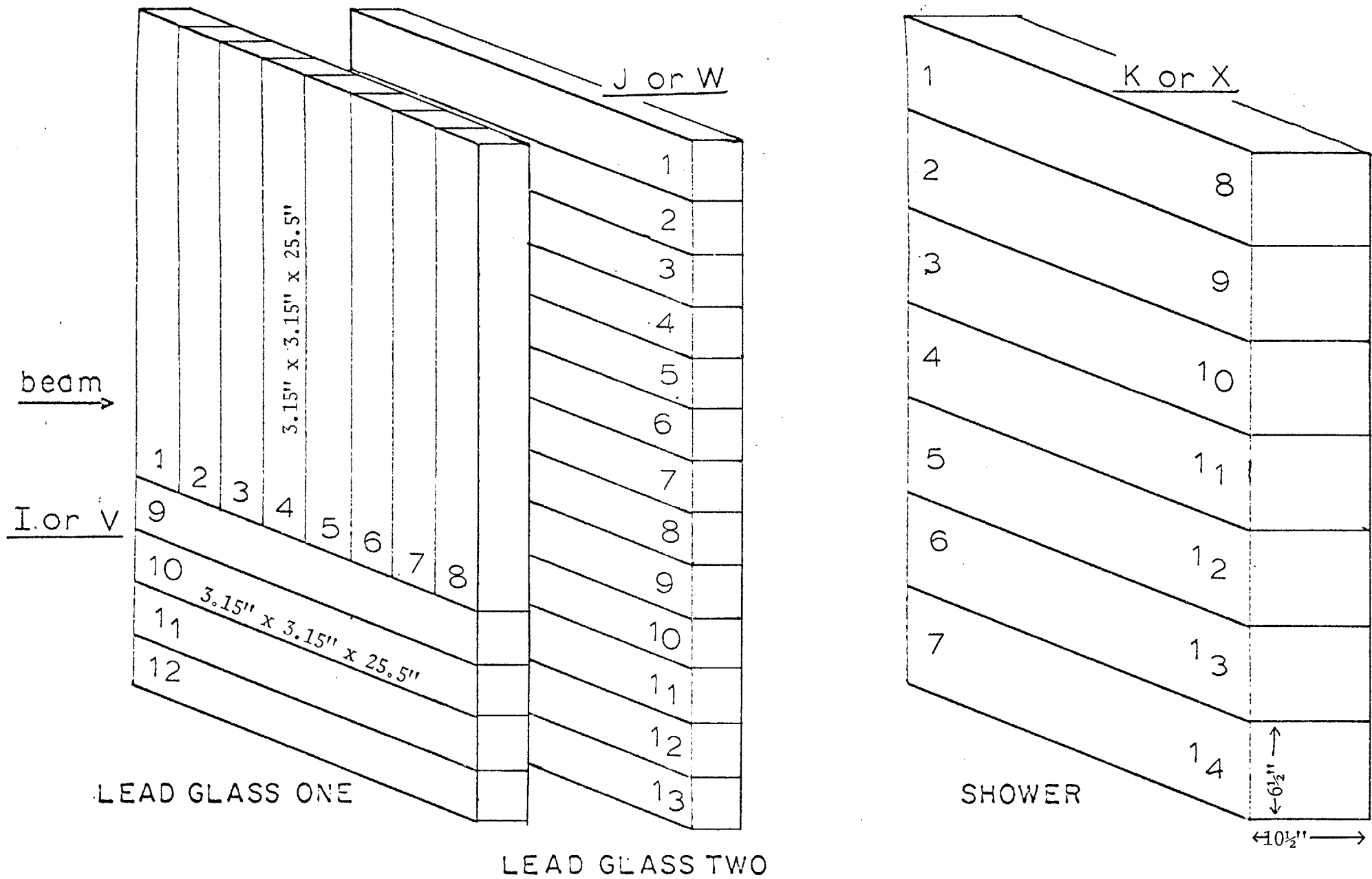


Fig. 9

SCHEMATIC ARRANGEMENT OF LEAD GLASS AND SHOWER COUNTERS

PROPORTIONAL WIRE CHAMBERS

Proportional wire chambers may be compared to an array of geiger counters except lower field strengths are used at the cathode causing discharge in the proportional region. When charged particles pass through a gas, electrons are liberated by ionization. When these electrons are nearby sensing wires of positive potential, they are accelerated towards the wire and induce secondary ionizations which result in an avalanche of electrons. The charge collection yields a negative pulse on the wire. Charpak exploited this effect to construct large multiwire arrays when transistorized amplifiers sensitive to such signals made it feasible.¹ The wire chambers feature spatial resolution of the order of mm, good resolution time and small dead time. The time resolution is limited by the drift times of electrons which vary depending (20-50ns) where the charged particle passed between the two sensing wires. The dead time (200-300 ns) is limited to the length of time for the collection of all electrons.

The spectrometer has four proportional wire chambers, A \emptyset , A, B and C. Chambers A, B and C each had three planes of sensing wires rotated 60 $^{\circ}$ ^(fig.10). This configuration required that a charged particle passing through the chambers fire wires whose sum of wire number coordinates from the three

planes equal a constant. Also each chamber was rotated 20° relative to the preceeding to reduce parallel track ambiguities.

Because AØ was placed at the opening of M2, the high rates required a special design. The purpose of AØ was to provide an additional check on the horizontal track position to improve track reconstruction. For one set of vertical wires high rates of 2×10^7 /sec yielded 1 particle/50 ns. The dead time was approximately 350 ns, hence the amount of tracks lost is for 100 effective wires,

$$(350/50) (1/\# \text{wires}) = 7\%$$

for one plane. Using 2 sets of wires, slightly rotated $\pm 5^\circ$ as to decouple the dead times will improve the situation.

The chambers had sense wires 2 mm apart sandwiched between high voltage wire planes with a separation of 6 mm between planes. The wires were strung with 50-70 grams of tension and glued onto G10 frames. Thin mylar windows in front and back sealed the chambers gas tight. The mylar windows were also aluminized to shield the wires from R.F. pickup.

The chamber was filled with a special gas mixture of 80% argon and 20% methylal. This was obtained by bubbling argon through methylal at 2°C where the partial pressure is 0.2 atm. This mixture allowed the chambers to operate in

high radiation without "ageing" and further allowed chamber operation at low voltages of 3.2 kV with amplifier thresholds of 250 μ V.

The wire readout system is the Sippach² design. Fig. 11a shows a block diagram of the system. The signal is amplified and discriminated on IC boards on the chamber and the pulse is sent along a 200 ft. cable to the coincidence register in trailer. The signal reaches the coincidence register, which is a combination OR/LATCH device that from 32 wire signals forms 32 bit words that will enter the Track Encoder. The coincidence register performs coincidence of all 8800 wires with the event trigger of 30 ns which is stored in the latch. The Track Encoder forms wire chamber numbers from the 32 bit words and the address information from the coincidence register so only the numbers of the fired wires are passed on. The Interface and DR11B are the interface devices to match the electronics to the UNIBUS system of the PDP11. There the computer will process the data onto tape.

¹G. Charpak et al., Nucl. Instr. and Meth. 62(1968)13.

²H. Cunitz et al., Nucl. Instr. and Meth. 91(1971)211.

Configuration Of Wire Planes In Proportional Chambers

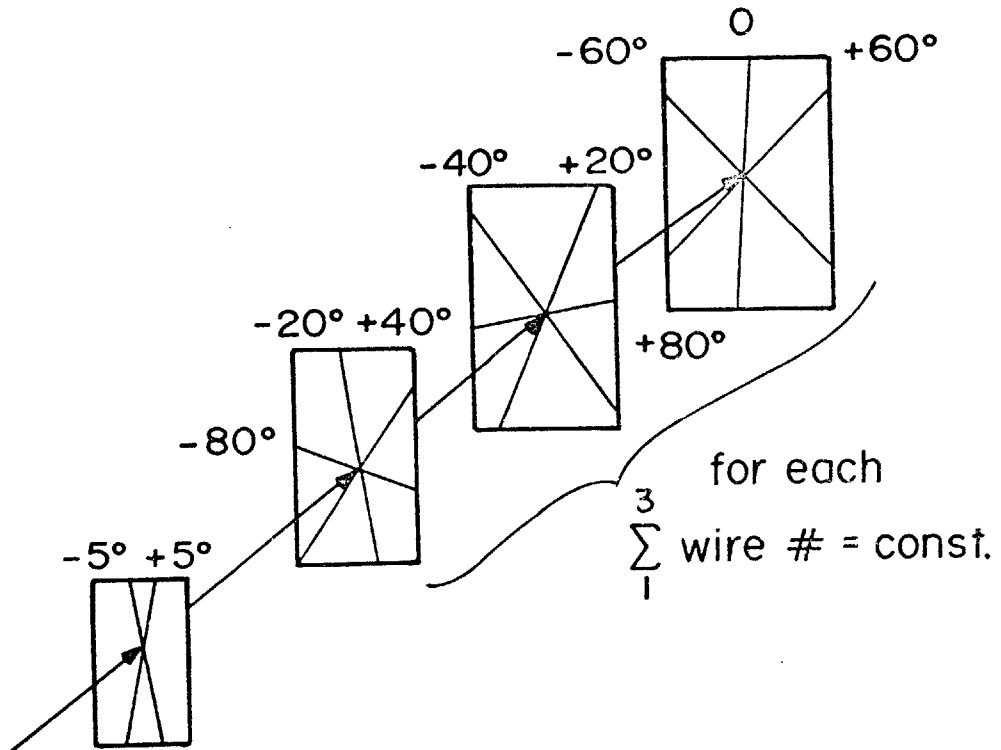


Fig. 10 Relative orientation of the planes of wires in the proportional chambers.

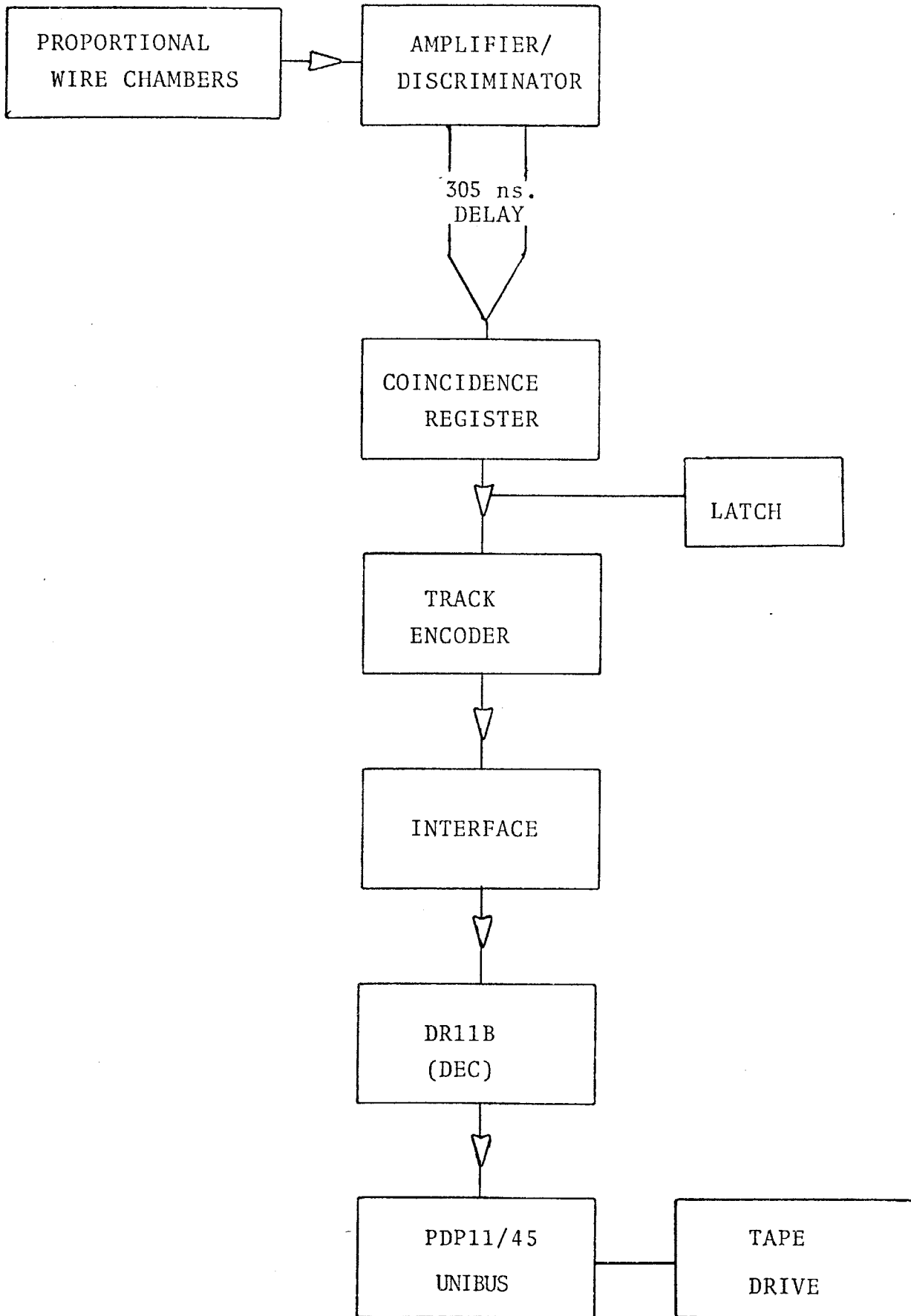


Fig. 11a WIRE CHAMBER READOUT

SHIELDING

The shielding requirements for the experiment were immense since beam intensities of 10^{12} protons/pulse were used. The shielding is used primarily to stop neutrons. Generally neutrons interacting strongly reach a maximum hadronic cascade at roughly 6 interaction lengths long and 3 wide¹. Consequently 12' of concrete (10" collision length) shielding was around the target area and 6' of concrete was around the spectrometer beyond M2 magnet to protect the experimental area.

To shield the spectrometer arms from gamma rays and neutrons, the hodoscopes and chambers were positioned such that they did not see the target directly through the opening of the magnets. Also a large lead brick and uranium collimator was constructed around MØ magnet and CB counters to stop charged secondaries and γ rays. To stop soft neutrons, bags of Borax (rich in Boron content) were placed between M1 and M2 magnets and around CE counters.

1. J. Engler et al., Nucl. Inst. and Met. 106, 189 (1972).

TARGET

The targets were either flat 1" metal strips in quantities of one to nine pieces. The choice of targets included Be, Cu, Ni, Pb, etc.

The flat strip targets provided a large surface for the incident beam to strike, which is important for absolute cross section measurements since no part of the beam should miss the target.

The choice of the number of targets had different merits. The single target piece has the advantage of producing experimental data that can be analyzed with simpler acceptance calculations with a single target center. The many-piece target has the advantage of producing a cleaner reaction. For a given total target thickness, if the target is divided into smaller sections, spread out along the beam axis, there is less chance of a secondary scattering, multiple scattering and bremsstrahlung in the case of electrons.

Normally, Be targets were used because the small fermi motion of the nucleons produced better defined kinematics. However, Ni targets were used on one occasion because of its high fermi motion in an attempt to produce a reaction with higher CM energy. The Pb and Cu targets were used on electron calibration runs to maximize the production of pairs by Bethe-Heitler production of γ 's from π_0 decay.

The targets were mounted on an adjustable tray that was

was surveyed into position. The tray held cross marked scintillator flags. These flags were monitored by a T.V. camera. The entire tray and its supporting table were inside a Helium bag to reduce multiple scattering of particles entering the spectrometer. The He gas protection of secondary particles entering the spectrometer was extended by a handmade 4 mm polyethylene bag to the first window of CO counters. Down stream of the box followed an aluminum beam pipe filled with He that continued to the beam dump behind the spectrometer. This was to reduce background due to further proton interactions.

BEAM CHARACTERISTICS

The beam was a slow extracted 28.5 GeV proton beam with a spill length ~.7 sec and a repetition rate of 2.4 seconds. The beam line, 96" above the AGS floor, used four upstream quadrupoles to focus the beam into a spot size $3 \times 6 \text{ mm}^2$. The last quadrupole focused in the vertical plane to accurately position the beam vertically which is necessary for correct track reconstruction. The beam intensities were variable from 10^{10} - 2×10^{12} protons/pulse. Fig.^{11b} shows the target area.

BEAM POSITION MONITORS

The beam was monitored in several ways. The most important method used the T.V. camera to view the scintillator flags. The targets were also monitored by 5 small spectrometers of 3 telescope counters each viewing the target at 75°. The secondary rate of the center piece target was checked by the middle monitor spectrometer. The spill rate was checked by a small scintillation counter, in the target area, whose output was integrated and displayed on a sweep triggered by the beam gate to give a profile of the beam spill. This spill monitor allowed measurement of the beam spill length and partial identification of beam problems. Large spills indicated that the beam was hitting the beam pipe wall. Jagged spills indicated uneven extraction.

BEAM INTENSITY MONITOR

The beam intensity was determined by a Secondary Emission Monitor whose integrated output accumulated on a scaler. Generally one count of the scaler corresponded to 10^9 protons. The AGS beam diagnostics group initially calibrated the S.E.M. in the proton synchrotron against current transformers. Later during actual runs, aluminum and polyethylene foils were placed in the beam. Using known cross sections and half lives for C^{11} ($\sigma = 2.5 \times 10^{-26} \text{ cm}^2$ and $\tau_{1/2} = 20.5 \text{ min.}$) produced by 28.5 GeV protons incident on polyethylene and Na^{24} ($\sigma = 8.0 \times 10^{-27} \text{ cm}^2$ and $\tau_{1/2} = 15 \text{ hrs.}$) produced in reactions using aluminum targets, the number of incident protons could be determined. However, this measurement was sensitive to beam conditions and caused a 5% fluctuation between different measurements.

TRIGGER ELECTRONICS

A block diagram of the trigger electronics is shown in fig. 12. All discriminators, except for CB's, were set at 30 mV threshold with output widths of 10 ns. The CB counters which had high rates were set at 3 ns output widths with 200 mhz discriminators (all others used 100 mhz units).

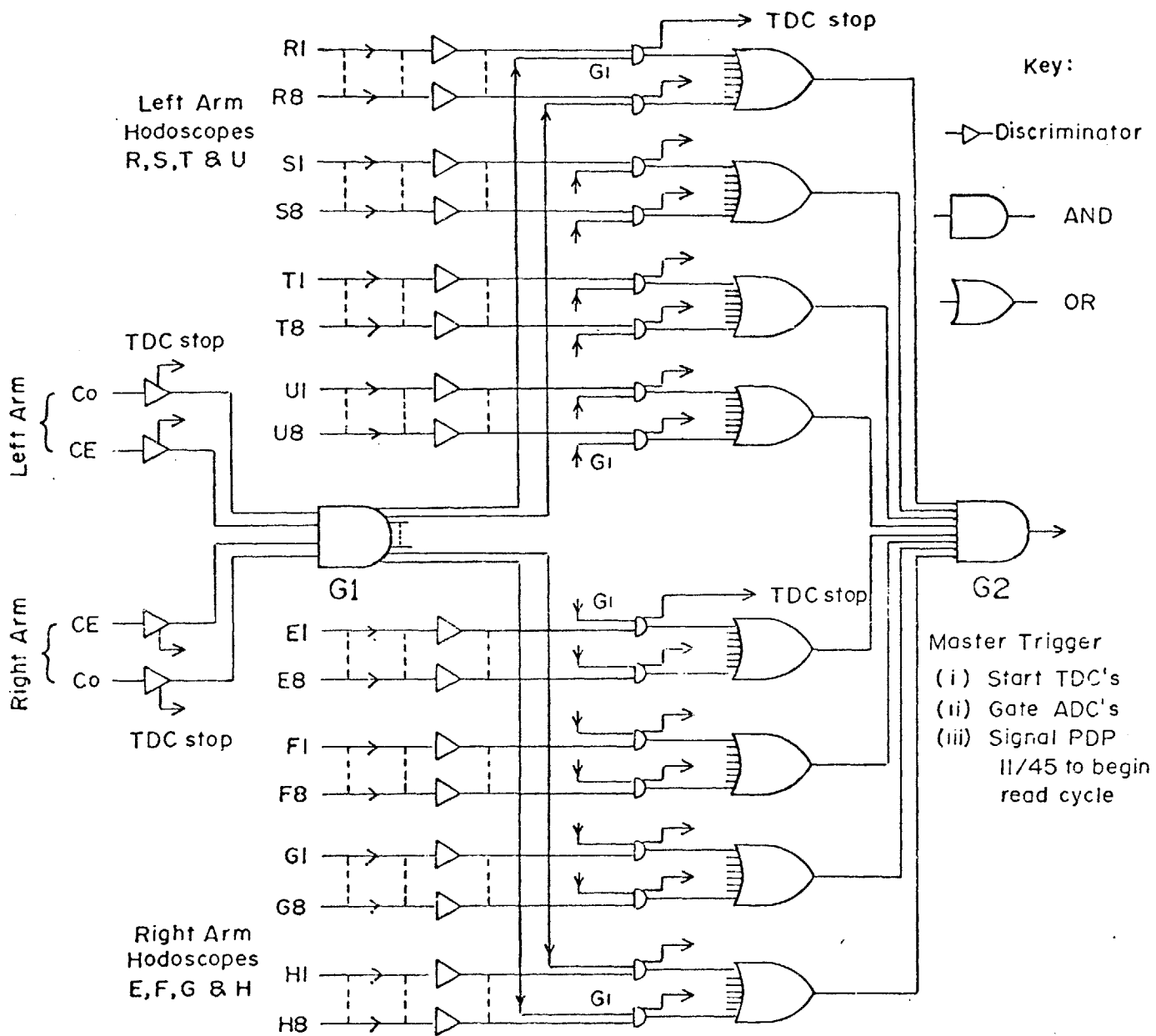
The first gate, G1, was a coincidence of four Cerenkov counters and strobed all the hodoscope discriminators with a 50 ns gate. The G1 rate was 1 khz.

The master trigger G2 was a coincidence of all eight hodoscope planes for the hadron pair experiment

$$G2 = (\Sigma E) (\Sigma F) (\Sigma G) (\Sigma H) (\Sigma R) (\Sigma S) (\Sigma T) (\Sigma U) A Z$$

G2 started the data collection, opened the 60 ns gate on the ADC units and provided the start pulses for the TDC units. In addition G2 initiated a 1 ms. veto over itself to stop triggers during data collection and transfer to the computer.

To provide a dead timeless trigger, that is monitored on a scaler, for an absolute count of the real trigger rate, a separate trigger, G3, was formed with the identical electronics and wiring as G2 except without a veto.



BLOCK DIAGRAM OF THE ELECTRONICS

Fig. 12

DATA ACQUISITION SYSTEM

The data acquisition system was controlled by a software program on a PDP11/45 computer. The block diagram of the system is shown in fig. 13. Starting with G2, an interrupt is sent through the DR11B interface to the computer to start the PDP11 and CAMAC read sequence. When this reading is completed the wire numbers are read in and finally the veto is cleared and the system is ready for another interrupt. Four to five events were accumulated in the memory and then written on one tape record in 16 bit words on an IBM 7-track tape drive.

The event data is listed in fig.14 . The 3 word buffer prefix contains the number of events and number of 16 bit words in the entire record. The 25 PDP11 words contain the numbers of CAMAC words and wire number words, data, time and run number. The 180 CAMAC words contain timing and charge data. The TDC (time to digital converter) CAMAC units had 512 channels at 0.2 ns per channel. Generally the first 200 channels were found to be linear and consequently the average timing signal was centered about channel 80. The ADC (analogue to digital converter) CAMAC units had 256 channels at 1.0 picocoulombs per channel. The phototube outputs of the lead glass and shower counters were fed into adjustable attenuators which scaled the EQ and hence the ADC spectrum.

To provide additional checks on counters, their discriminator outputs were fed into CAMAC scalers and dumped onto tape and then reset every 10 beam spills. Fig. 15 lists a typical dump.

SOFTWARE

HARDWARE

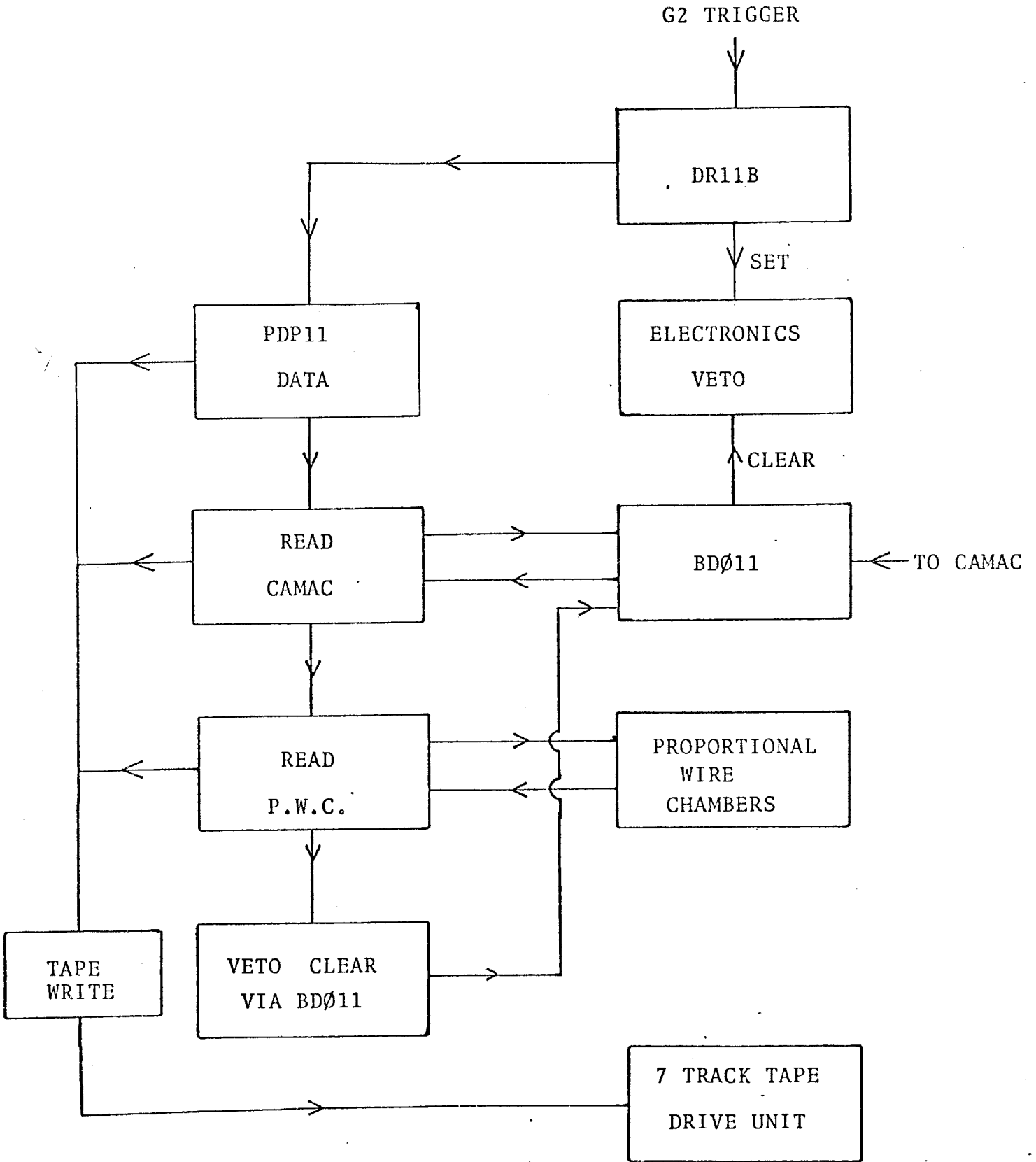


Fig.13 DATA ACQUISITION SYSTEM

TDC	D1	0	D5	0	Q1	0	Q5	0	A1	0	AE1	16	MT0	13		
	D2	0	D6	0	Q2	0	Q6	0	A2	0	AE2	17	MT1	14		
	D3	0	D7	0	Q3	0	Q7	98	Z1	98	AK1	21	MT2	14		
	D4	0	D8	0	Q4	0	Q8	0	Z2	130	AK2	16	MT3	14		
TDC	E1	0	F2	0	G3	0	H4	0	R5	0	S6	0	T7	81	U8	0
	E2	0	F3	0	G4	0	H5	0	R6	0	S7	0	T8	0	CK1	0
	E3	0	F4	0	G5	0	H6	0	R7	91	S8	0	U1	0	CK2	118
	E4	0	F5	0	G6	0	H7	0	R8	0	T1	0	U2	0	CE1	0
	E5	0	F6	0	G7	0	H8	0	S1	0	T2	0	U3	80	CE2	107
	E6	0	F7	0	G8	0	R1	0	S2	0	T3	0	U4	0		
	E7	0	F8	0	H1	0	R2	0	S3	90	T4	0	U5	0		
	E8	0	G1	0	H2	0	R3	0	S4	0	T5	0	U6	0		
	F1	0	G2	0	H3	0	R4	0	S5	0	T6	0	U7	0		
ADC	I1	14	I5	22	I9	12	J1	45	J5	8	J9	7	J13	5	V4	5
	I2	13	I6	21	I10	53	J2	52	J6	16	J10	15	V1	3	V5	0
	I3	10	I7	20	I11	23	J3	10	J7	14	J11	16	V2	3	V6	5
	I4	21	I8	13	I12	23	J4	8	J8	18	J12	11	V3	0	V7	0
ODC	V12	18	V9	20	W3	6	W4	15	W10	7	W7	18		11		12
	V8	13	W2	21	V11	18	W9	11	W6	15		12	W13	14		9
	W1	17	V10	17	W8	17	W5	16	W11	10	W12	10		13		11
ODC	K5	0	K7	0	K12	0	K14	0	X5	0	X7	0	X12	2	X14	0
	K1	0	K3	0	K8	0	K10	0	X1	94	X3	0	X8	233	X10	4
	K6	0		0	K13	0		0	X6	0		0	X13	0		0
	K2	0	K4	0	K9	0	K11	0	X2	3	X4	0	X9	30	X11	2
TDC	C01	0	N1	0	N3	0	N5	0	CBL1	517	CBL3	516				
	C02	0	N2	0	N4	0	N6	0	CBL2	517	CBL4	517				
SCAL	G1	8251553	G2	16196	G3	27496	IONCH	27967	SEMA1	3169	MC	2699				

FIG. 14 CAMAC READOUT DUMP

CBR1	0	C02	3089433	T	1024188	RC02X	12082	RCE2X	17199	CBL4	0
CBR2	0	CE2	1133018	U	14197389	RCE2	181163	CBL1	0	C01	13799212
CBR3	0	R	12039647	R10	3283834	RD	19431	CBL2	0	CE1	791827
CBR4	0	S	2380808	RC02	111799	RE	12178	CBL3	0	E	15438168
SCAL											
F	8313179	L10	5916876	LCE1	153711	LCE1K	20841	LC01KD	1379	REX	4095
G	6980477	LC01	198813	LD	40897	LC01D	140532	LCE1D	2349		
H	2684624	LC01K	37475	LE	10088	LEK	2093	LCE1KD	907		
SCAL											
RC02D	87750	LK	1457547	RE	148	G1	6805	GCBL2	0	GCBL4	0
RCE2D	2082	LKD	27176	RED	103	G2	4833	GCBR2	0	GCBR4	0
RC02XD	313	RX	261103	LEKD	60	GCBL1	0	GCBL3	0		0
RCE2XD	418	RXD	6504	REXD	39	GCBR1	0	GCBR3	0		0
SCAL											
E1	3577654	F4	2011440	G7	2784584	R2	5599171	S5	3043116	T8	2087829
E2	3697460	F5	3816210	G8	2505284	R3	3936981	S6	3657953	U1	437518
E3	3018058	F6	4310812	H1	2192699	R4	3139682	S7	3942172	U2	867746
E4	3745488	F7	5328479	H2	1611556	R5	3215284	S8	4938009	U3	899827
E5	3825911	F8	5644148	H3	1605512	R6	3583127	T1	2492773	U4	1019938
E6	3396769	G1	2634800	H4	1596956	R7	2837326	T2	3621320	U5	2566571
E7	10967478	G2	2783831	H5	3057916	R8	5202794	T3	2059491	U6	2925057
E8	2965881	G3	3355893	H6	3027104	S1	1126459	T4	2324378	U7	2888230
F1	2383453	G4	6067115	H7	3472333	S2	1189714	T5	1919299	U8	3480172
F2	1951180	G5	2430692	H8	4116879	S3	1558940	T6	2496943		
F3	1954475	G6	2796491	R1	4153574	S4	1436798	T7	2031268		
SCAL											
K1	1307937	K6	899760	K11	687684	X2	129612	X7	380790	X12	547124
K2	898035	K7	675881	K12	258711	X3	376222	X8	302310	X13	277857
K3	2185916	K8	2191878	K13	765233	X4	717557	X9	1092919	X14	578756
K4	1050844	K9	1095002	K14	758097	X5	57167	X10	613108		
K5	2081973	K10	1076395	X1	207147	X6	243690	X11	127464		

FIG. 15 SCALER READOUT

ON-LINE ANALYSIS

The on-line analysis with the PDP11 computer consisted of histogramming CAMAC and wire chamber numbers as well as simple differences, efficiencies and 3 or 4 fold coincidences (fig. 16). The histogramming program sampled events when the computer was not processing data. Consequently at lower rates the histogramming was more efficient. The histograms could be produced on a linear or log scale. The wire chamber histograms had a special histogram program to produce fine lines to display compactly the number of counts of each wire (fig. 17). Accumulated histograms were stored on disk and constantly updated.

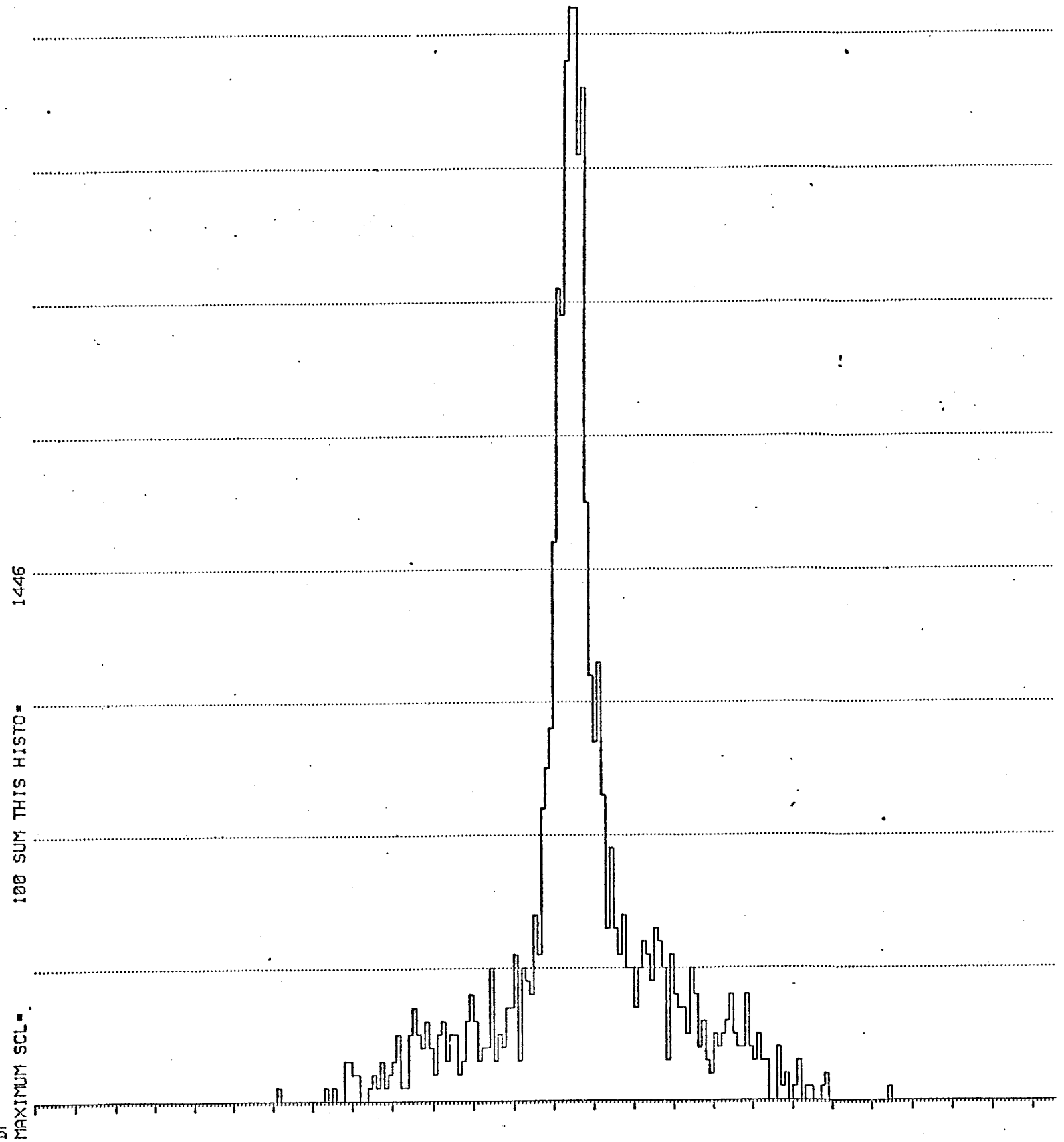
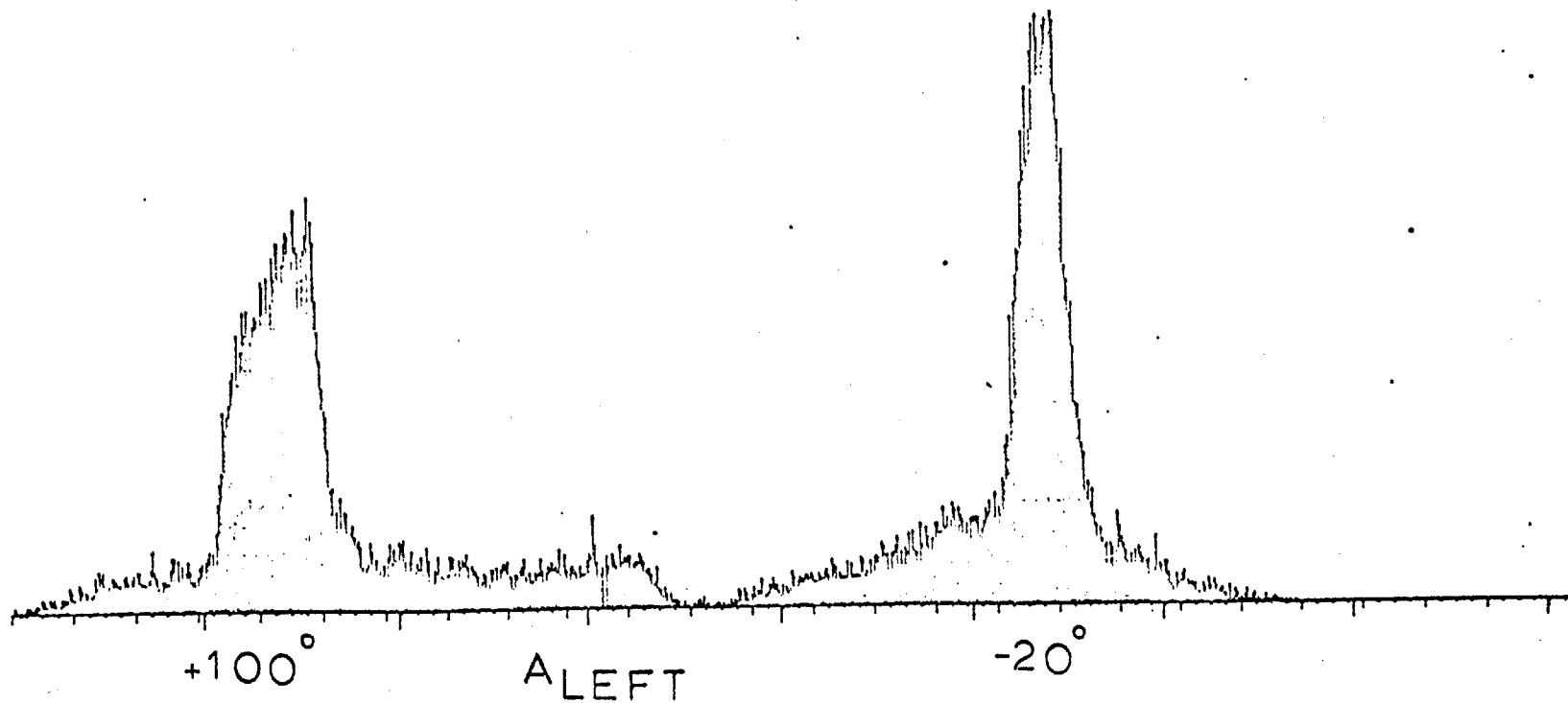


Fig. 16 Timing difference between EFGH and RSTU hodoscopes taken from an on-line computer printout. Each horizontal unit is 0.2 nanoseconds.

Fig. 17 Histogram of two from the three planes of the left A-Chamber. Taken during a high intensity run to check the efficiency. For this a $5 \times 10 \text{ cm}^2$ trigger counter was incorporated into the trigger. The peaks are projections thereof.



EXPERIMENTAL MODIFICATIONS

The entire layout of the modified spectrometer is shown in fig. 18 & 19. For hadron pairs, the spectrometer was modified by installing a new target system, new Cerenkov counters, a pair of scintillation counters near the end of the spectrometer arms, and a set of scintillation counters at the forward opening of M2.

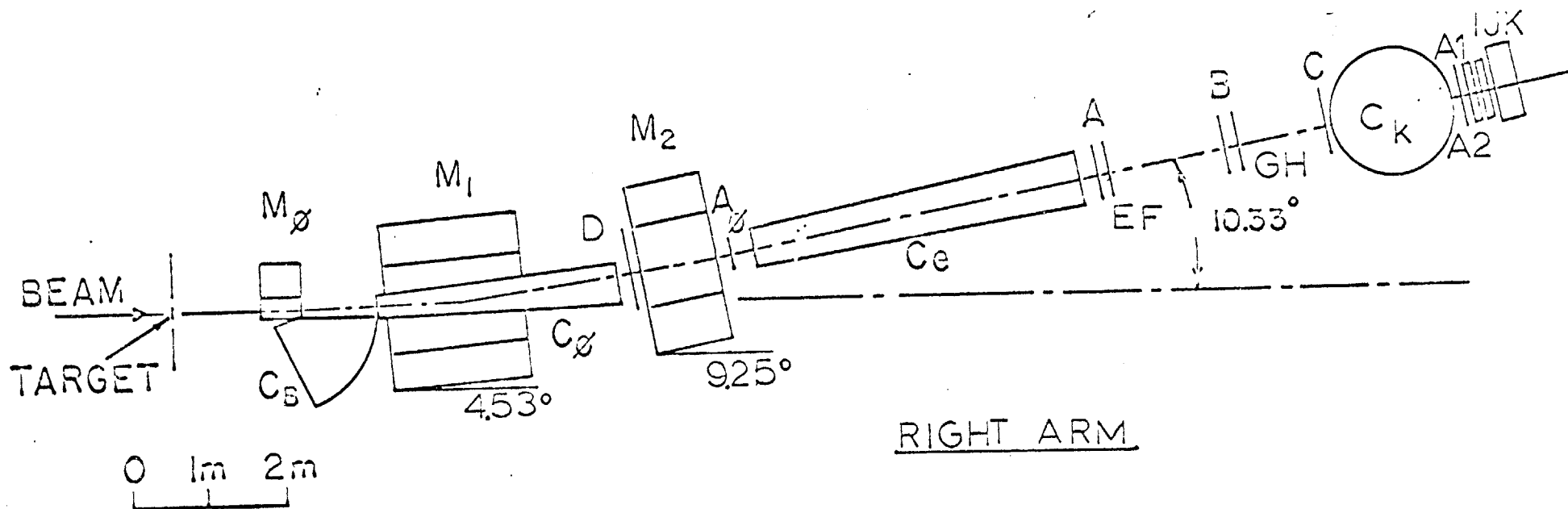
The new target system consisted of five $(.4 \text{ cm})^3$ Be cubes held by thin piano wire. By constraining the vertex to ± 2 mm on the beam axis this matches the accuracy of the wire chambers and yields improved momentum resolution. When searching for long lived particles this enhances the signal relative to the background. Additionally, this reduced the accidental background which was anticipated to be much higher. Occasionally Al_2O_3 target cubes, which fluoresce under proton bombardment, were used to check the beam position.

To identify the protons, kaons and pions, CE was filled with isobutane to be efficient on π 's and a new gas threshold counter CK, filled with ethylene of 6-22 atm. detects kaons and pions to provide adjustable large index of refraction so the threshold of kaon detection can be adjusted for different magnet settings. Before installation, the CK's were tested in the AGS test beam in a similar

manner as CE and CØ.

To provide a new G1 trigger that included protons, large scintillators, "A" and "Z", 23" x 36" x 1/4" thick, were installed near the end of the spectrometer arms. Each had phototubes, at the top and bottom, connected to a mean timer to improve the timing resolution.

Finally, D and Q counters (a set of eight 1.6 mm thick vertical strip scintillators) were added in the right and left arm between CØ and M2 magnet to reduce the trigger rate by requiring additional coincidences further upstream of the spectrometer arm.



SIDE VIEW OF THE SPECTROMETER

- M_0, M_1, M_2 - dipole magnets
- A_0, A, B, C -4400 proportional wire chambers
- EF, GH - 8x8 hodoscopes
- IJK - 3 banks of Pb-glass Shower counters
- D - 8 vertical strip hodoscopes
- A_1, A_2 - counter (2 phototubes)
- C_B, C_e, C_K -gas Cerenkov threshold counters

Fig. 18

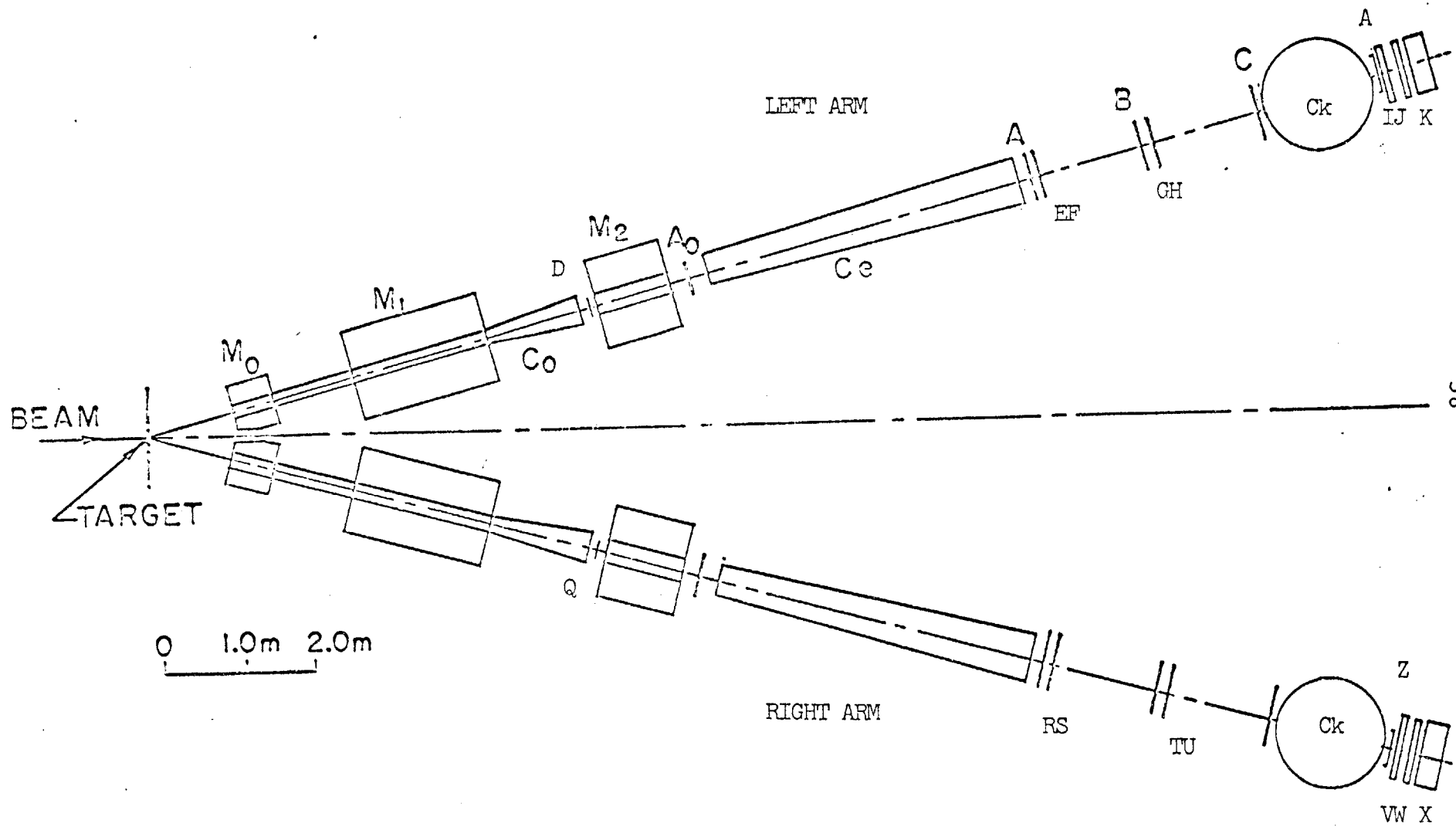


Fig. 19

SPECTROMETER CHECKS

Before an actual data taking run, at least a full week is spent systematically checking and calibrating all components of the spectrometer. In this section we describe the methods applied on all parts of the spectrometer.

All 64 hodoscopes were checked for efficiencies. One plane of eight hodoscopes were plateaued at a time. From fig. 3 we describe how the E counters were plateaued. The others follow analogously. Using a moderate beam intensity of 10^{11} protons/pulse we trigger with (Σ).F8.H8. This restricts the geometry to the end of the counter opposite to the phototubes. The total triggers and counts from all E hodoscopes are collected by the PDP11 which computes the efficiencies. This is done at normal voltages (determined from test beam measurements) and at +50, -100 and -200 volts relative to normal to check the correct position of the knee.

To plateau the Cerenkov counters a small test counter with a scintillator roughly 1"x2" was placed directly behind the center of the EF hodoscopes. This was to plateau on central rays in the Cerenkov counter. Using a trigger of EFGH.test.C01, the CE1 efficiency (CE1 counts/triggers) was measured at normal, -400, -500, -700 and -800 volts. The normal voltage setting of the Cerenkov counter was roughly 500 volts above the knee.* This method was applied in like

*Since pions emit in isobutane more light than electrons in hydrogen.

manner to CK and CØ.

Next the timing of the hodoscopes and Cerenkov counters were checked. Before the actual run the trigger electronics is thoroughly checked with a pulser such that all the discriminator outputs are in time. Consequently, the only necessary changes in timing are made by adding or removing cable to the line between the discriminator input and phototube output. All the timing is checked by using known reference values of the TDC units. If an e^+e^- pair, for example, fires all the counters, the signal from the counters arrive all at the same time at the discriminator outputs. The TDC units cross check this and the stability.

The two arms are timed in using CE1 or CE2 versus a small test counter. The test counter is placed behind CE1 and used as a start for the TDC. The TDC channel is compared to the TDC channel of CE2 when the same test counter is physically moved into an identical position in the other spectrometer arm. Due to the RCA 31000M tubes, these counters have excellent timing as seen in fig.24a. Appropriate cable is added or removed so the signals arrive at the same TDC channel. Now CE1 and CE2 are in time and can be compared to other counters in the corresponding arm. Next the entire right arm is aligned by using CE1 discriminator output as the TDC start for all the TDC units of the right arm. Appropriate cable is then added or subtracted so that all the signals

appear in the same TDC channel. Finally CE1 and CE2 each are aligned relative to themselves so their own stop signal will arrive in the same TDC channel as the others. Hence, all the signals are in time.

The proportional wire chambers were initially voltage plateaued with a test counter in five positions: in the four corners and the center. The trigger consisted of the test counter and the particular hodoscope segments that cover the test counter scintillator. The test counter was placed behind "C" chamber and all planes of the wire chambers of that arm were plateaued at one time for each test counter position (fig. 20). The timing of the wire chamber signals was checked by delay curves. A single arm trigger was used to gate out all coincidence registers (see PROPORTIONAL WIRE CHAMBERS) and systematically delayed, while the efficiency (chamber counts/triggers) was recorded by the PDP11. Plotting this efficiency as a function of delay, the final amount of delay used was checked to fall in the center of the plot between the steep early and late edges of the plot.

The lead-glass and shower counters, although not used in this run, were used in the next electron/hadrons runs and will be described here. To calibrate the counter on electrons, an electron trigger (CØ.CE1) was used and the ADC histogram was produced by the PDP11 (fig. 21). Extrapolating by eye where the low end of the electron shower ends, the number of

events within the shower are counted and the ratio of this number to the total triggers is plotted as a function of voltage (fig. 22). Setting the final voltage 100 volts above the knee, the attenuators, that reduce the signal voltage from the phototubes that are fed into the ADC units, are adjusted so the peak of the shower falls in the center channel 150.

AUG 23 1974
~ 3PM - X 11

RUN 44
CHAMBER CL
SET: low P
TARGET: 9 x Be.
PULSE: 4 x 10¹¹
EVENTS: 1000
G2 RATE: 10/PULSE
TRIG: G=DX
G2=RSITIU-TEST

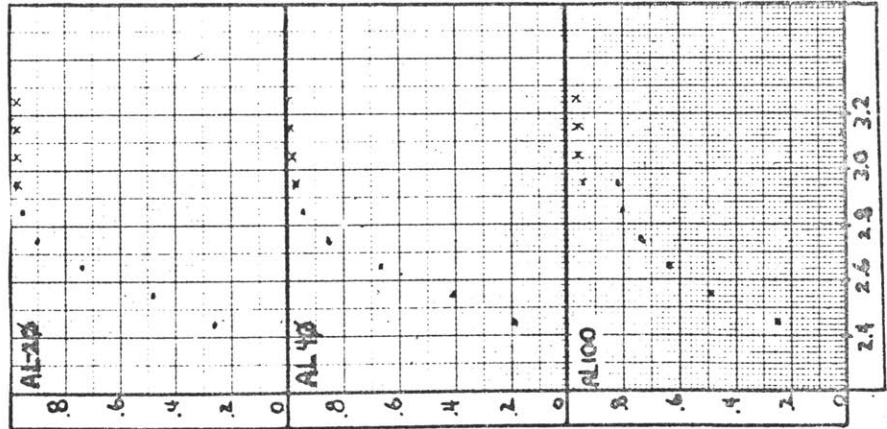
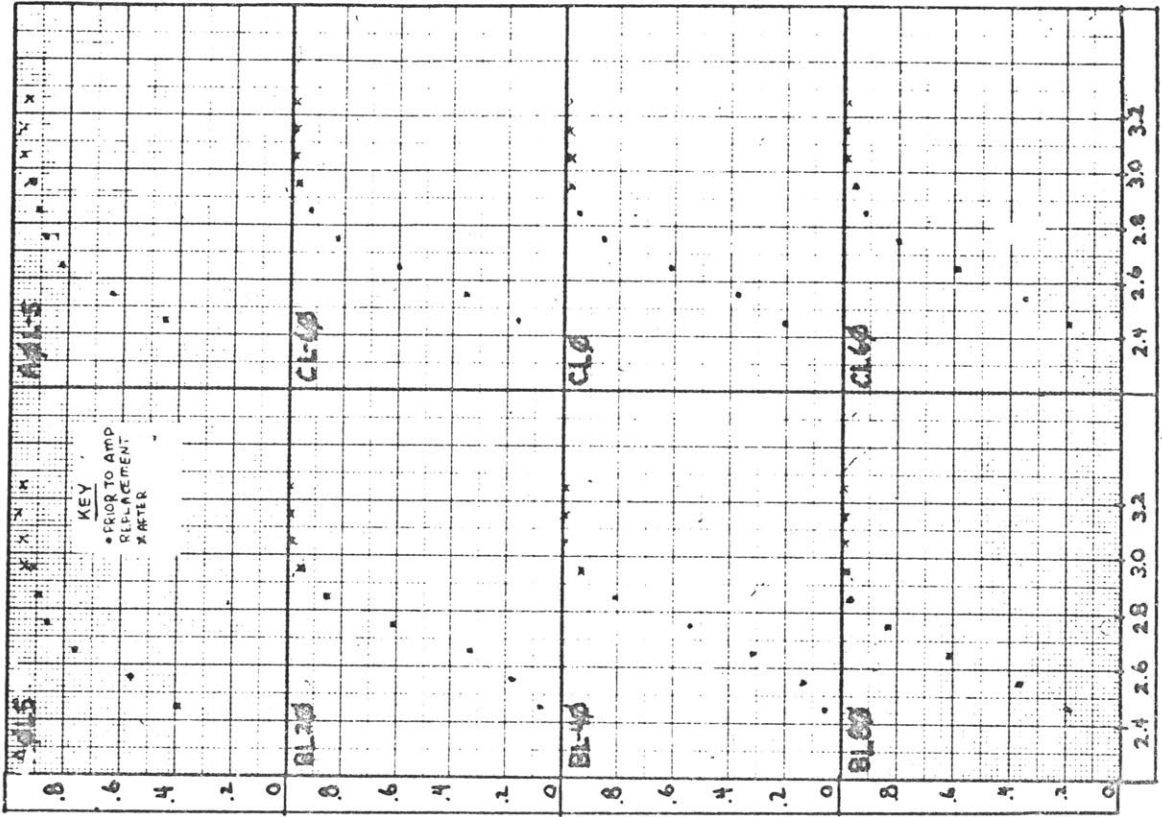
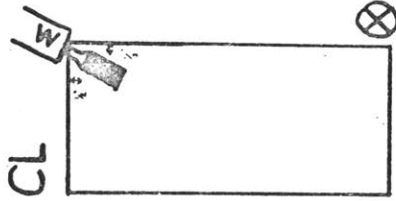


Fig. 20 Efficiency of all the wire planes as a function of the applied voltage. The position where this measurement was made is indicated by the sketch in the top left hand corner. These are graphs taken directly from the log book.

Pulse Height Spectrum In Shower Counter

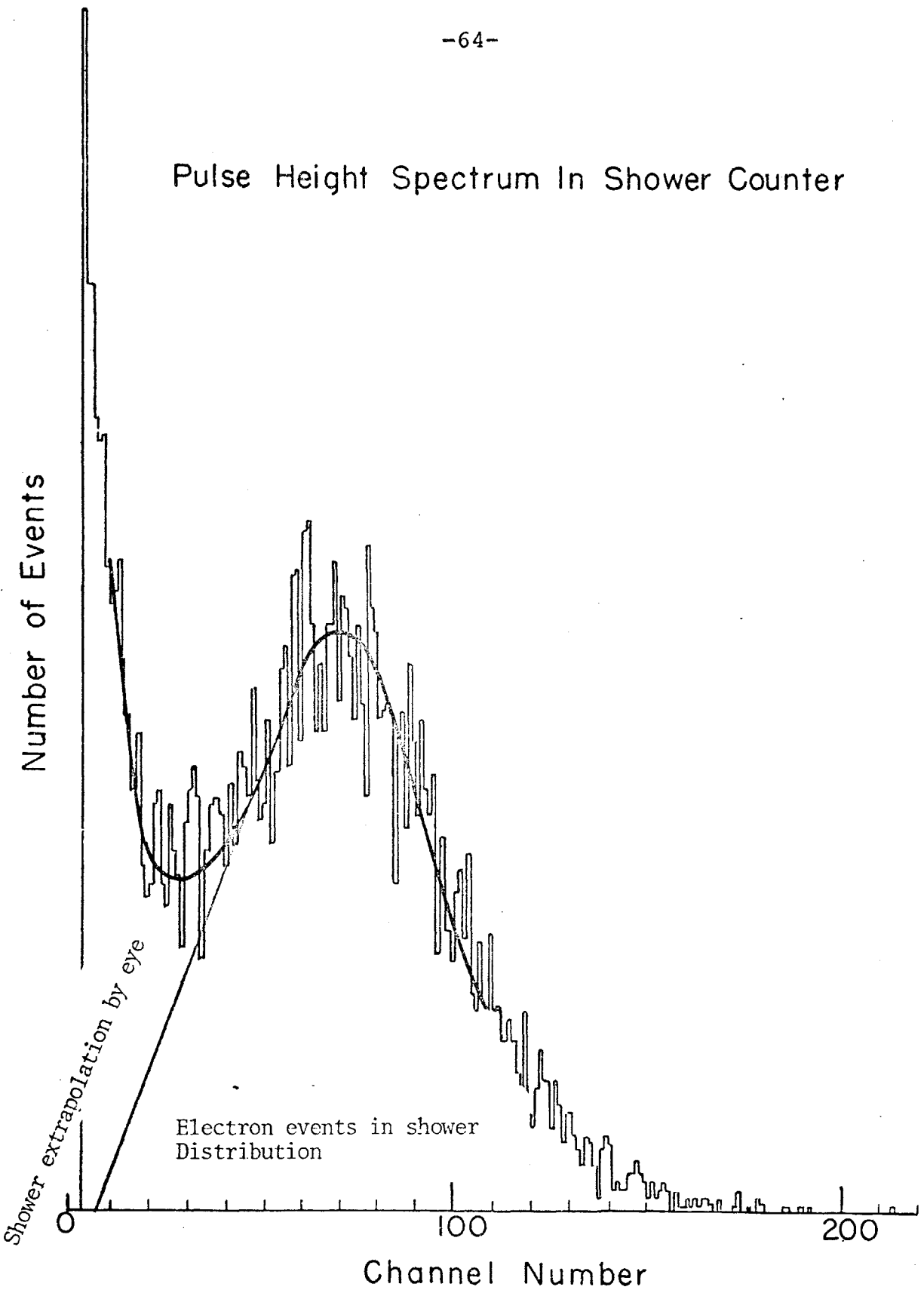


Fig. 21 A typical pulse height spectrum for electrons in one of the shower counters. The electron peak is clearly visible.

HIGH VOLTAGE PLATEAU of LEAD GLASS COUNTER

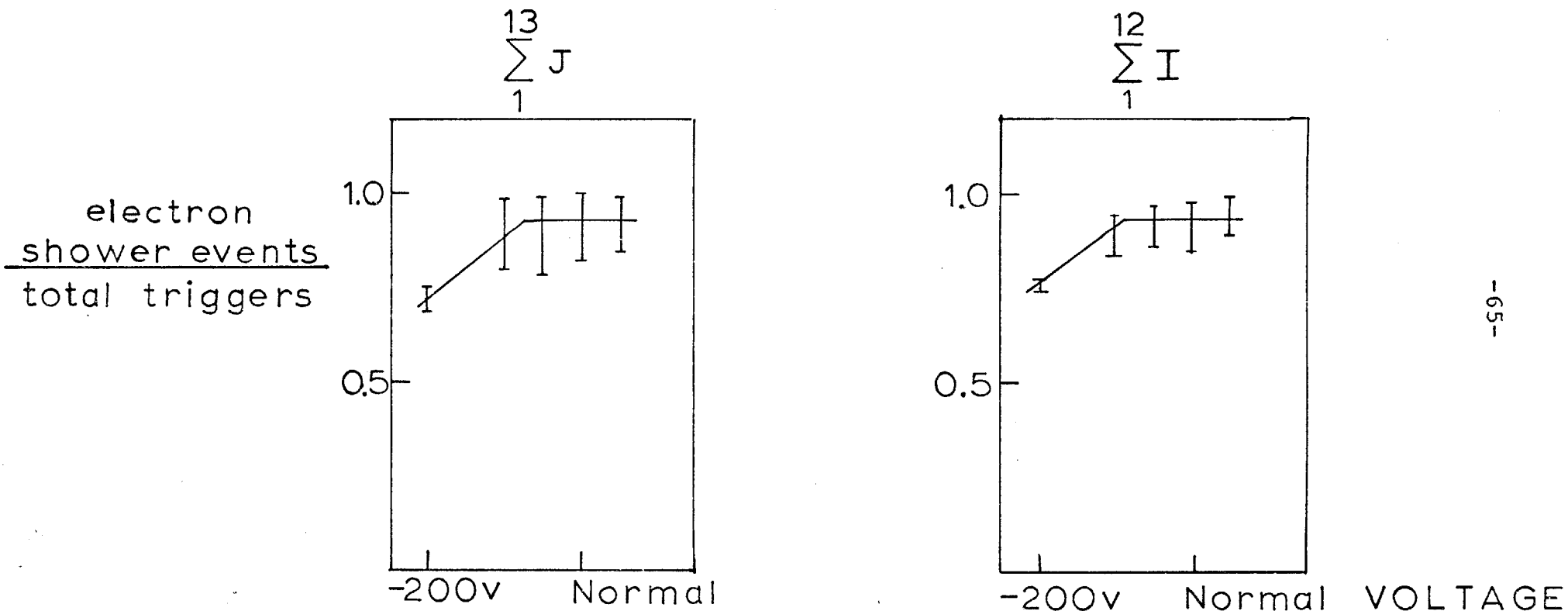


Fig. 22 ratio of electron shower events to total triggers as function of high voltage. The graph on the left is the sum of all J lead Glass counters and the right is of the I lead Glass counters. Every bar gives the systematic difference between a reasonable and no background subtraction.

DATA TAKING

Data was taken in runs filling a tape. For every run a data information (fig. 23) was filled noting Cerenkov counter pressures, magnet settings and polarities, beam energy and conditions, etc.

To check all detectors, scaler rates were taken every 15-30 minute intervals and the PDP11 was used to produce their histograms from the CAMAC readout. The beam was monitored with the spill monitor and the T.V. monitor. Several important ratios were plotted to check long-term stability. As a check of both, beam and detector, the ratio of events/Secondary Emission Monitor was plotted and checked to be constant, as well as the counter rate between the left and right arm, to safeguard against beam asymmetries. Also the ratio of the telescope counters viewing the target over the SEM counts was used to check that the beam was properly steered onto the target.

Additional checks performed every 30 minutes include checking high voltages of all counters, Cerenkov gas pressures, magnet currents, argon flow rates to the wire chambers and the methylal consumption rate of the chambers.

Data for the h^+h^- runs were taken in February 1975 in five overlapping mass regions. Tables 3&4 lists the name of the magnet settings, the momentum range and the Cerenkov counter

thresholds for π , K and P. Intensities between 10^{10} and 10^{11} protons/pulse were used on $3xBe$, $5xBe$ and $3xAl_2O_3$ targets.* Generally the loss of events from electronics and data collection dead time was 10-20%.

There were three main triggers; for all h^-h^+ pairs,

$$G2 = (\Sigma D) (\Sigma Q) (EFGH) (RSTU) \cdot A \cdot Z$$

for h^-h^+ pairs except π^-p , with right arm positive polarity,

$$G2 = (\Sigma D) (\Sigma Q) (EFGH) (RSTU) (CK1 CE2) \cdot A \cdot Z$$

and for h^-h^+ pairs except π^-p and $\pi^-\pi^+$, again with right arm positive,

$$G2 = (\Sigma D) (\Sigma Q) (EFGH) (RSTU) (CE2 CK1) (CE1 CE2) \cdot A \cdot Z$$

The last two triggers were used to suppress the most abundant modes, π^-p and $\pi^-\pi^+$, to detect the other modes at faster rates. As will be reported later the data used for cross section calculations had only the all inclusive h^-h^+ trigger so the relative cross sections between different modes is uniformly measured.

*targets were 4 mm cubes, 6" apart.

TABLE 3 Hadron Pair Runs

-69-

Trigger	Magnet	#Tapes	#Trig's	#Inc. P	Target*
h^-h^+	Med-10	50	1.9 Meg	2.08×10^{15}	5xBe
h^-h^+	Low	37	1.44	5.45×10^{14}	3xBe
$h^-h^+(\pi^-p)$	Low-Med	20	.80	5.04×10^{14}	3xBe
$h^-h^+(\pi^-p, \pi\pi)$	Low-Med	52	2.04	2.62×10^{15}	3xBe
h^-h^+	Med-High	10	.391	8.77×10^{14}	3xBe
$h^-h^+(\pi^-p)$	Med-High	40	1.57	4.43×10^{15}	3xBe
$h^-h^+(\pi^-p)$	Med P	32	1.24	2.14×10^{15}	3xBe
h^-h^+	80%Low P	259	11.5	4.11×10^{15}	3xAl ₂ O ₃
$h^-h^+(\pi^-p, \pi\pi)$	Med-10	100	3.17	1.35×10^{16}	3xAl ₂ O ₃
$h^-h^+(\pi^-p, \pi\pi)$	Med P	62	2.73	1.06×10^{16}	3xAl ₂ O ₃
h^-h^+	Med P	10	.394	4.59×10^{14}	3xAl ₂ O ₃

*5xBe= 3 pieces of 4mm Be target pieces 6" apart, 4% collision length

3xBe= 5 pieces of 4mm Be target pieces 6" apart, 6.7% collision length

3xAl₂O₃= 3 pieces of 4mm Al₂O₃ target pieces 6" apart, 6.9% collision length

TABLE 4 Cerenkov Counter Gas Pressure Setting and Momentum Thresholds

Mag. Set.	P range	CE Press.	Gas	$n(n-1)$	P_{π}	CK Press.	Gas	$n(n-1)$	P_k	P_p
Low P	3.0-7.0	1.0 atm.	Isobutane	1.37×10^{-3}	2.6 Gev	19.6 atm.	Ethylene	.0155 atm	2.8	5.3
Med P-10%	4.0-8.5	"	"	"	"	11.1	"	.0081	3.9	7.4
Med P	4.5-10.0	"	"	"	"	9.0	"	.0065	4.3	8.2
Med-High	5.0-10.5	"	"	"	"	6.5	"	.0047	5.1	9.6

ANALYSIS

In this section, off-line track reconstruction is described. This analysis was carried out on the Laboratory for Nuclear Science IBM 360 computer and the Brookhaven CDC 7600 computer. It was completed early in the summer of 1975.

Track reconstruction began by finding the point positions where the charged particles passed through the wire chambers. For a genuine track through the chambers, the sum of the wires must be constant which allowed for a ± 2 mm tolerance in position. From these positions in the A and C chambers, straight tracks were defined and checked to have a corresponding point in B chamber within .4 inches. The momentum is determined by re-extrapolating this track to the target. An iteration by Newton's interpolation is done starting with 50 GeV momentum in the first try and 1% less in the second to find its vertical projection from the beam axis. Forming a derivative of the momentum as a function of that vertical projection from the beam axis, the momentum is extrapolated to a value such that it has zero vertical projection from the beam axis. The process is iterated until the vertical projection deviates less than .02 inches from the actual beam height. This defines the momentum and the intersection of the track with the beam axis which we refer to as the target

position. Fig.24b displays the average position of the reconstructed target position $(z_{\text{Left}} + z_{\text{Right}})/2$, where z_{Left} is the target position of the particle that went through the left arm and z_{Right} is for that of the right arm. Multiple scattering causes the spread in vertex positions and the absolute number in each target piece is different because of the difference in acceptance for each target piece. Having determined momentum and opening angle for each particle the invariant mass of the pair is reconstructed as,

$$\begin{aligned}
 M_{h^+h^-} &= (\{E_1+E_2\}^2 + \{P_1+P_2\}^2)^{1/2} \\
 &= m_1^2 + m_2^2 + 2\sqrt{P_1^2+m_1^2} \sqrt{P_2^2+m_2^2} - 2 P_1 P_2 \cos\theta_{12}
 \end{aligned}$$

The particles were identified by requiring the following combinations of counts from the cerenkov counters for each event,

	CE	CK
π	YES	YES
K	NO	YES
P	NO	NO

One limit to this identification was for kaons. High momentum protons will count in CK and lead to misidentification.

Consequently the kaons and protons require a momentum cut.

From a momentum distribution of events with CE not counting and CK counting the kaon and proton events are separated by eye (fig.25). This was serious in the K^+ events because of the high proton rates, whereas for K^- events, the contamination was small due to the rarity of anti-proton events. The first peak is due to kaons and the second is due to protons. The characteristic shape is due to a production mechanism that rapidly decreases at higher momentum and a spectrometer acceptance that increases with higher momentum.

To pick out the genuine pair signal the timing difference between counters in the left and right arm were used. Fig.24b shows the timing difference between CE1 and CE2 for $\pi^+\pi^-$ pairs. A cut is made around the peak for those intimate signals. The timing is very sharp, FWHM = 0.9ns, and the random accidentals quite small. The following table lists the combination of Cerenkov counters used for identification and the cuts applied to the data.

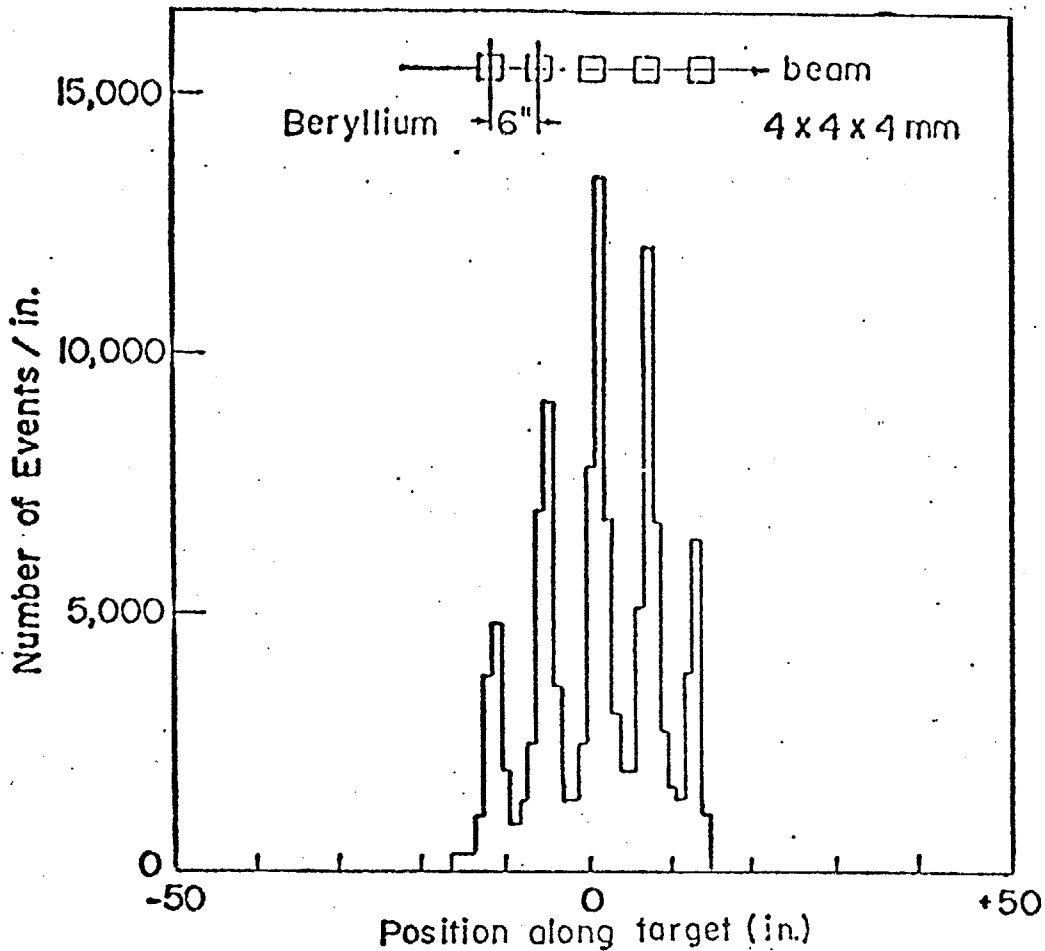


Fig. 24a. Reconstruction of the pair vertex at the target; using information from the proportional chambers. The five pieces of beryllium are seen clearly.

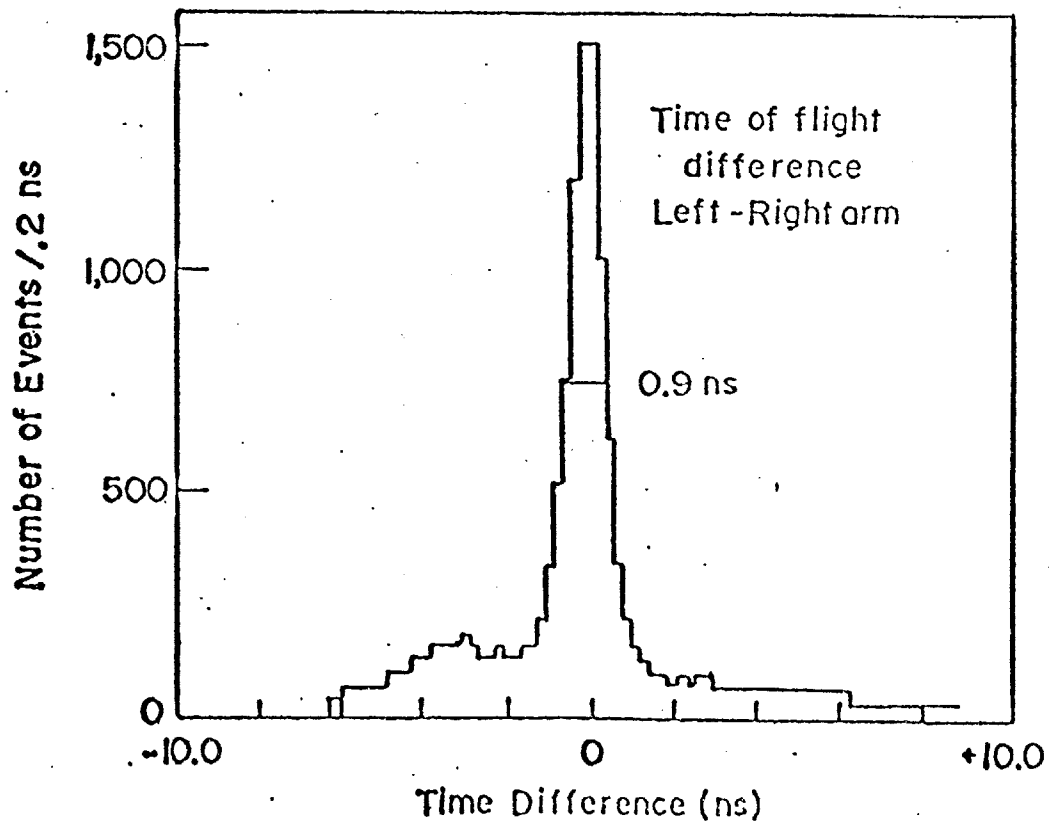


Fig. 24b. Time difference between additional scintillation counters in the left and right arms. The resolution obtained is 0.9 ns and little background is present.

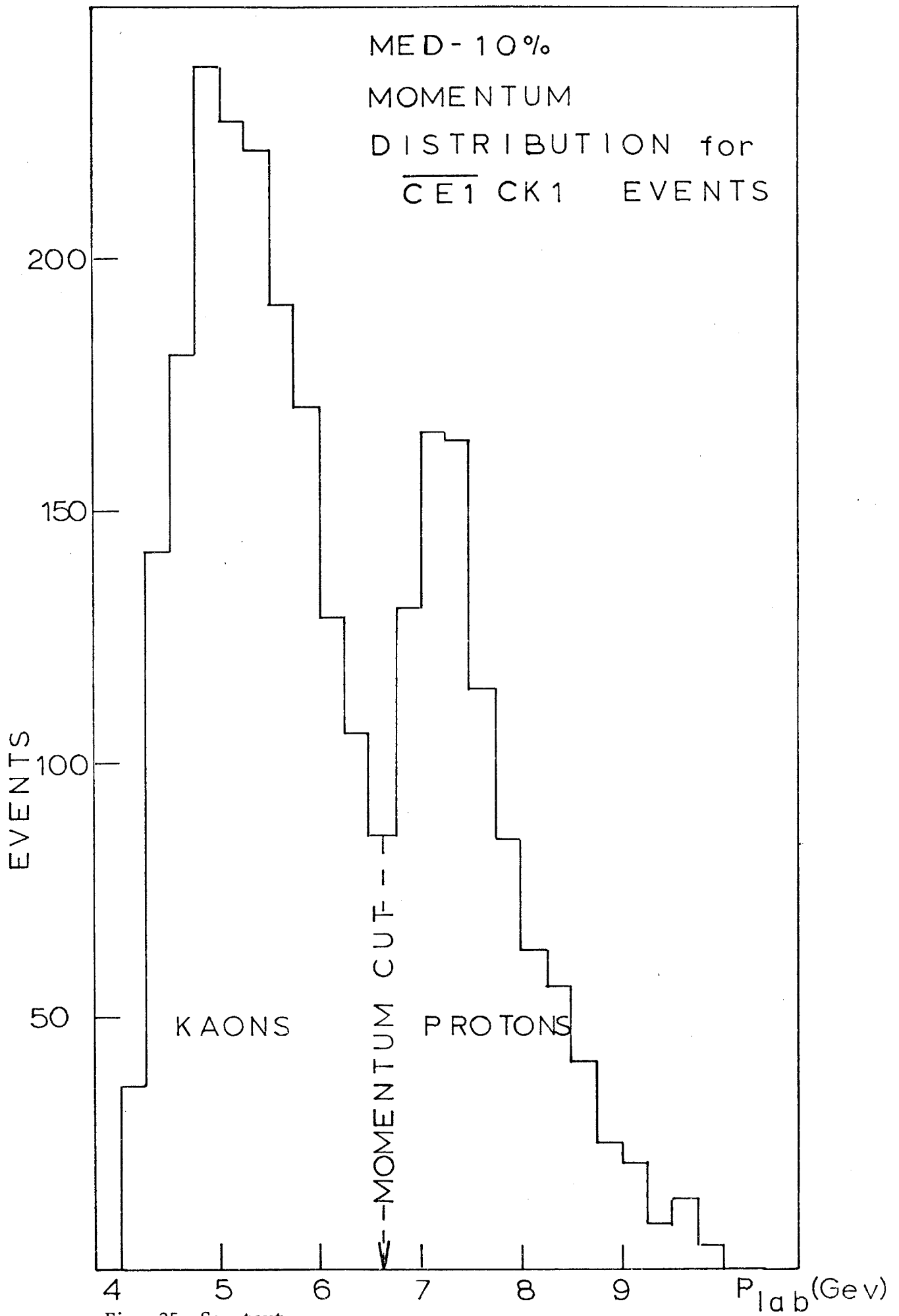


Fig. 25 See text.

TABLE 5 CUTS APPLIED TO h^-h^+ DATA

RIGHT ARM	LEFT ARM	CERENKOV CUT	TIMING CUT	TARGET CUT
π	π	CE1 CE2	$ CE1-CE2 < 1.5ns$	$ Z_{right} - Z_{left} < 4''$
π	K	CE1 $\overline{CE2}$ CK2	$ CK1-CK2 < 2.5$	"
π	P	CE1 $\overline{CE2}$ $\overline{CK2}$	$ A-Z < 4.5$	"
K	π	$\overline{CE1}$ CK1 CE2 CK2	$ CK1-CK2 < 2.5$	"
K	K	$\overline{CE1}$ CK1 $\overline{CE2}$ CK2	$ CK1-CK2 < 3.0$	"
K	P	$\overline{CE1}$ CK1 $\overline{CE2}$ $\overline{CK2}$	$ A-Z < 4.0$	"
P	π	$\overline{CE1}$ $\overline{CK1}$ CE2	$ A-Z < 5.5$	"
P	K	$\overline{CE1}$ $\overline{CK1}$ $\overline{CE2}$ CK2	$ A-Z < 4.0$	"
P	P	$\overline{CE1}$ $\overline{CK1}$ $\overline{CE2}$ $\overline{CK2}$	$ A-Z < 4.0$	"

TABLE 6 MOMENTUM CUTS APPLIED TO h^-h^+ DATA

MAGNET SETTING	P_p	P_K
80% Low P	0-4.5	2.25-4.5 Gev
Low P	0-5	2.5-5.0 Gev
Med P-10%	0-7	3.5-7.0 Gev
Med P	0-8	4.0-8.0 Gev
Med-High P	0-10	5.0-10.0 Gev

RESULTS

Roughly 20 million events were analyzed. The results of the analysis are presented in mass plots in figs. 26-34. The mass plots are in 12.5 MeV bins, which is consistent with the observed FWHM of the J particle. The cuts applied to these mass plots are listed in tables 5&6.

The results of all overlapping mass plots are smooth distributions increasing because of increasing acceptance and decreasing because of the production mechanism. The results are presented in events instead of cross sections in order to view the statistics involved in searching for sharp resonances. There are no sharp resonances in all nine reactions. A comparison of all overlapping mass plots shows no structure outside of statistical fluctuations. This result contradicts many theoretical attempts to understand the J particle in terms of the charm model¹. The charm model predicts a sharp resonance near 3 GeV in $p\bar{p}$ and around 2 GeV in π^+K^- . None of these were found in these measurements for proton collisions at $E_{cm} = 7.43$. There may be wide resonances with larger widths than 300 MeV, however, this would depend on an exact calculation of the acceptance.

To place an upper limit on the production of sharp narrow resonances, particles at masses of 2.25, 3.1 and 3.7 GeV were monte carlo generated with a production

mechanism of

$$E \frac{d^3\sigma}{dp^3} = C e^{-6p_1}$$

which decay into h^-h^+ pairs isotropically in its rest frame.

To produce a peak 5 standard deviations above the background, the required cross section times branching ratio, σ_B , yields the following cross sections to which these measurements are sensitive, at three different masses,

h^-h^+	2.25 Gev	3.1 Gev	3.7 Gev	MASS
π^+K^-	1×10^{-33}	4×10^{-35}	1×10^{-35}	cm^2
$K^+\pi^-$	4×10^{-33}	8×10^{-35}	4×10^{-35}	
$P\bar{P}$...	4×10^{-34}	2×10^{-35}	
K^-K^+	1×10^{-33}	5×10^{-35}	1×10^{-35}	
$\pi^-\pi^+$	8×10^{-33}	5×10^{-34}	3×10^{-35}	
$P K^-$	7×10^{-33}	4×10^{-34}	3×10^{-35}	
$K^+\bar{P}$	2×10^{-33}	4×10^{-35}	8×10^{-36}	
$P \pi^-$	4×10^{-32}	4×10^{-33}	5×10^{-34}	
$\pi^+\bar{P}$	2×10^{-33}	4×10^{-35}	7×10^{-36}	

¹T. Appellequist and H. D. Politzer, Phys. Rev. Lett., 34, 43 (1975)

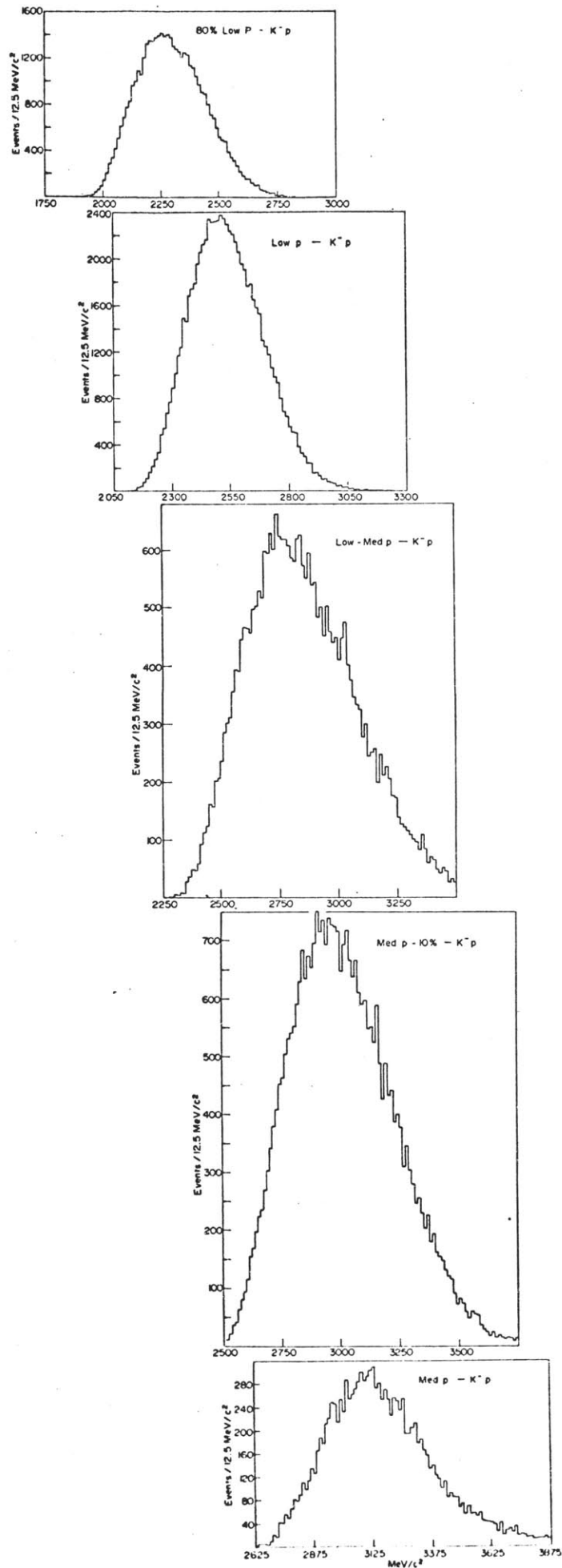


Fig. 26 K^-p mass spectra for five mass ranges from MIT-BNL.

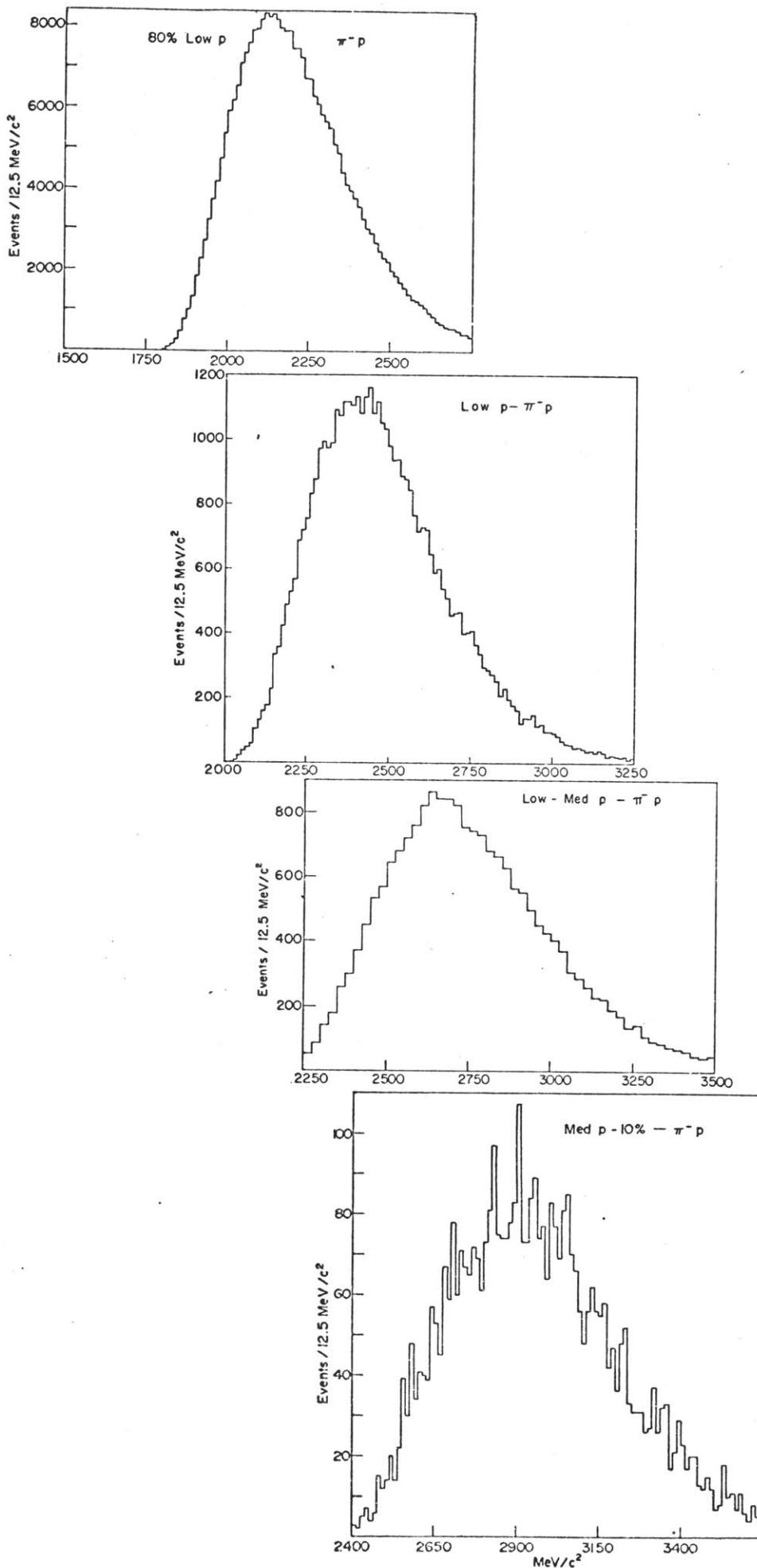


Fig. 27 $\pi^- p$ mass spectra for four mass ranges from MIT-BNL.

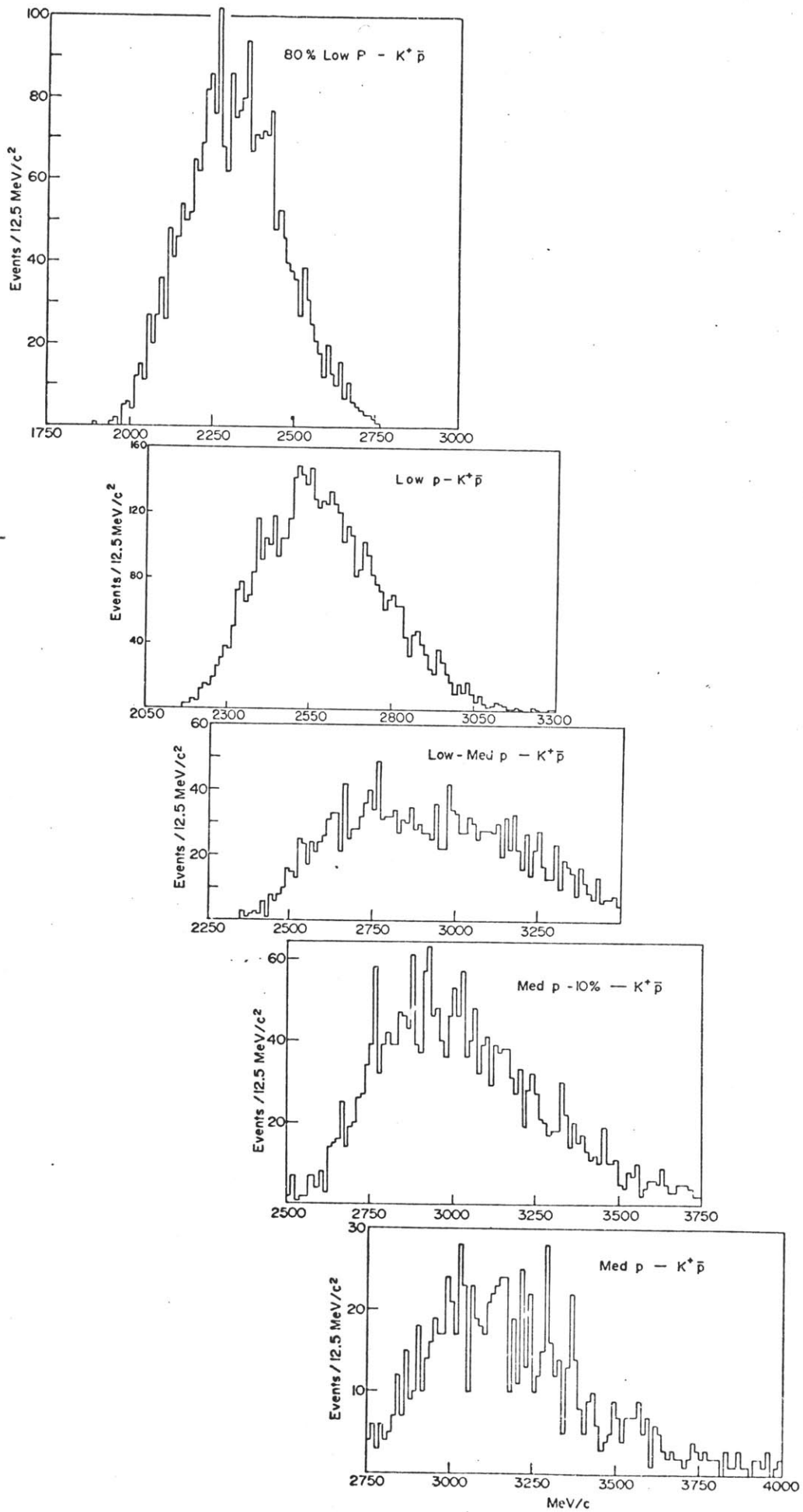


Fig. 28

$\bar{p} K^+$ mass spectra for five mass ranges from MIT-BNL.

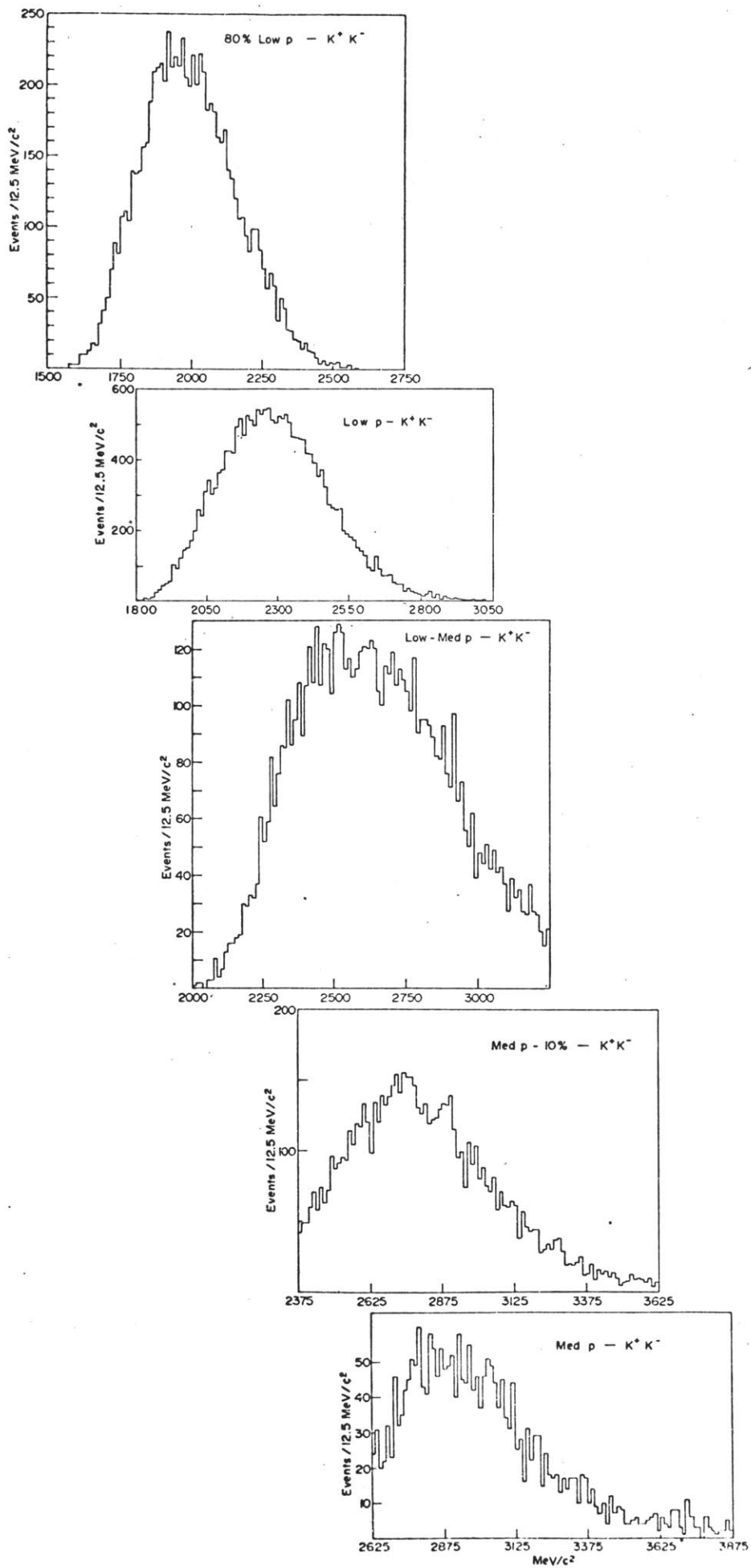


Fig. 29 K^-K^+ mass spectra for five mass ranges from MIT-BNL.

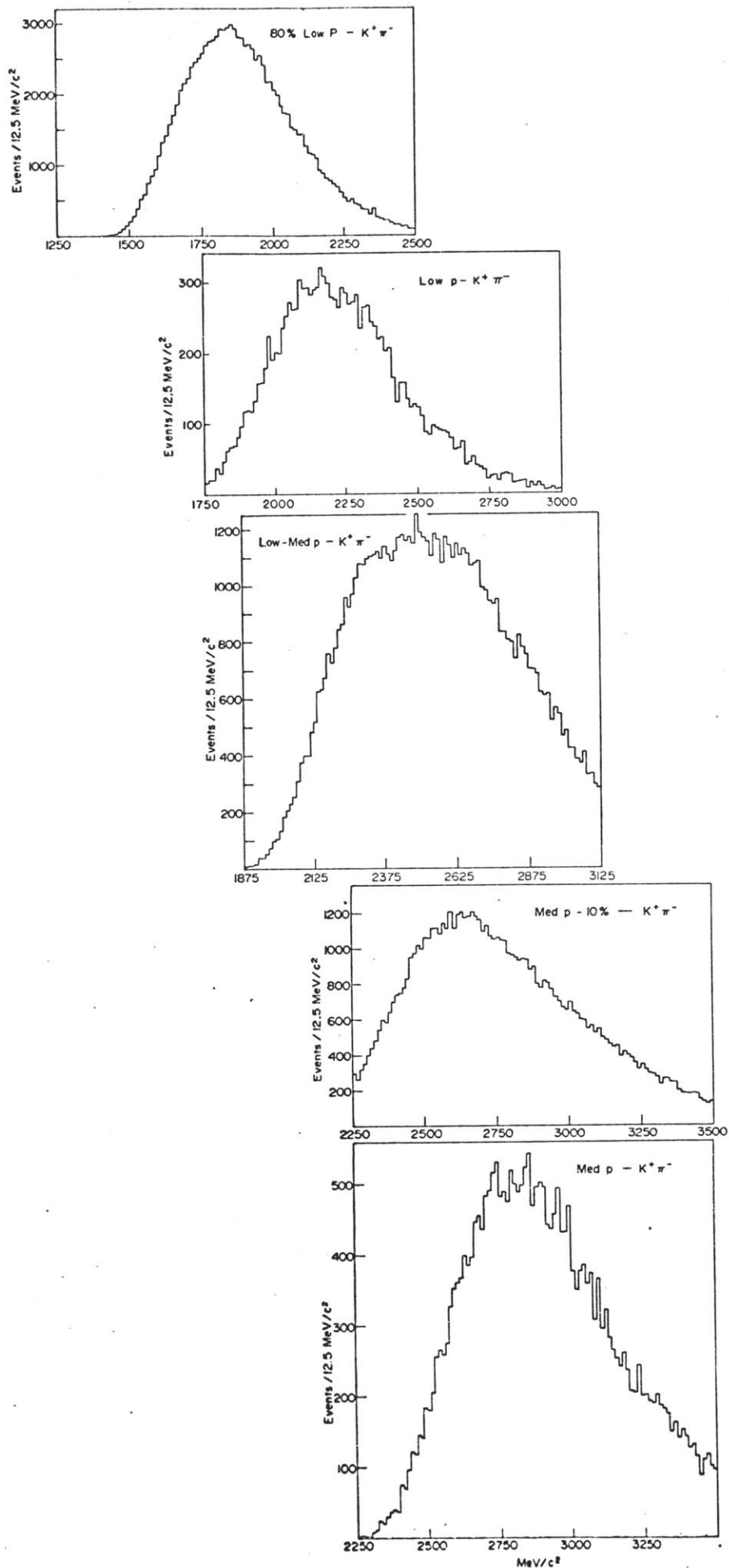


Fig. 30

π^-K^+ mass spectra for five mass ranges from MIT-BNL.

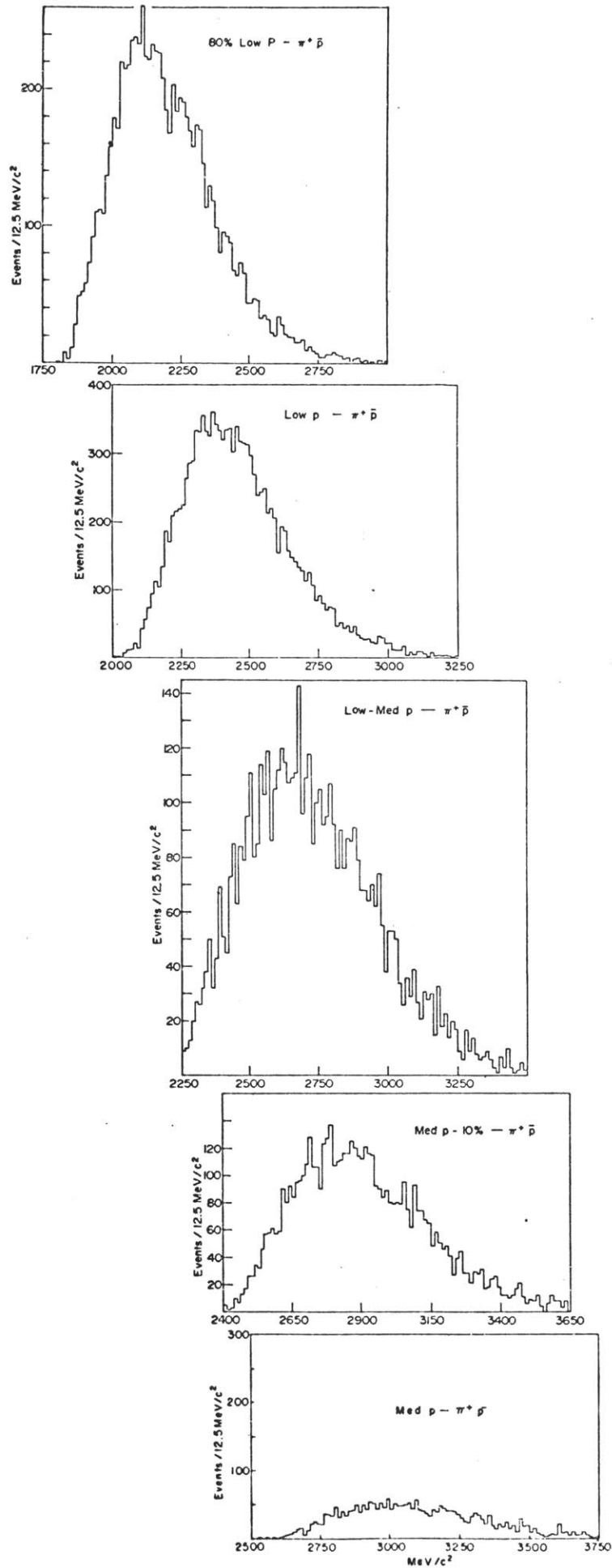


Fig. 31 $\bar{p}\pi^+$ mass spectra for five mass ranges from MIT-BNL.

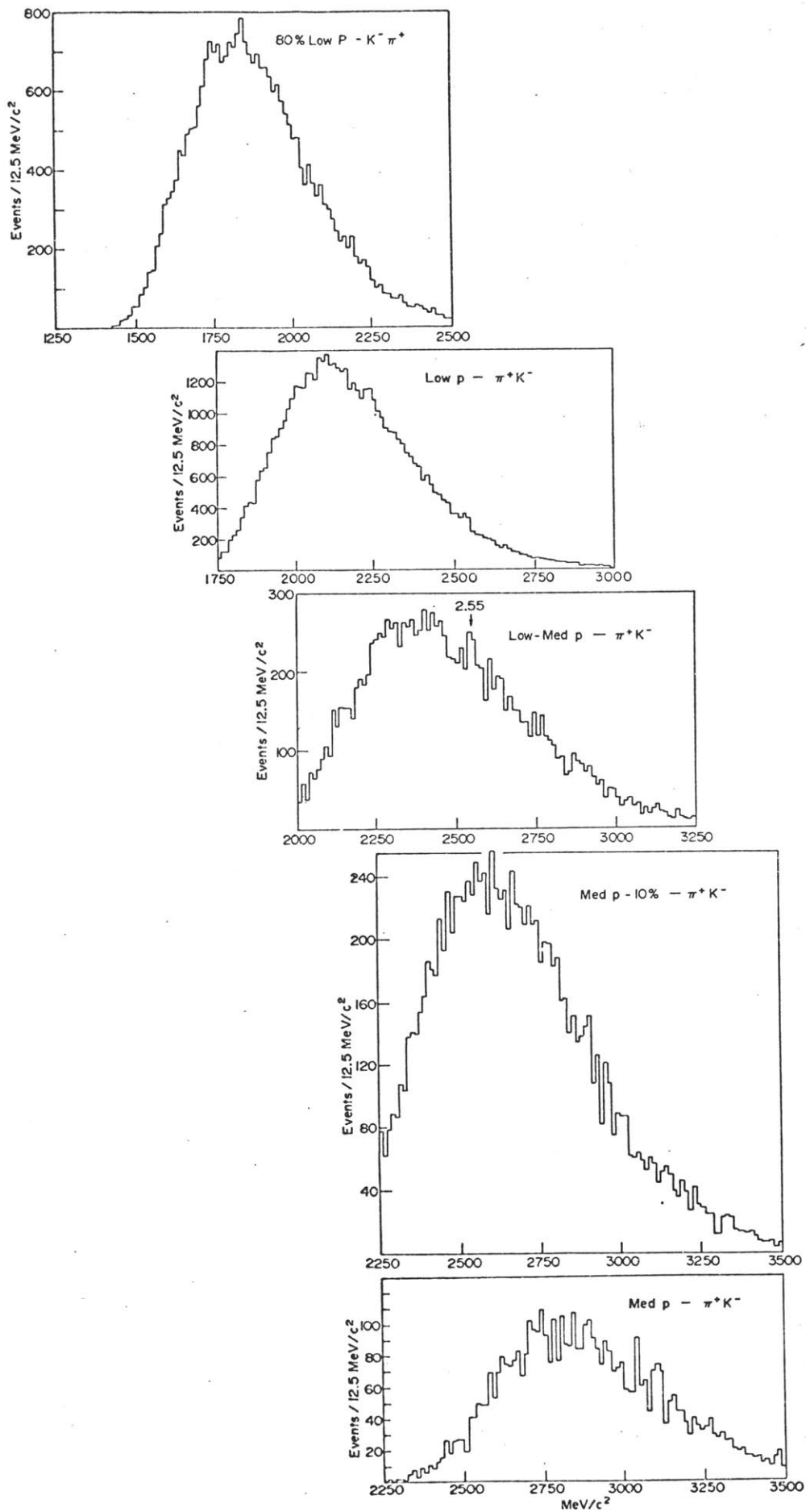


Fig. 32 $K^- \pi^+$ mass spectra for five mass ranges from MIT-BNL.

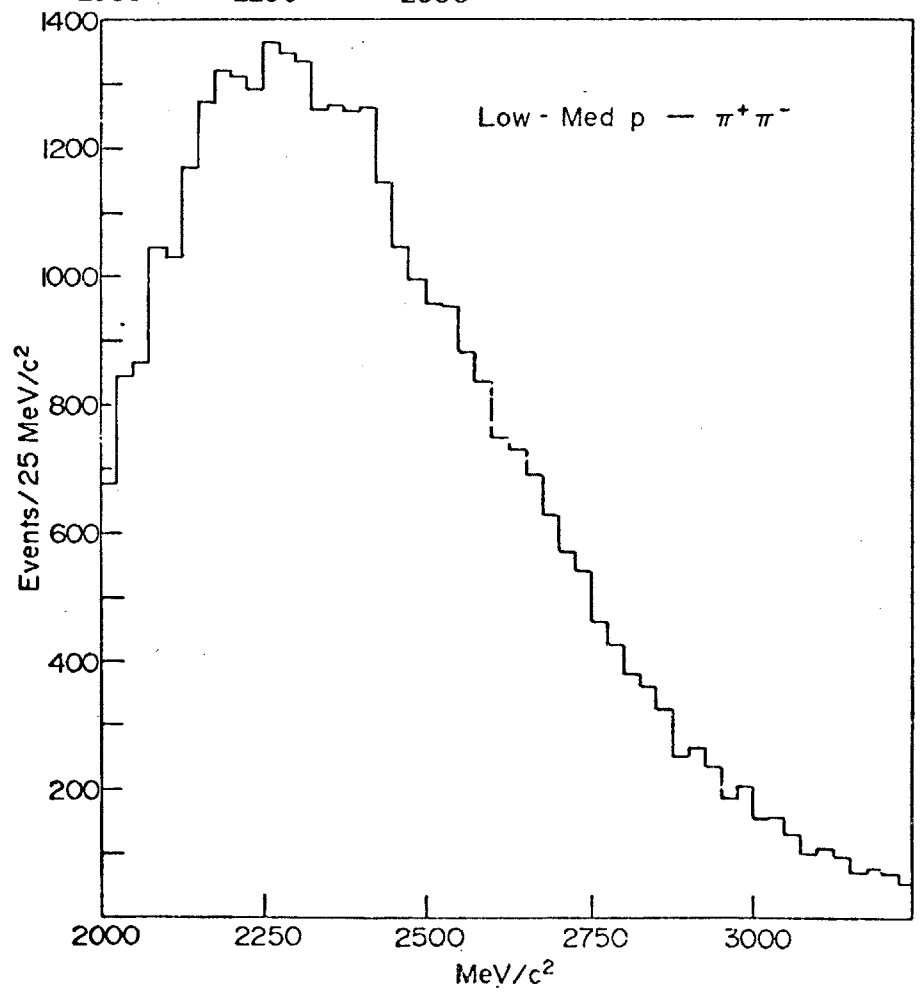
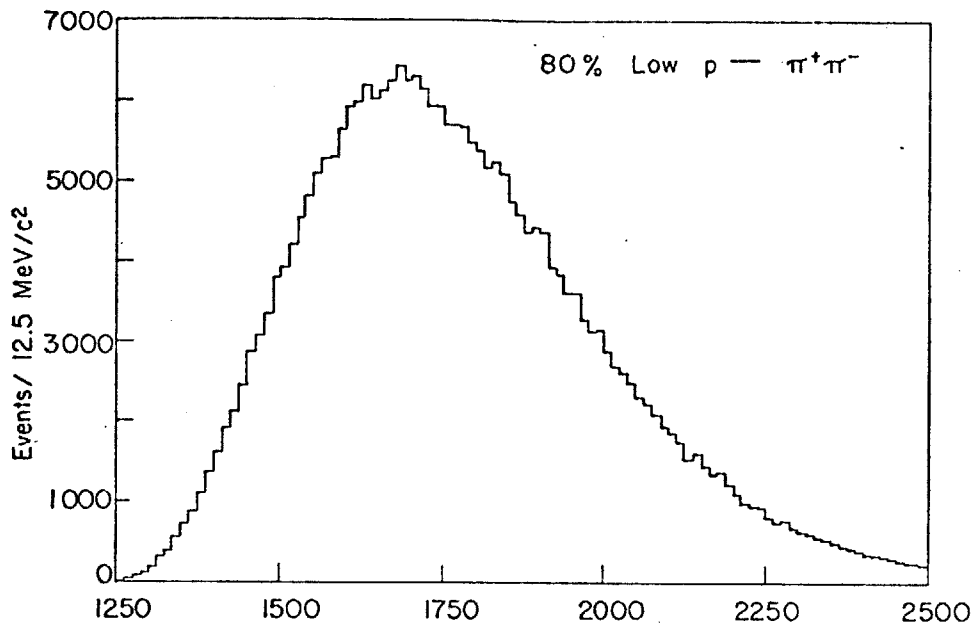


Fig. 33 $\pi^-\pi^+$ mass spectra for two mass ranges from MIT-BNL,

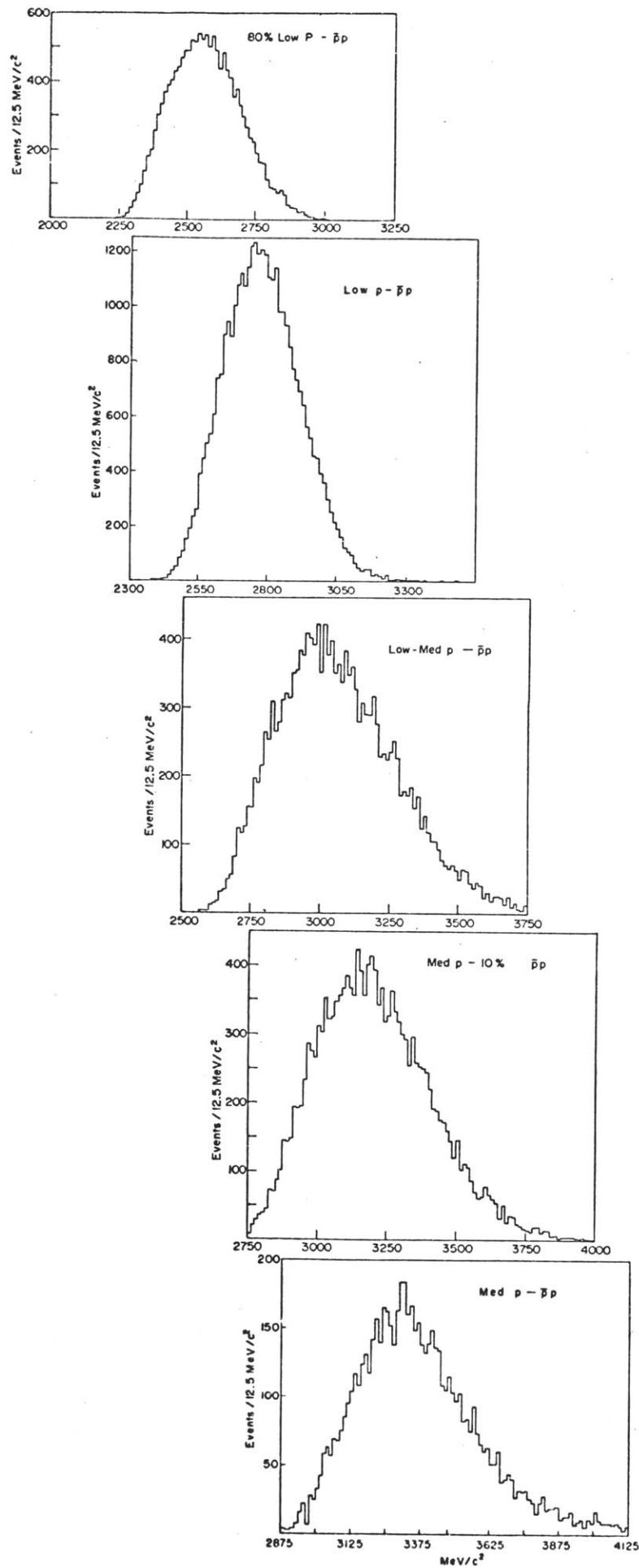
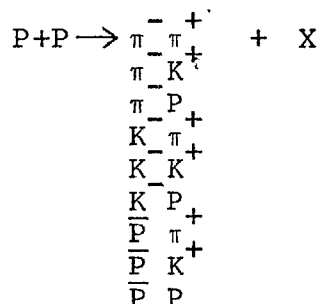


Fig. 34 $\bar{p}p$ mass spectra for five mass ranges from MIT-BNL.

CROSS SECTION

To obtain cross sections from the simultaneously measured reactions,



the yields of the final hadron states are assumed to come from the decay of a particle, $A \rightarrow h^+ h^-$ with mass $m_{h^+ h^-}$, that decays isotropically.

To calculate the acceptance from Monte Carlo simulation, events are generated according to a flat mass distribution, $m_{h^+ h^-}$, a flat $X = P_L / \sqrt{S/2}$ distribution and a P_{\perp} distribution fitting the data. Given now the complete kinematics of A in the C.M.S., A then isotropically decays into a hadron pair $\pi\pi$, πK , πP , KK , KP , and PP . The acceptance for each pair must be calculated separately. The program then tries to transport each decay particle through the magnets, allowing for decay. These calculations were carried out for each magnet setting and each of the previously listed pairs.

The cross section for a reaction is related to the number of events, N, monte carlo events, $N_{M.C.}$, and target in

the following relation,

$$N = \frac{N_{\text{ACCEPTED}}^{\text{M.C.}}}{N_{\text{GENERATED}}^{\text{M.C.}}} \times \sigma \times (\# \text{ target nucleons/cm}^2)$$

for the number of N events detected per incident proton.

$N_{\text{GENERATED}}^{\text{M.C.}}$ is the total number of monte carlo tries, $N_{\text{ACCEPTED}}^{\text{M.C.}}$ is the total number of events detected in the simulation, and σ is the reaction cross section. The first quantity of the right hand side of the equation is called the acceptance and represents the efficiency to which the experimental apparatus can detect a reaction. Using data and monte carlo events from the same 12.5 MeV bins, the differential cross section is,

$$d\sigma = N_{\text{DATA/bin}} \left(\frac{N_{\text{GEN}}^{\text{MC}}}{N_{\text{ACCEPT/BIN}}^{\text{MC}}} \right) \frac{1}{(\# \text{ target nucleons/cm}^2)} \frac{1}{(\# \text{ INCIDENT PROTONS})} \frac{dm}{M_0} \frac{dX}{X_0}$$

where M_0 is the width of the random mass generation and X_0 is the interval of random X generation, $-0.15 < X < 0.1$.

The statistical errors are

$$\sqrt{\frac{1}{N_{\text{ACCEP/BIN}}^{\text{M.C.}}} + \frac{1}{N_{\text{DATA/BIN}}}}$$

Thus,

$$\Delta \left(\frac{d\sigma}{d\Omega dX} \right) = \frac{d\sigma}{d\Omega dX} \sqrt{\frac{1}{N_{ACC}^{M.C./BIN}} + \frac{1}{N_{DATA/BIN}}}$$

The target nucleons/cm² for the Beryllium and Al₂O₃ are

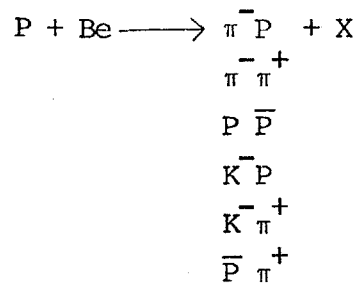
$$\text{target nucleons} = (\# \text{nucleons/nuclei}) \times (\text{target thickness}) \\ \times (\text{density}) \times (6.02 \times 10^{23})$$

for a cross section per interacting nucleon.

The # incident protons was measured by the Secondary Emission Counter, as explained earlier. However, since 4 mm target cubes were used, for improved momentum resolution, parts of the beam could have missed the target. Conservatively, the overall absolute cross section of all the measurements is estimated to be uncertain with a factor of 3.

Since measurements were taken simultaneously for all h⁺h⁻ pairs, the relative yields between different h⁺h⁻ pairs should be accurate to ±20%. The primary cause of these errors is due to protons causing counts in CK and hence being falsely identified as kaons. This is due to proton interactions in C wire chamber which had a total of 1" aluminum and in the wall of CK which was 5/16" thick steel. This totaled to a 15% collision length. Even though this effect was verified later to be ~20%, the modes with K⁺ in the h⁺h⁻ pair are omitted.

The cross sections for the following reactions



are shown in fig. 35 . In this figure, $\frac{\partial^2 \sigma}{\partial m \partial x}$ is plotted versus mass at $x = 0$. Two important observations are:

- 1) All cross sections $\frac{d^2 \sigma}{dm dx}$ decrease as $\approx e^{-5m}$
- 2) The cross section falls into three bands; $\pi^- p$ in the first, $\pi^- \pi^+$, $p \bar{p}$ and $K^- p$ in the second, and $K^- \pi^+$ and $\pi^+ p^-$ in the last. Each band is roughly an order of magnitude apart.

We note that for a particle A produced near $x = 0$ the production can only depend on the energy E like e^{-5E} . Assuming the production to be isotropic in the C.M.S.

$$\langle (P_{\perp}^2) \rangle = 2/3 \langle (p^2) \rangle,$$

and defining the kinetic energy

$$T = E - m = (m^2 + 3/2 P_{\perp}^2)^{1/2} - m,$$

we have

$$E \frac{d^3\sigma}{d^3p} = Ce^{-5E} = Ce^{-5m}e^{-5T}$$

where C is a constant. The e^{-5T} term describes the P_{\perp} dependence as a function of mass. The data in fig. 35 clearly displays the first term. The prediction for T dependence at different masses is shown in fig. 36.

To check this relation, we note for small mass, the P_{\perp} behavior is,

$$E \frac{d^3\sigma}{d^3p} \propto e^{-5\sqrt{(3/2)P_{\perp}^2}} \approx e^{-6P_{\perp}}$$

which is well known from inclusive single particle production.¹

The P_{\perp} dependence of our data is verified by comparing the T dependence with the $\pi^{-}\pi^{+}$ invariant cross section. Mass independence is demonstrated in three narrow mass bands of $1.9 < m < 2.1$, $2.4 < m < 2.6$ and $2.9 < m < 3.1$ Gev in fig. 37.

To further study the P_{\perp} dependence of other particles we include the ρ° and ω mesons.² This is compared in fig. 38 with the $e^{-5(m+T)}/E$ relation against the $d\sigma/dp_{\perp}^2$ data points of ρ° and ω mesons produced from 24 Gev protons incident on liquid Hydrogen. All these results show good agreement with this simple description for the mass and P_{\perp} behavior of inclusive particle production and resonances.

¹M. Banner et al., Phys. Lett. 44b, 537(1973).

1

²V. Blobel et al., Phys. Lett. 73, 48B(1974)

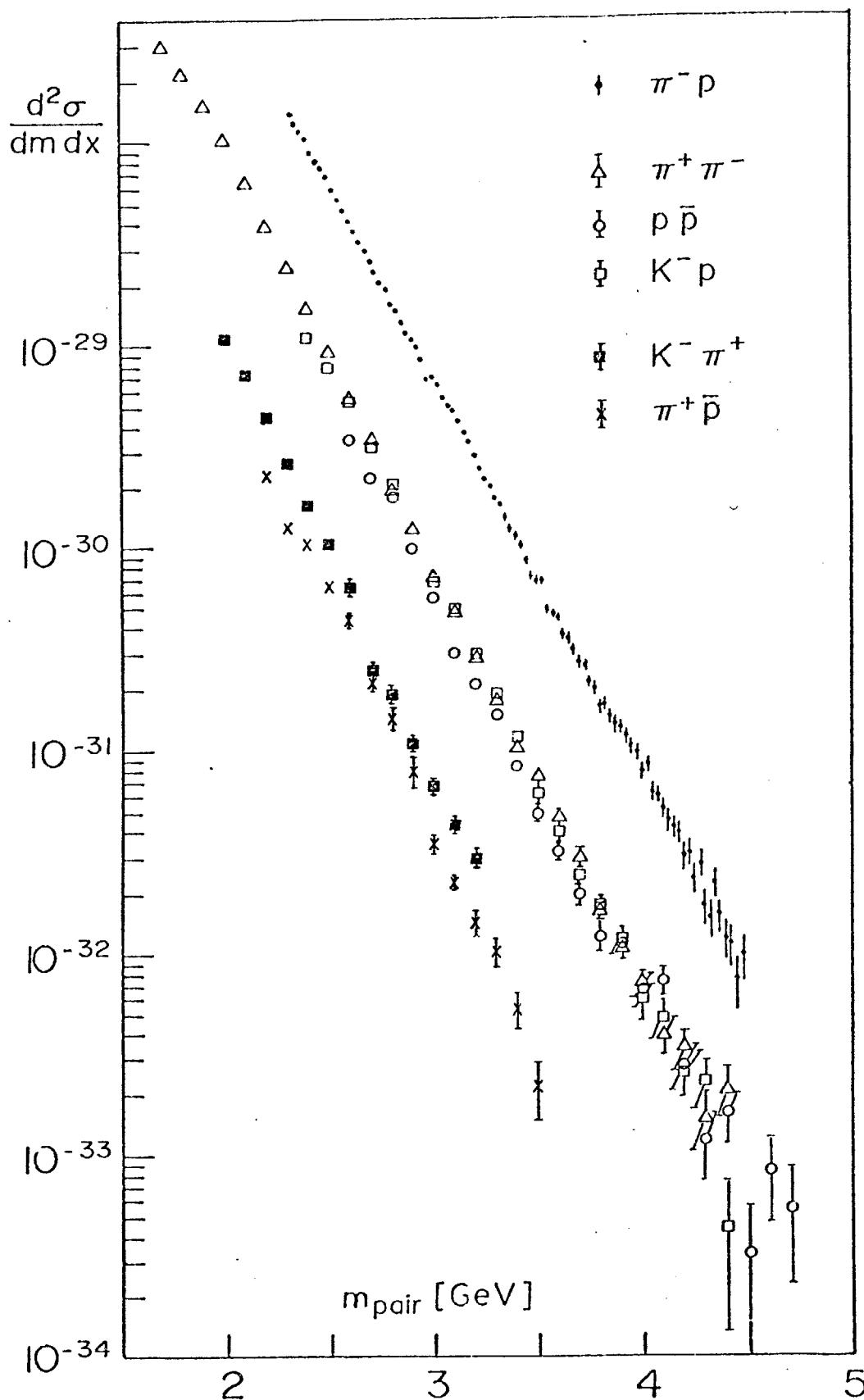


Fig.35 The measured cross section ($P_{\pm} \approx 0, X \approx 0$) as a function of the pair mass. The absolute cross section is accurate to a factor of ~ 3 . The relative yields between different reactions is accurate to $\sim 20\%$.

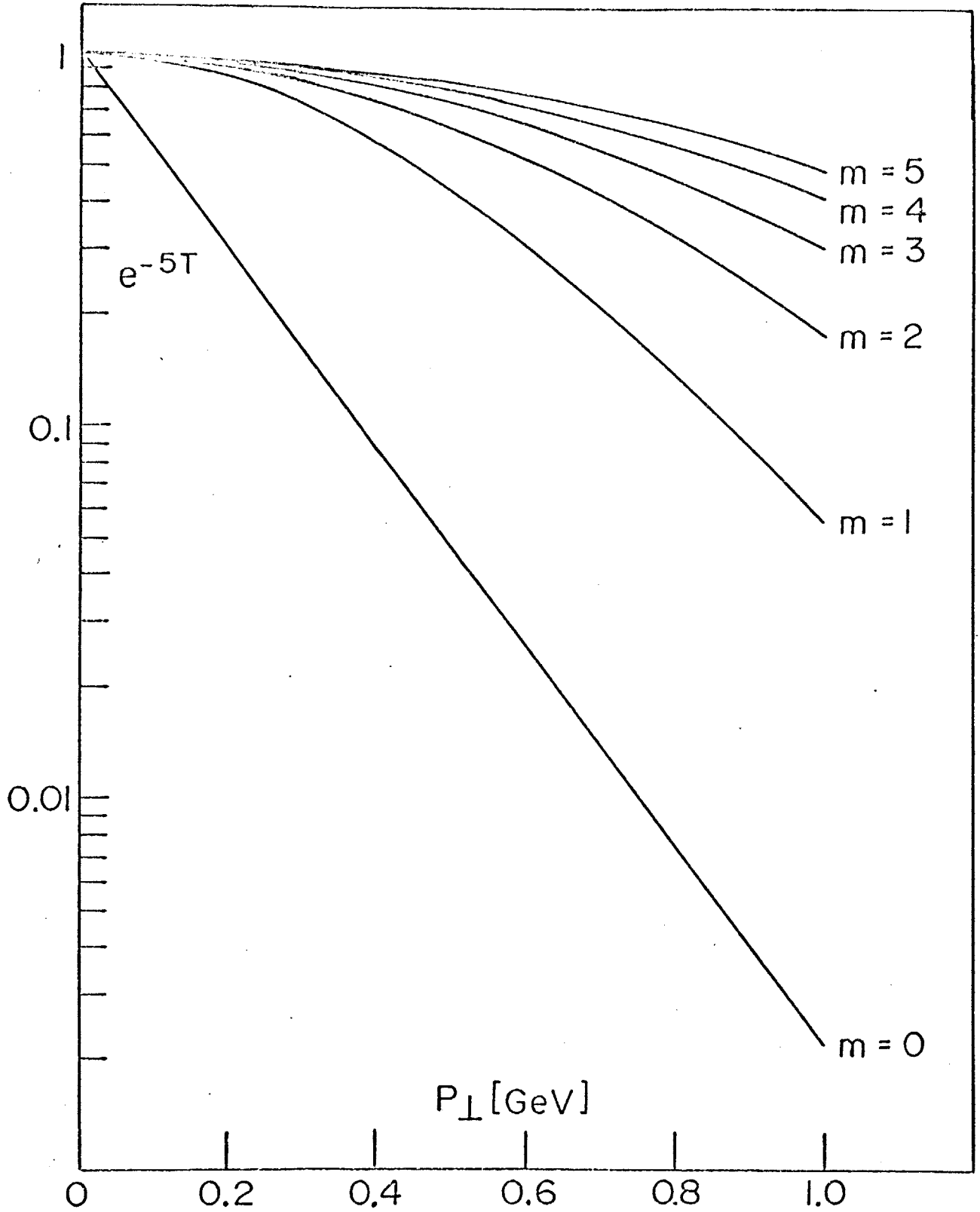


Fig.36 The P_{\perp} behavior of e^{-5T} as a function of M .

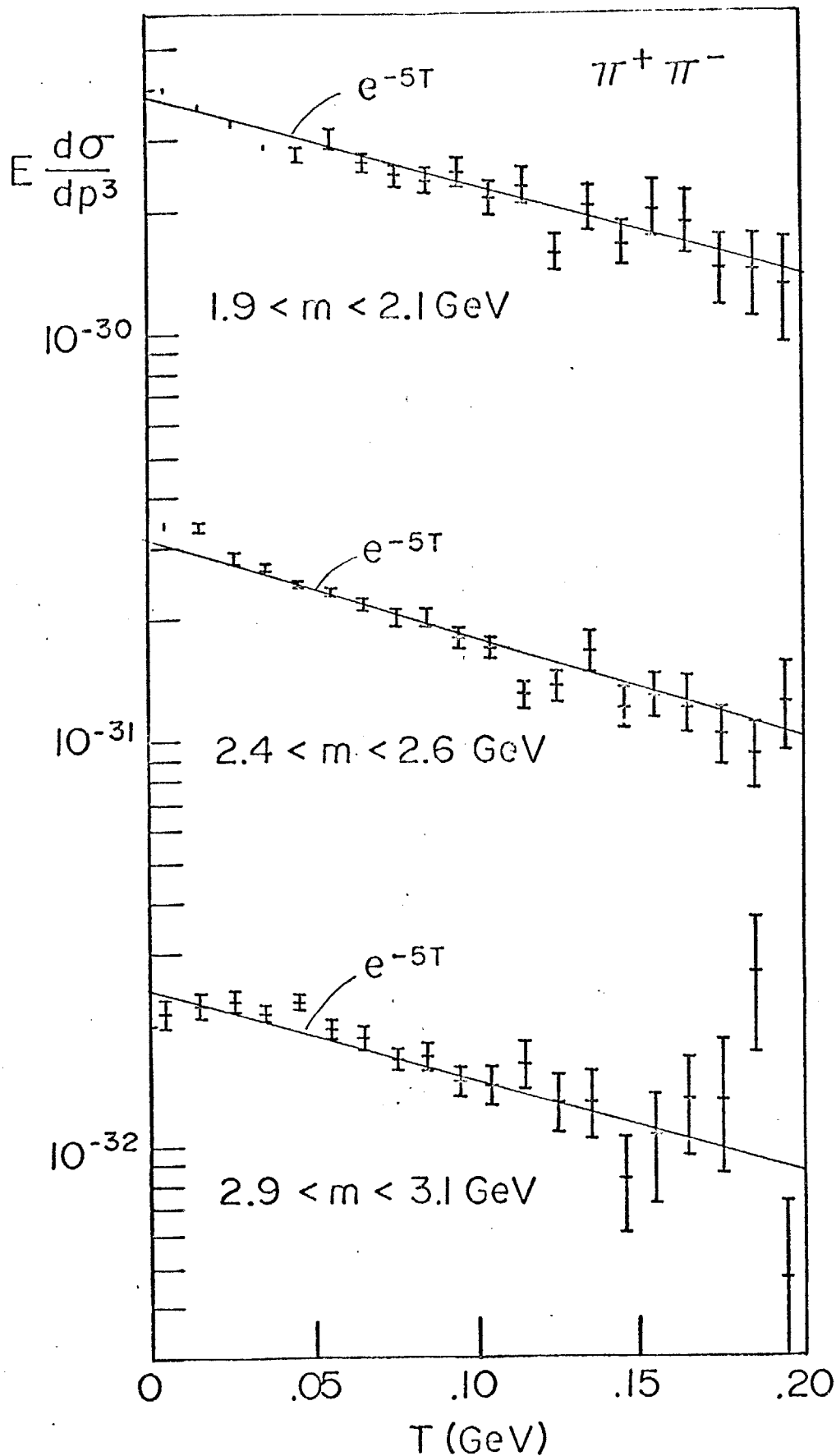


Fig. 37 The T dependence of the invariant cross section (in units of cm^2/GeV^2) for $\pi^+ \pi^-$ at three narrow mass bands. The e^{-5T} line is a visual fit to the data.

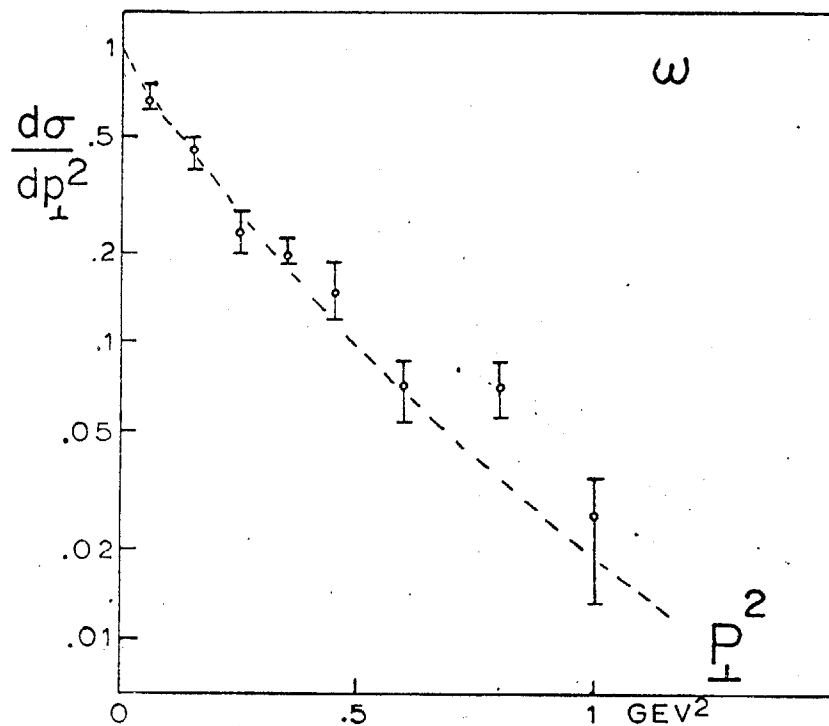
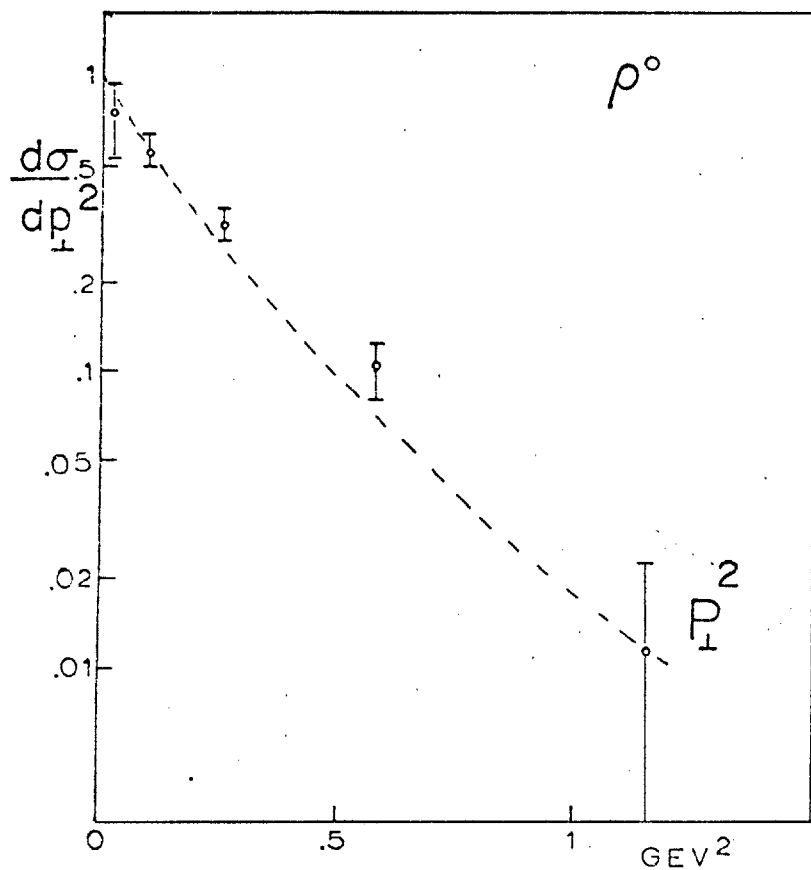


Fig. 38 P_{\perp}^2 distributions of ρ^0 and ω mesons produced from 24 Gev protons incident on liquid hydrogen. The dashed line is $e^{-5\sqrt{m^2+(3/2)P_{\perp}^2}/\sqrt{m^2+P_{\perp}^2}}$. The vertical height is adjusted by eye.

shows only electrons (positrons) of less than 1.2 GeV can be detected, hence this method cannot possibly eliminate all π^0 's. the double arm trigger, 17% radiation length copper converter plates were placed in the gap of $M\emptyset$ magnet on the electron (positron) arm. In this manner the dominant fraction of events are one hadron plus an e^-e^+ pair from a converted γ entering the electron (positron) arm. Thus the ratio, from the off-line analysis of these special runs, of the number of events with CB counting over the total number of events represents the fraction to which CB can detect π^0h^+ events. The results shown in table 9 yield detected fraction of $40 \pm 4\%$. Hence the estimated number of π^0h^+ events in regular runs will be the number of events with CB counting times a factor 2.5.

TABLE 7 Electron-Hadron Runs

MODE	MAGNET	TARGET	#TRIGGERS	#TAPES	#INC. PROTONS
e^+h^-	Low P	5xBe	139K	11	1.75×10^{15}
e^+h^-	Low P	5xBe/Cu Con.	39K	2	1.51×10^{14}
e^+h^-	Low Med P	5xBe	32K	7	1.43×10^{15}
e^-h^+	Low Med P	5xBe	90K	9	1.28×10^{15}
e^-h^+	Low Med P	5xBe/Cu Con.	36K	2	1.56×10^{14}
e^-h^+	Low P	5xBe	195K	10	1.14×10^{15}
e^-h^+	Low P	5xBe	419K	18	1.26×10^{15}
e^-h^+	Med P-10%	5xBe	132K	6	2.52×10^{15}

TABLE 8 CUTS APPLIED TO ELECTRON-HADRON DATA

LEFT	RIGHT	CERENKOV AND LEAD GLASS/SHOWER CUT*				TARGET CUT [†]	TIMING CUT	
e	π	$\overline{CO1}$	$\overline{CE1}$	$\overline{CK1}$	$\overline{LG/SH}_R$	CE2 CO2 CK2 LG/SH _L	$ Z_L - Z_R < 3.5''$	$ CE1 - CE2 < 1.2ns$
e	K	$\overline{CO1}$	$\overline{CE1}$	$\overline{CK1}$	$\overline{LG/SH}_R$	"	"	$ CK1 - CE2 < 1.2$
e	P	$\overline{CO1}$	$\overline{CE1}$	$\overline{CK1}$	$\overline{LG/SH}_R$	"	"	$ A - Z < 2.4$
e	e	CO1	CE1	CK1	LG/SH _R	"	"	$ CE1 - CE2 < 1.2$

*LG/SH; Lead Glass/Shower sum with large pulse height

$\overline{LG/SH}$; " " small "

†In addition to this target cut, $(Z_L + Z_R)/2$ had to be within 2" of the survey point

TABLE 9 CB Efficiency with 17% Converter Plate

Mode	Setting	Total Events	CB Events	Detected
$e^+ \pi^-$	Low P	783	333	43±3%
$e^+ K^-$	"	27	9	33±13%
$e^+ \bar{P}$	"	-	-	-
$e^- \pi^+$	Low Med	402	163	41±4%
$e^- K^+$	"	72	29	40±9%
$e^- \bar{P}$	"	517	212	41±3%

OFF-LINE ANALYSIS

The only modification from the h^-h^+ analysis is the incorporation of the lead glass and shower counters.

The analysis program summed the pulse heights of at least two adjacent lead glass and shower counters around the trajectory from the wire chamber. Fig. 39 gives the histogram of this summation from electrons and hadrons. The hadron produced a minimum ionizing curve which is the steep curve on the left. The electrons produce a shower according to a poisson distribution on the left. With the pulse heights clearly separated, the cut was applied by eye roughly where the hadron tail extrapolates to zero.

Table 8 lists the cuts applied to the electron-hadron data.

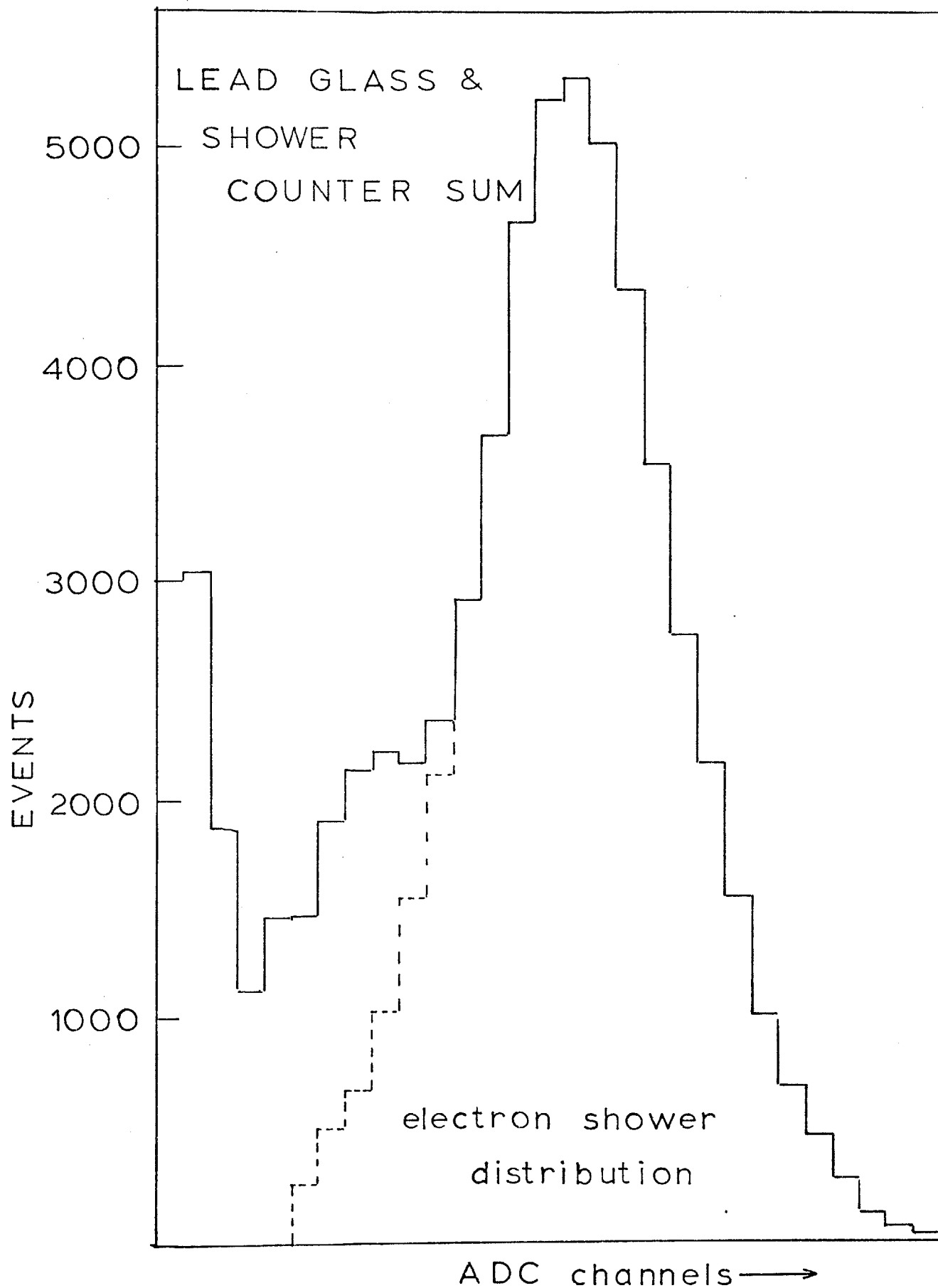


Fig. 38 Summation of lead glass and shower counters in off-line analysis.

RESULTS

We report here on the e^+h^- signal from the measurement described before. A substantial amount of data in the e^-h^+ mode has been taken but will not be reported because the e^- of the pair could be contaminated with knock on electrons.

There is a clear $e^+\pi^-$ signal as shown in fig. 40 which displays the time difference between the two Cerenkov counters CE1 and CE2. Fig. 39 confirms this signal by showing clean target reconstruction. There is also background in the timing signal (see fig. 40) which we subtract from the intime signal,

$$N_{\text{signal}} = N(t=0, \pm 1.2\text{ns}) - N_{\text{background}}$$

$$\Delta N_{\text{signal}} = \sqrt{N(t=0, \pm 1.2\text{ns}) - N_{\text{background}}}$$

This signal is reported in table 10 for the different spectrometer settings. Fig. 41 shows the reconstructed mass spectrum taken from a measurement from Low P. The mass spectrum for the low momentum setting shown in fig. 41 does not show any significantly different shape from $\pi^+\pi^-$ mass spectrum shown in the Low P runs in fig. 33.

Fig. 42a shows the corresponding timing plot of e^+K^- which is obtained by the T.O.F. difference of the A and Z counters. Fig. 42b shows the corresponding T.O.F. difference A and Z for the e^+p^- signal. And for comparison we show the A and Z T.O.F. difference from the π^-e^+ signal in Fig. 42c. It is obvious

that whereas a clear $\pi^- e^+$ is seen that $\bar{p} e^+$ and $K^- e^+$ is marginal. This certainly conflicts with the idea that most of the observed electron hadron pairs comes from Charmed meson decays,

$$D^0 \rightarrow e^+ K^- \bar{\nu} \quad 1a)$$

$$D^0 \rightarrow e^+ \pi^- \bar{\nu} \quad 1b)$$

There one expects equation 1a) to be preferred by the $\cos^2 \theta_c$, where θ_c is the Cabibbo angle, whereas 1b) proceeds with the $\sin^2 \theta_c$.

Also from the shape of the $e^+ \pi^-$ spectrum we have no hint that this signal emerges from a three body decay. The observed signal can be converted into upper cross section limits relative to the 7 J events observed during the runs,

$$\int_{1.5}^{3.5} \frac{\partial \sigma(e^+ K^-)}{\partial m} dm = \frac{25 \pm 11}{7} \sigma(J) < 10^{-33} \text{ cm}^2 \quad 2a)$$

$$\int_{1.5}^{3.5} \frac{\partial \sigma(e^+ \bar{p})}{\partial m} dm = \frac{1 \pm 1}{7} \sigma(J) < 10^{-34} \text{ cm}^2 \quad 2b)$$

These spectra may still contain physical background from internal and external π^0 gamma conversions. An estimate assuming $\pi^- \pi^0$ ($\pi^0 \rightarrow e^- e^+ \gamma$) are produced at the same rate as $\pi^+ \pi^-$ pairs which were measured will yield rates of the magnitude observed. However, the π^0 must have a substantially higher momentum to produce an acceptable e^+ via decay. Such unsymmetrical pairs have not been measured.

As mentioned in the previous section, π^0 decays may be recognized to the $40 \pm 4\%$ level by the help of CB, suggest that up to ~80-90% of the observed signal may come from Dalitz decays confirming the above estimate. In this case the upper limits of equation 2a,b may be lower by an order of magnitude.

1. M.K. Gailliard, B. Lee, and J. Rosner, Rev. Mod. Phys., 47, 310 (1975).

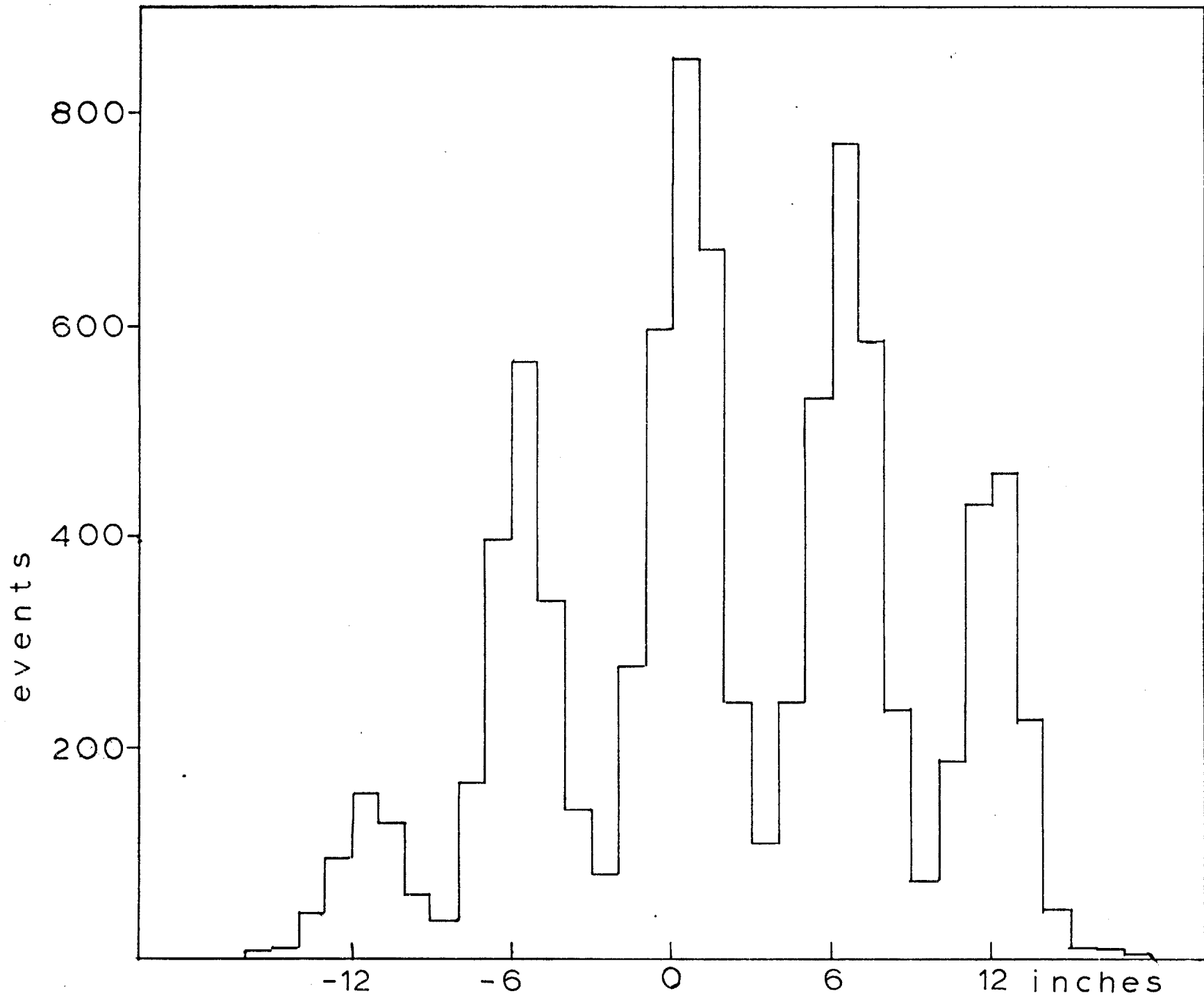
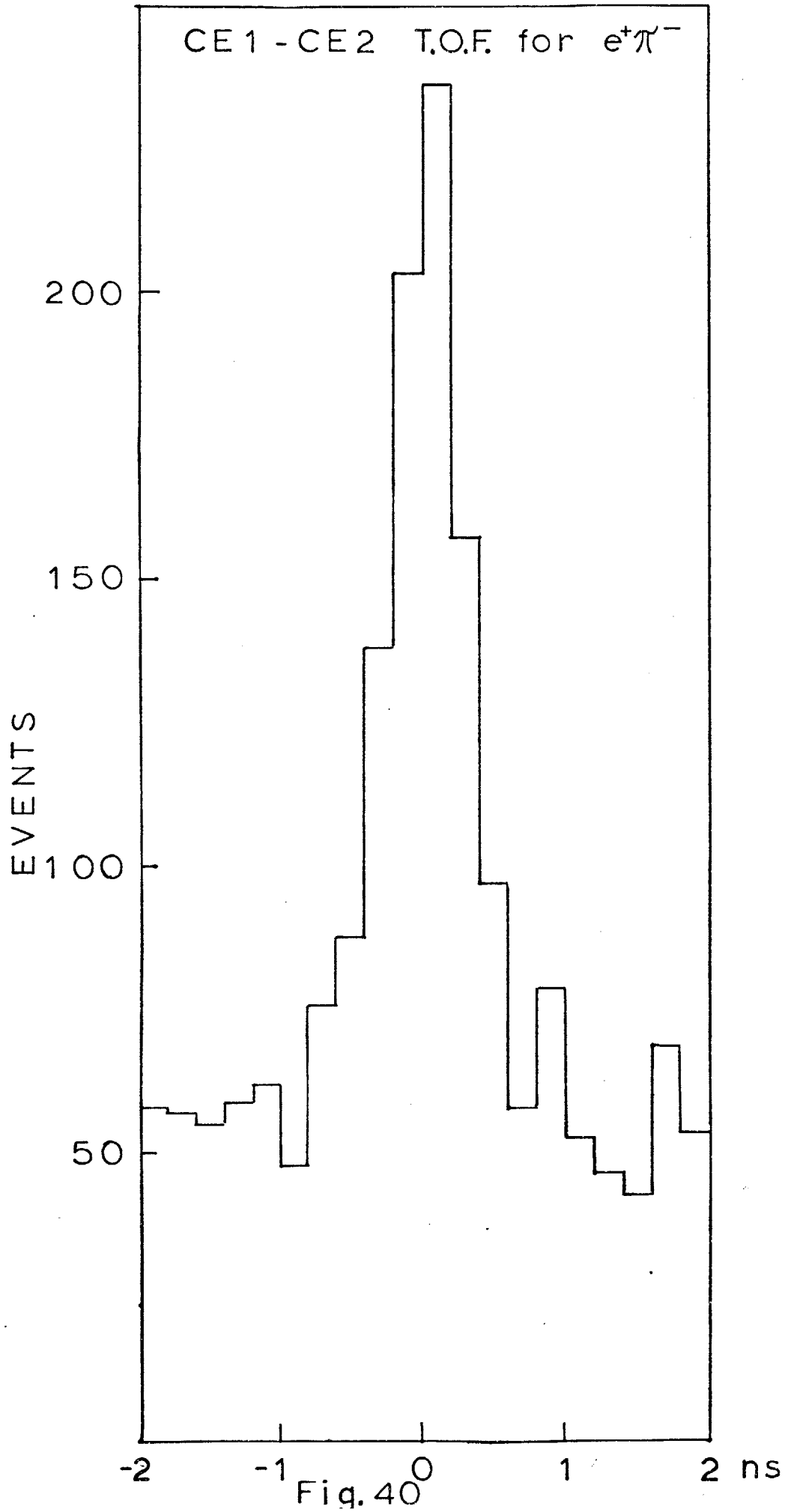


Fig. 39 TARGET RECONSTRUCTION



EVENIS

$e^+ \pi^-$ MASS

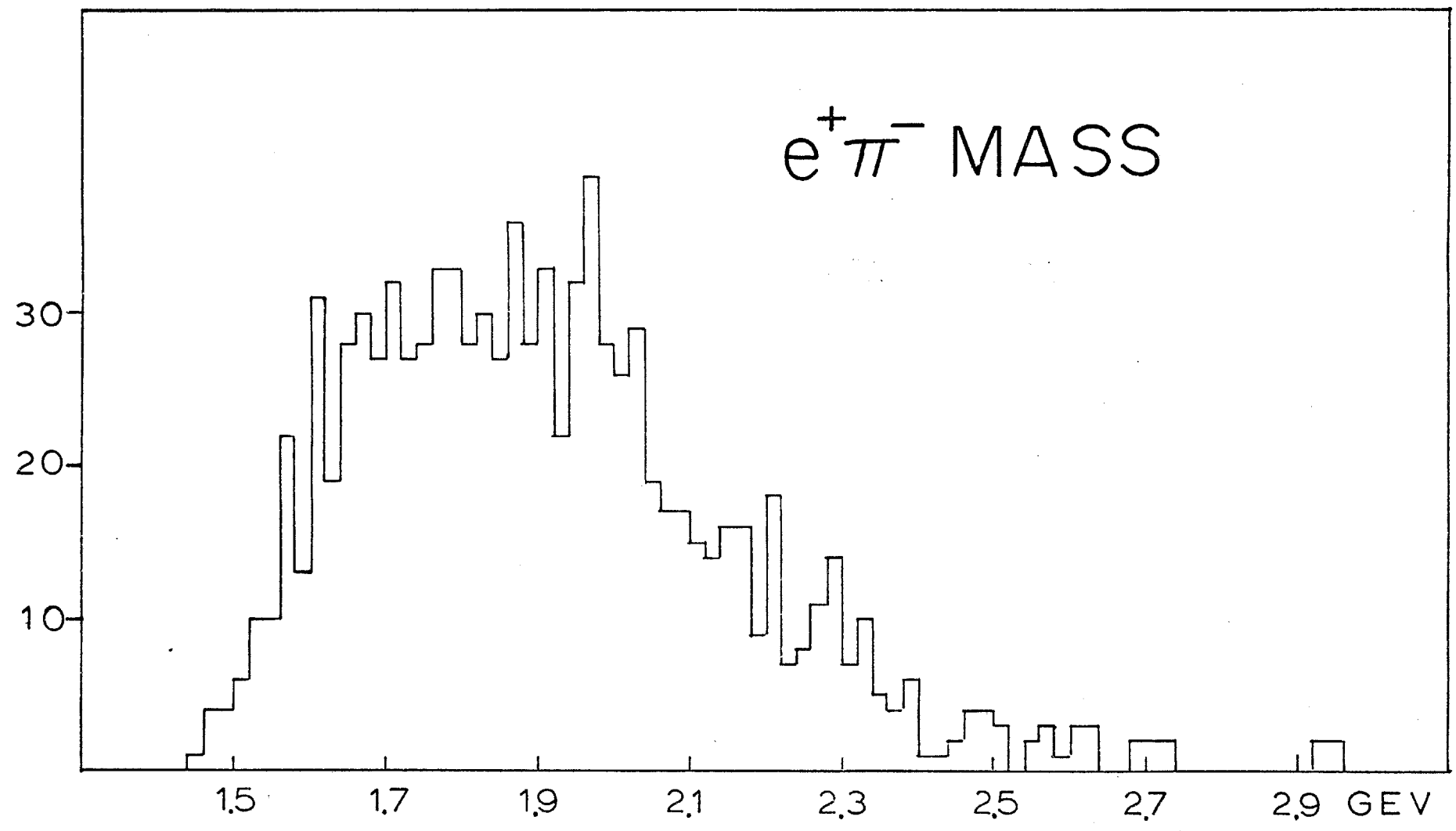


Fig. 41 $e^+ \pi^-$ pair mass from the Low P runs.

TABLE 10 e^+h^- EVENTS

MODE	SETTING	INC. PROTONS	EVENTS	%CB EVENTS	CB EFF.	% π h EVENTS
$e^+\pi^-$	Low P	1.08×10^{15}	676 ± 47	$36 \pm 2\%$	$43 \pm 3\%$	$84 \pm 9\%$
e^+K^-	"	"	20 ± 9	$31 \pm 9\%$	$33 \pm 13\%$	$94 \pm 46\%$
$e^+\bar{P}$	"	"	1 ± 1	--	--	--
$e^+\pi^-$	Low Med	1.46×10^{15}	340 ± 30	$31 \pm 3\%$	--	--
e^+K^-	"	"	5 ± 6	$25 \pm 14\%$	--	--
$e^+\bar{P}$	"	"	--	--	--	--

Note: %CB Events = $\frac{\text{\#Events w/CB counting}}{\text{Total \#Events}}$

% π h Events = $\frac{\text{\%CB Events}}{\text{CB Eff.}}$

A-Z T.O.F. DIFFERENCE

Fig. 42a

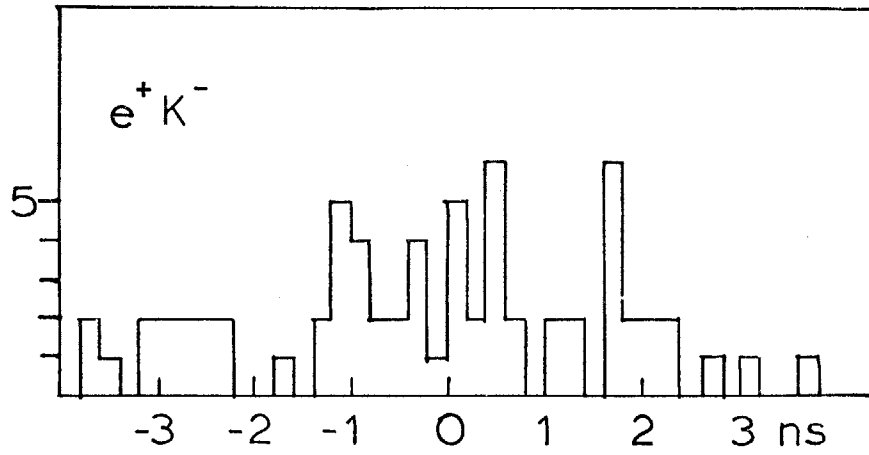


Fig. 42b

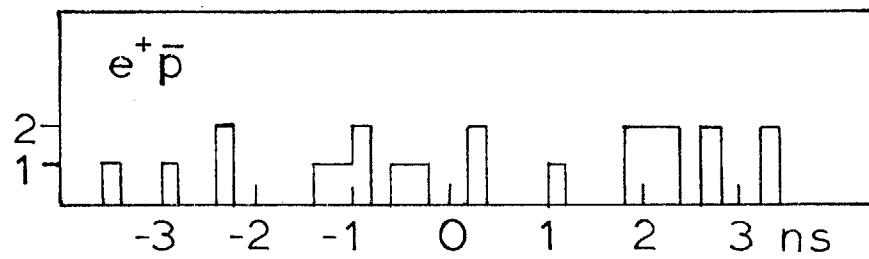
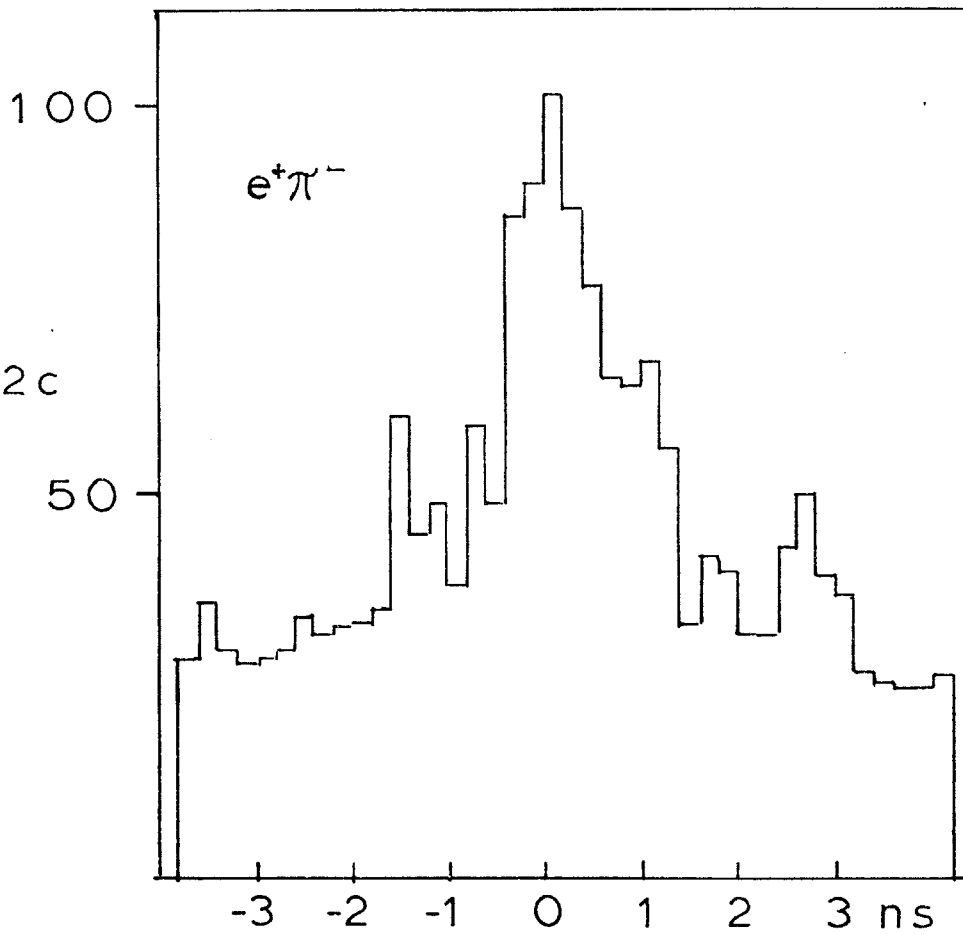


Fig. 42c



Comparison of time of flight differences between the A and Z counters for different particle pairs.

SUMMARY AND CONCLUSIONS

In conclusion a systematic study of hadron pairs and electron-hadron pairs has been performed on opposite charged pair combinations of π^+ , K^+ and P^+ and $e^+\pi^-$, e^+K^- and e^+P^- .

In the hadron pairs no sharp resonance was seen to a sensitivity comparable to the J cross section.

In the search for eh pairs no evidence for a large signal was found with cross sections for e^+K^- and $e^+\bar{P}$ limited to

$$\int_{1.5}^{3.5} \frac{\partial \sigma(e^+K^-)}{\partial m} dm < 10^{-33} \text{ cm}^2$$

$$\int_{1.5}^{3.5} \frac{\partial \sigma(e^+\bar{P})}{\partial m} dm < 10^{-34} \text{ cm}^2$$

And the production of e^+K^- events appears to be smaller than $e^+\pi^-$ events. All these results are inconsistent with Charm particle theory since:

1) no sharp resonances were found, particularly in the $P\bar{P}$ and $K\pi$ -modes.

2) no sizeable e^+h^- signal was found in the mass region 1.5-3 GeV which could originate from the semileptonic decay of charmed mesons .

3) the e^+K^- rate appears to be smaller than the $e^+\pi^-$ rate, contrary to Charm theory where decays involving strange

particles are preferred.

The hadron pair cross sections in the mass range 2.5-4.5 GeV displayed simple degeneracies. All modes show an exponential decrease as e^{-5m} forming three bands of

1) $\pi^- p$

2) $\pi^+ \pi^-$, $p\bar{p}$, $K^- p$ and

3) $K^- \pi^+$ and $\pi^+ \bar{p}$, each band about factor ~10 apart. The

mass and P dependence of these results are well described by

$$E \frac{d^3\sigma}{dp^3} \propto e^{-5M} e^{-5T}, \text{ where } T = \sqrt{m^2 + \frac{3}{2} P_{\perp}^2} - m$$

Recent theoretical papers have attempted to explain this simple structure. Chodos and Willemsen¹ use a quark counting model. Hagedorn² also gave an explanation for the production dynamics similar to the aforementioned formula.

To further study the nature of the inclusive h^+h^- pair results, single particle production has been measured to find correlations to pair as suggested by Bjorken.³

Search for more sharp resonances at higher masses could be done with the same spectrometer at N.A.L. to see how extended the class of new particles is which started with the discovery of the J.

1. A. Chodos and J.F. Willemsen, Phys. Rev. Let. 35, 334 (1975).
2. M. Chaichian and R. Hagedorn, Phys. Let., (1976).
3. J. Bjorken, private communication.

ACKNOWLEDGEMENTS

First, I would like to express my great appreciation to Professor Becker for his advice and guidance of this thesis. His direct physical insight as well as his genuine interest in teaching tempered with patience and understanding was remarkable.

Many people were involved in the setup and running of the experiment. Professor Ting, uncompromising in his demand for first rate physics, provided the group leadership necessary to pursue experimental physics vigorously and accurately. Professor Chen, with his keen knowledge of physics, always quickly responded to the numerous problems occurring during the experiment. Dr. J. Burger, who was in charge of the experiment during long runs, set an example of complete dedication and hard work. Others who deserve special mention are Drs. P. Biggs, G. Everhart, T. Lagerlund, J. Leong, T. Rhoades, J. J. Aubert and S. Wu and the technical specialists who include J. Donahue, T. Jones, G. Krey, D. Osborne, Ingrid Schulz and E. Weiner.

I would also like to thank Drs. J.W. Glenn III, Y.Y. Lee and D. Lowenstein and the staff of the A.G.S. for the fine operation of the accelerator.

Finally I would like to acknowledge my parents, whose support and encouragement throughout my education enabled me to complete so many long years.

BIOGRAPHICAL NOTE

Walter H. Toki was born on August 7, 1951 in Oakland, California. He attended public schools in Richmond and El Cerrito and began course work at the University of California at Berkeley while still in high school. While at Berkeley, he witnessed the social and political turmoil during those difficult years resulting in a very broad education. In June 1973, he graduated in physics, with Great Distinction honors and election to the Honor Society and Phi Beta Kappa. Entering the Massachusetts Institute of Technology in September 1973 as a teaching assistant, he began work in experimental high energy physics with the M.I.T. group at the Alternating Gradient Synchrotron at Brookhaven National Laboratories in January 1974.